AD-757 880

ORBITAL PARAMETER DETERMINATION BY WEIGHTED LEAST SQUARE ERROR AND KALMAN FILTERING METHODS

Joseph J. Pollard

Air Force Institute of Technology
Wright-Patterson Air Force Base, Ohic

December 1972

DISTRIBUTED BY:

NTIS

National Technical Information Service
U. S. DEPARTMENT OF COMMERCE
5285 Port Royal Road, Springfield Va. 22151

DISCLAIMER NOTICE

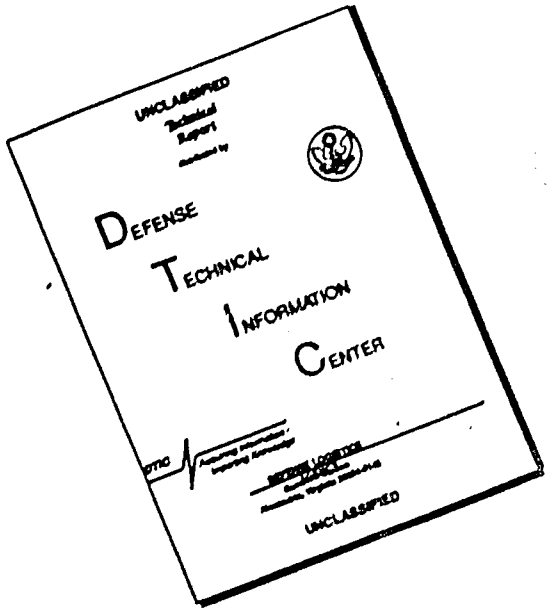

THIS DOCUMENT IS BEST QUALITY AVAILABLE. THE COPY FURNISHED TO DTIC CONTAINED A SIGNIFICANT NUMBER OF PAGES WHICH DO NOT REPRODUCE LEGIBLY.

Reproduced by
NATIONAL TECHNICAL
INFORMATION SERVICE
U S Department of Commerce
Springfield VA 22151

UNCLASSIFIED

Security Classification

DOCUMENT CONTROL DATA - R & D

(Security classification of title, body of abstract and indexing annotation must be entered when the overall report is classified)

1. ORIGINATING ACTIVITY *(Corporate author)*

Air Force Institute of Technology (AFIT/ENE)
Wright-Patterson Air Force Base, Ohio 45433

2a. REPORT SECURITY CLASSIFICATION

Unclassified

2b. GROUP

3. REPORT TITLE

Orbital Parameter Determination by Weighted Least Square Error and Kalman Filtering Methods

4. DESCRIPTIVE NOTES *(Type of report and inclusive dates)*

AFIT Thesis

5. AUTHOR(S) *(First name, middle initial, last name)*

Joseph J. Pollard
Captain USAF

6. REPORT DATE	7a. TOTAL NO. OF PAGES	7b. NO. OF REFS
December 1972	145	21

8a. CONTRACT OR GRANT NO.	9a. ORIGINATOR'S REPORT NUMBER(S)
b. PROJECT NO.	GGC/EE/73-13
c. N/A	9b. OTHER REPORT NO(S) *(Any other numbers that may be assigned this report)*
d.	

10. DISTRIBUTION STATEMENT

This document has been approved for public release and sale; its distribution is limited.

11. SUPPLEMENTARY NOTES	12. SPONSORING MILITARY ACTIVITY

13. ABSTRACT

The Extended Kalman Filter and Weighted Least Square Error filtering techniques are used to determine estimates of the classical orbital parameters of a passive near-earth satellite. Modelling of the geopotential is complete through $J_{6,6}$. Modelling of the earth's atmosphere includes day-night variations as well as altitude variations. Kalman smoothing is also performed. Both filter techniques were used on a simulated orbit as well as a polar circular orbit and a low perigee eccentric orbit obtained from actual radar data. The determination of the orbital parameters of the simulated orbit yielded an absolute as well as a relative comparison of the filter techniques. The analyses of the orbits determined from actual data yielded a relative comparison of the filter techniques. Comparable results were achieved with both filter techniques. Analyses include discussion of orbital perturbations as well as mean orbital elements. All orbits considered were multi-pass with a limited number of observations per revolution.

DD FORM 1 NOV 68 1473

UNCLASSIFIED

Security Classification

14. KEY WORDS	LINK A		LINK B		LINK C	
	ROLE	WT	ROLE	WT	ROLE	WT
Orbit Determination						
Atmospheric Modelling						
Geopotential Modelling						
Extended Kalman Filter						
Weighted Least Square Filtering						
Kalman Smoothing						
Filtering						
Orbital Perturbations						

ORBITAL PARAMETER DETERMINATION BY WEIGHTED LEAST SQUARE ERROR AND KALMAN FILTERING METHODS

THESIS

GGC/EE/73-13 Joseph J. Pollard
Captain USAF

APR. 13
RECEIVED
DDC
REPRODUCED
APR 2 1973
RECEIVED
E

This document has been approved for public release and sale; its distribution is unlimited.

159

ORBITAL PARAMETER DETERMINATION BY WEIGHTED LEAST SQUARE ERROR AND KALMAN FILTERING METHODS

THESIS

Presented to the Faculty of the School of Engineering

of the Air Force Institute of Technology

Air University

in Partial Fulfillment of the

Requirements for the Degree of

Master of Science

by

Joseph J. Pollard, B.S.E.E.
Captain USAF

Graduate Guidance and Control

December 1972

This document has been approved for public release and sale; its distribution is unlimited.

ic

Preface

This thesis is a continuation of the work done by other students at the Air Force Institute of Technology. The most recent of these theses was by Captain Jackson R. Ferguson, Jr., GA-72. A sincere respect for their previous work has been cultivated over the past year, and a sincere debt of gratitude is owed them.

I would also like to express my appreciation and thanks to Lt. Col. Russell A. Hannen, AFIT-ENE, my advisor, for his advice and instruction in stochastic control theory. I also gratefully acknowledge the assistance of Captain Jackson R. Ferguson, Jr., 1st Aerospace Con Squadron, ENT AFB, Colorado in obtaining actual radar data and analysis of it. Last but far from least, I wish to thank my wife, Mike, for her help and deep understanding over the year during which this thesis was prepared.

Joseph J. Pollard

Contents

		Page
Preface		ii
List of Figures		v
List of Tables		viii
List of Symbols		ix
Abstract		xi
I.	Introduction	1
	Statement of the Problem	2
	Assumptions and Limitations	2
	Plan of Development	2
II.	Modelling and Dynamics	4
	Earth's Physical Shape	4
	Earth's Geomagnetic Field	5
	Earth's Atmospheric Density	5
	Geometric Differentiation	6
	The Satellite	9
	The Radar	10
	Coordinate Systems	10
	Dynamics - State Equations	11
	Initial Conditions	12
	Measurements	14
III.	Kalman Filtering	16
	Prediction	17
	Filtering	18
	Smoothing	19
	Reverse Integration	20
	Class I Filter Modification	21
IV.	Weighted Least Square Error Filtering	22
V.	Simulation Study	25
	The Simulation Orbit	25
	Simulation Data Generation	29
	Orbital Perturbations	30
	Secular Perturbations	30
	Oblate Earth Perturbations	37
	Filter Operation	38
	Kalman Smoothing	61

Page

Fixed Interval Smoothing 61
Fixed Point Smoothing. 61
Covariance Matrix Behavior 63
Initial Covariance Matrix, P(0). 63
Experimentation with the Kalman Gain, K. 68
Experimentation with the value of P. 68
Experimentation with the value of Q. 69
Pointing Information from Prediction 69

VI. Actual Data: Ent Set I. 71

Radar Characteristics. 73
Comparison of Orbital Parameters 73
Kalman Smoothing 81
Interpass Pointing Data. 84
Filter Covariance. 84
Filter Effectiveness 84

VII. Actual Data: Ent Set II 90

Data 90
Radar Characteristics. 90
Comparison of Orbital Parameters 90
Kalman Smoothing 110
Covariance of the Filters. 110
Interpass Pointing Data. 117

VIII. Conclusions and Recommendations. 119

Simulation Conclusions 119
Actual Data Conclusions. 120
Recommendations. 121

Bibliography 123

Appendix A: Derivation of the Gravitational Field of the Earth. . 125

Appendix B: Direction Cosine Matrices 128

Appendix C: Derivation of the System Matrix, F. 129

Appendix D: Measurement Sensitivity Matrix, M 131

Appendix E: Gaussian Distribution Density Curves. 132

Appendix F: Determination of θ_{g_o} 141

Appendix G: Determination of Classical Orbital Elements from the State Vector. 142

Vita: Joseph J. Pollard 145

List of Figures

Figure		Page
1	Density Modelling.	8
2	Earth Centered Inertial and Rotating and Station Centered Topocentric Coordinate Systems	13
3	Gaussian Density Distribution 500 Points	27
4	True Simulated Semi-Major Axis	31
5	True Simulated Eccentricity.	32
6	True Simulated Angle of Inclination.	33
7	True Simulated Line of Nodes	34
8	True Simulated Period.	35
9	Semi-Major Axis Error Pass 1	42
10	Semi-Major Axis Errors Pass 2.	43
11	Eccentricity Errors Pass 1	44
12	Eccentricity Errors Pass 2	45
13	Angle of Inclination Errors Pass 1	46
14	Angle of Inclination Errors Pass 2	47
15	Line of Nodes Errors Pass 1.	48
16	Line of Nodes Errors Pass 2.	49
17	Angle at Perigee Errors Pass 1	50
18	Angle at Perigee Errors Pass 2	51
19	Height at Perigee Errors Pass 1.	52
20	Height at Perigee Errors Pass 2.	53
21	Period Errors Pass 1	54
22	Period Errors Pass 2	55
23	Kalman Determined Semi-Major Axis, Simulated Orbit	56
24	Kalman Determined Eccentricity, Simulated Orbit.	57

Figure		Page
25	Kalman Determined Angle of Inclination, Simulated Orbit. .	58
26	Kalman Determined Line of Nodes, Simulated Orbit	59
27	Kalman Determined Period, Simulated Orbit.	60
28	Covariance Simulated Data P_{xx}, Simulated Orbit	64
29	Covariance Simulated Data $P_{xx}^{\cdot\cdot}$, Simulated Orbit	65
30	Standard Deviation of Position, Simulated Orbit.	66
31	Standard Deviation of Velocity, Simulated Orbit.	67
32	Semi-Major Axis Ent Set 1.	76
33	Eccentricity Ent Set 1	77
34	Angle of Inclination Ent Set 1	78
35	Line of Nodes Ent Set 1.	79
36	Period Ent Set 1	80
37	Covariance of P_{xx}, Ent Set 1	86
38	Covariance of $P_{xx}^{\cdot\cdot}$, Ent Set 1	87
39	Standard Deviation of Position, Ent Set 1.	88
40	Standard Deviation of Velocity, Ent Set 1.	89
41	Semi-Major Axis, Kalman, Ent Set 2	94
42	Eccentricity, Kalman, Ent Set 2.	95
43	Angle of Inclination, Kalman, Ent Set 2.	96
44	Line of Nodes, Kalman, Ent Set 2	97
45	Period, Kalman, Ent Set 2.	98
46	Semi-Major Axis, WLS, Ent Set 2.	99
47	Eccentricity, WLS, Ent Set 2	100
48	Angle of Inclination, WLS, Ent Set 2	101
49	Line of Nodes, WLS, Ent Set 2.	102
50	Period, WLS, Ent Set 2	103

Figure		Page
51	Semi-Major Axis, Kalman Revised, Ent Set 2.	105
52	Eccentricity, Kalman Revised, Ent Set 2	106
53	Angle of Inclination, Kalman Revised, Ent Set 2	107
54	Line of Nodes, Kalman Revised, Ent Set 2.	108
55	Period, Kalman Revised, Ent Set 2	109
56	Covariance of P_{xx}, Kalman Revised, Ent Set 2.	113
57	Covariance of $P_{\dot{x}\dot{x}}$, Kalman Revised, Ent Set 2.	114
58	Standard Deviation of Position, Kalman Revised, Ent Set 2	115
59	Standard Deviation of Velocity, Kalman Revised, Ent Set 2	116
60	Gaussian Density Distribution 100 Points.	133
61	Gaussian Density Distribution 200 Points.	134
62	Gaussian Density Distribution 300 Points.	135
63	Gaussian Density Distribution 400 Points.	136
64	Gaussian Density Distribution 600 Points.	137
65	Gaussian Density Distribution 700 Points.	138
66	Gaussian Density Distribution 800 Points.	139
67	Gaussian Density Distribution 900 Points.	140

List of Tables

Table		Page
I	Theoretical Radar Parameters.	26
II	Gaussian Distribution Data Analysis	28
III	Orbital Perturbation Analysis	36
IV	Kalman Filter Analysis.	40
V	WLS Filter Analysis	41
VI	Kalman Smoother Analysis.	62
VII	Theoretical Interpass Pointing Data Kalman Filter	70
VIII	Orbit Data Ent Set I.	72
IX	Radar Parameters Ent Set I.	74
X	Ent Data Set I Results.	75
XI	Smoothing Data at First Observations Ent Set I.	82
XII	Interpass Pointing Data Ent Set I	85
XIII	Orbit Data Ent Set 2.	91
XIV	Sensor #344 Ent Set 2 Parameters.	92
XV	Ent Data Set 2 General Perturbations.	93
XVI	Ent Data Set 2 Special Perturbations.	104
XVII	Smoothing Data at First Observations Ent Set 2, Special Perturbations	111
XVIII	Final Covariances Ent Data Set 2.	112
XIX	Interpass Pointing Data Ent Set 2	118

List of Symbols

A	State Sensitivity Matrix, Weighted Least Squares
B	Ballistic Coefficient, m^2/kgm, .015 for this study
C_d	Drag Coefficient, 2.2, for this study
F	State Sensitivity Matrix
G	Gravitational attraction of the earth
I	Identity matrix
J	Cost Functional, Weighted Least Squares
$J_{k,m}$	Coefficient used in earth modelling
M	Measurement Sensitivity Matrix
N	Index used with Kalman smoothing
P	Covariance of the states; period
P_k^m	Associated Legendre Polynomial
R	Covariance of the measurement noise
S	Frontal area of the satellite
U	Earth's geopotential
V	Velocity
X	State Vector
X_s, Y_s, Z_s	Coordinates of the sensor of interest
a	azimuth angle
$a_{d_x}, a_{d_y}, a_{d_z}$	Components of drag acceleration
$a_{g_x}, a_{g_y}, a_{g_z}$	Components of gravitational attraction
e	eccentricity; elevation angle; geocentric rotating frame
h	Non-linear measurement matrix
i	Angle of inclination; inertial frame
i,j,k	indices

ℓ	length of the vehicle
m	mass of the vehicle
q	constant used with Level I modification, 1×10^{-12} usually
t	time; tangent frame
w	earth rotation rate
y	measurement vector
γ	point of Ares, Vernal Equinox
ϵ	criterion of convergence, Weighted Least Squares
θ_{g_o}	offset angle between inertial and rotating geocentric
λ_E	East Longitude
ρ	range, atmospheric density
ϕ	State Transition Matrix; North Latitude
Ω	Line of Nodes
ω	Argument of Perigee
$\underline{\ }$	Vector Quantity
$\|\|F\|\|$	Norm of F where F is a vector
A^T	Transpose of matrix A
A^{-1}	Inverse of matrix A
$x(k\|j)$	Value of x at kth iteration given information through the jth iteration
b_o	b evaluated at the time, t_o

Abstract

The Extended Kalman Filter and Weighted Least Square Error filtering techniques are used to determine estimates of the classical orbital parameters of a passive near-earth satellite. Modelling of the geopotential is complete through $J_{6,6}$. Modelling of the earth's atmosphere includes day-night variations as well as altitude variations. Kalman smoothing is also performed. Both filter techniques were used on a simulated orbit as well as a polar circular orbit and a low perigee eccentric orbit obtained from actual radar data. The determination of the orbital parameters of the simulated orbit yielded an absolute as well as a relative comparison of the filter techniques. The analyses of the orbits determined from actual data yielded a relative comparison of the filter techniques. Comparable results were achieved with both filter techniques. Analyses include discussion of orbital perturbations as well as mean orbital elements. All orbits considered were multi-pass with a limited number of observations per revolution.

ORBITAL PARAMETER DETERMINATION BY WEIGHTED LEAST SQUARE ERROR AND KALMAN FILTERING METHODS

I. Introduction

When the first vehicles were orbited in the late 1950's and early 1960's, a demand for greater accuracy and higher speed in the computation of orbital parameters became evident. Both engineers and scientists combined their knowledge of the earth's non-uniform gravitational field, the earth's oblate spheroidal shape, and the non-linear time varying atmosphere of the earth to produce highly accurate models. Communications engineers strained at the problem of more accuracy from their radars while the age of computer technology paced the speed which could be achieved in the determination problem.

Previous AFIT theses (Ref: 6,7, & 17) have addressed many of the problems of orbital determination in both simplified simulations and quasi-real world environments using both weighted least square error and Kalman filtering methods. Success has been demonstrated in the application of these filtering methods on both simulation and actual radar data measurements.

However, as yet, all of these concepts have not been gathered together using extremely accurate modeling or even exercising the filtering and smoothing capabilities of stochastic theory to the extent possible. The purpose of this study is to apply both the Weighted Least Square Error and Kalman filtering theory to the problem of real-world near-earth orbital determination using extremely accurate models of the earth and its atmosphere. Smoothing algorithms will be used in conjunction with the Kalman filtering algorithms to determine the classical orbital

parameters. Perturbations occuring in the elements will be investigated and compared with theoretical predictions.

Special interest is shown in this study for the short term, fast determination problem and the capability to predict vehicle position and velocity on future passes in order to assist radar acquisition, provide pointing data, and/or aid intercept capability. The multi-pass multi-radar problem is studied assuming limited information availability on all passes.

The problem will be studied by first addressing highly accurate models to a simulated orbit, two pass, single radar problem. Having obtained a basis for comparison of both filter and smoothing capabilities on data with known true parameters, the study will shift to analyses of actual radar data. The first case to be studied will be a three pass, two radar problem of a satellite in near circular polar orbit. The second case will be a limited data problem using only one radar providing measurements of a satellite having an eccentric, inclined, low perigee orbit. In both cases, parameters obtained will be compared to parameters obtained through use of current operational capabilities. Use will be made of both general and special perturbation theory.

During this study the following assumptions are made:

1. The satellite under consideration is spherical, cylindrical, or of other common shape with no large solar panels or massive extended antennae such that its ballistic coefficient is accurately modeled as B=.015 m^2/kgm (Ref. 12:12-17).

2. The satellite is non-thrusting and therefore incapable of maneuvering.

3. The earth's gravitational field is accurately represented by

inclusion of zonal, tesseral, and sectoral harmonics through $J_{6,6}$.

4. The earth's atmosphere is non-rotating with respect to the surface of the earth. The complete atmospheric model is described in Chapter 2.

5. The earth's atmosphere has negligible effect above 800 kilometers.

6. The earth's atmosphere has sufficient density below 120 kilometers that orbital degradation and re-entry have begun.

7. All orbits considered occurred during a period of mean solar activity.

8. Uncertainties in latitude, longitude, and height of the tracking sensors are assumed negligible.

9. The noise in the tracking sensor data is assumed to be a zero-mean, white, Gaussian sequence.

This study is divided into eight chapters. The second chapter presents a detailed description of the models used, state equations, and initial conditions. Chapter 3 presents the Kalman prediction, filtering, and smoothing algorithms used. Chapter 4 introduces the statistical least square error filter. The fifth chapter presents the details of the simulated orbit analysis and its results. Chapter 6 presents an orbital analysis of an actual vehicle in a polar circular orbit. Chapter 7 deals with an eccentric, inclined, low perigee vehicle. The final chapter presents recommendations for future study along with the conclusions of this study.

II. Modelling and Dynamics

In order to accurately determine the orbital parameters of a satellite, the environment which the vehicle experiences must be accurately described and modeled.

The Earth's Physical Shape

For many years science has been aware that the actual physical shape of the earth is not spherical. Current geophysical theory models the earth as an ellipsoid. An ellipsoid is a surface of revolution having a smaller polar diameter than its equitorial diameter. From the analysis of orbital data, many values have been determined for the ellipticity of the earth. However, in 1964, a value of 1./298.30 was adopted as an international reference standard (Ref: 3:172). This value is used throughout this study. The international reference standard for the equatorial radius of the earth is also used. Thus, the following parameters are employed for the physical shape of the earth:

$$f = 298.30 \tag{1}$$

$$r_e = 6{,}378{,}165 \text{ meters (Ref: 3:171)} \tag{2}$$

The Earth's Geomagnetic Potential

The earth's gravitational potential, U, is given by

$$U = \frac{k_e{}^2 m}{r}\left(1 + \sum_{k=2}^{6}\left(\sum_{m=0}^{k}\frac{P_k{}^m(\sin\phi)}{r^k}\left(C_{k,m}\cos(m\lambda_E) + S_{k,m}\sin(m\lambda_E)\right)\right)\right) \tag{3}$$

where $P_k^m(\sin \emptyset)$ is an associated Legendre polynomial, r is the radius to the point of interest, λ_E is the east longitude and $\emptyset$ is the north latitude (Ref 3: 174-175). The coefficients $C_{k,m}$ and $S_{k,m}$ are determined by a combination of orbital analysis and geodetic survey. Another form of

equation (3) uses the coefficients $J_{k,m}$. However, since $J_{k,m} = \sqrt{C_{k,m}^2 + S_{k,m}^2}$ and from trigonometry it can be shown that

$$A \cos \phi + B \sin \phi = C \cos (\phi + \alpha)$$

where

$$C = \sqrt{A^2 + B^2}$$

and

$$\alpha = \tan^{-1} (B/A)$$

there is actually no difference between these forms. The $J_{k,m}$ are often referred to as zonal constants if $m = 0$, sectoral constants if $k = m$, and tesseral constants otherwise. The constants used in this study are found in Reference 8.

The associated Legendre polynomial is given by

$$P_k^m(x) = (1-x^2)^{m/2} \frac{d^m}{dx^m} P_k(x) \qquad (4)$$

where $P_k(x)$ is a Legendre polynomial. The Legendre Polynomials used in this study are given in Appendix A (Ref: 13:870).

Since from basic physics it is shown that

$$G = \nabla U \qquad (5)$$

it is necessary to take the first partial derivatives of potential with respect to x, y, and z in the geocentric rotating coordinate frame in order to define the gravitational force field. Additionally, the second partials with respect to all combinations of x, y, and z will be required in order to calculate the state equations. The derivation of the first partials is given in Appendix A. The second partials are determined by geometric approximation which will be discussed later in this chapter.

The Earth's Atmospheric Density

The basis for the atmospheric density model used in this study are the 1965 Cospar (Council on Space and Atmospheric Research) atmospheric

data tables (Ref: 1:175-186). The earth's atmospheric density is found to be a function of three basic variables: (1) height above the reference ellipsoid, (2) position with respect to the sun or local time, and (3) solar activity. The first two of these basic variables are fully accounted for by the model used in this study while solar activity is a completely random variable and is treated by the assumption made in chapter 1 that a condition of mean solar activity is present during all orbital calculations.

The raw data relating altitude, local time, and density was first fit with a curve relating density and altitude. After these coefficients were determined using a least square error fit, the resulting coefficients of a seventh order polynomial were fitted versus local time data. Altitude increments were 20 kilometers and time increments were two hours. The time versus fitted altitude/density coefficients fit was done using a fourth order curve. Thus an analytic model was formed from the raw data tables. Curves of all possible orders were fitted and the curve of least order which generated a good fit was chosen.

To verify that no undesired peaks or discontinuities had occurred due to the curve fitting, listings by altitude in increments of 1 kilometer and by time in increments of 3 minutes were made. No irregularities were detected. Figure 1 shows groupings which were made during the curve fitting analysis. All intersections were overlapped at the boundary points to assure continuity when the analytic model was formed.

Geometric Differentiation

The calculation of the various state equations which will be discussed later requires the evaluation of first partials of the density as well as

second partials of the gravitational potential. To accomplish this geometric differentiation was performed:

$$f'(x) = \frac{f(x + \Delta x) - f(x)}{\Delta x}$$

where $f(x)$ is the evaluation of the function at x

and $\Delta x = 1$ meter

The choice of the delta was done after experimentation showed that no change occurred when a smaller delta was chosen. This choice of delta is equivalent to one part in one million for applications in this study.

0 < t<8 hrs 120<h<240 km	0<t<8 hrs 240<h<500 km	0<t<8 hrs 500<h<800km
8<t<16 hrs 120<h<240 km	8<t<16 hrs 240<h<500 km	8<t<16 hrs 500<h<800km
16<t<24 hrs 120<h<240 km	16<t<24 hrs 240<h<500 km	16<t<24 hrs 500<h<800km

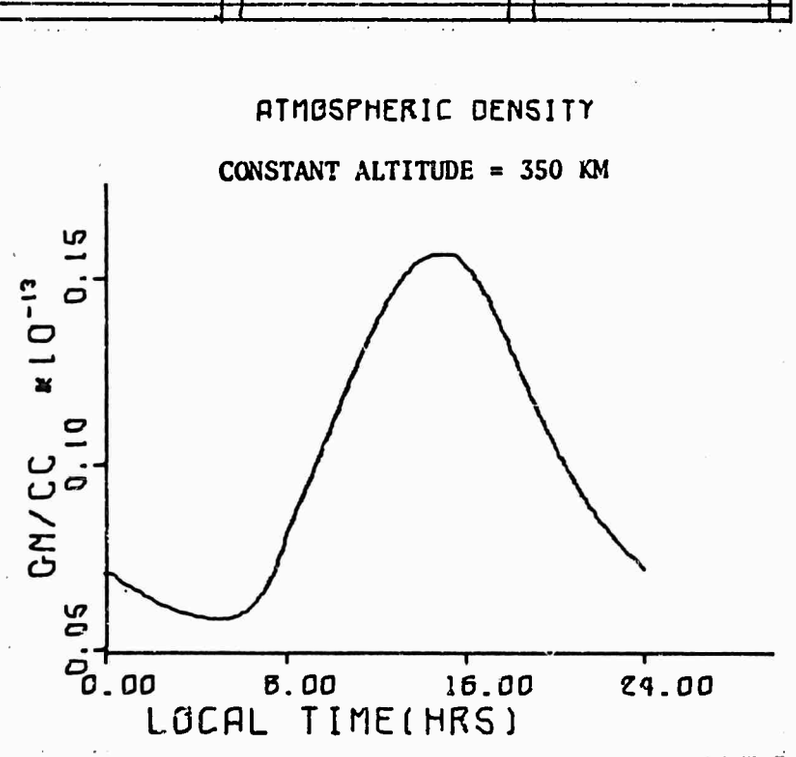

Figure 1. Density Modelling

The Satellite

The assumptions that the satellite is non-maneuvering and has a ballistic coefficient of .015 have previously been stated. A slight justification for the latter assumption is now presented.

King-Hele states (Ref 12:12-18) that for a satellite in an orbit with eccentricity between 0.0 and 0.2 the value of C_d ranges from between 2.1 to 2.2 for a sphere to 2.1 to 2.25 for a cylinder inclined to the airflow. For a cylinder tumbling end over end C_d is determined to be about 2.15. For cones with a semi-apex angle of 15 to 20 degrees, C_d is near 2.10. Therefore it appears that C_d may be assumed to be approximately 2.2 with only small error.

The average mean cross sectional area of a cylindrical satellite may be expressed by:

$$S = \ell d(.813 + .25\ d/\ell) \tag{7}$$

where

S = the mean cross sectional area

ℓ = the length of a cylindrical shape

d = the diameter of the cylinder

Since the drag force on a vehicle is given by

$$F_d = -\ 1/2\ C_d S \rho V^2 \tag{8}$$

Where ρ = the atmospheric density

V = the vehicle's velocity

and the other terms are as defined above.

The ballistic coefficient, B, is defined to be

$$B = C_d S/M \tag{9}$$

where M is the mass of the vehicle. Then the acceleration associated with the drag is given by:

$$a_d = - B\rho V^2/2 \tag{10}$$

In a typical case, using the above equations and the dimensions of the Discoverer series of satellites (Ref 11:182) the ballistic coefficient is determined to be

$$B = .02 \ m^2/kgm \tag{11}$$

which is sufficiently close to the assumed value of .015 m^2/kgm.

Since the models of the gravitational field and the atmosphere are for the earth thisstudy is necessarily restricted to satellites which are in near-earth orbits.

The Radar

The radars used in this study are assumed to have a priori biases and sigmas associated with the measurements of range, range rate, azimuth and elevation which they provide. Sampling periods of 6 and 10 seconds are used in this study since they are typical of operational radars.

The radar is assumed located at a Class A survey point from which we know its position exactly.

Coordinate Systems

In this study computation and measurements are done in three common coordinate systems.

The first of these is the inertial system, designated by i, which has its x-axis directed toward the Vernal Equinox (or the Point of Aries), the z-axis through the north geographic pole, and its origin located at the geocenter. For our purposes, this is a non-rotating, non-accelerating computation frame where Newton's laws of motion are directly applicable. This is the frame in which all orbital elements are calculated.

The second coordinate system to be considered is the rotating

geocentric system, e. This system has its origin colocated with the i frame at the geocenter; its x-axis passes through the Greenwich meridian in the equitorial plane. The z-axis of this system passes through the geographic north pole. The system is called rotating since the x-axis always passes through the Greenwich meridian rotating at approximately 15° per hour. Integration of the state equations is performed in this system.

The last coordinate system which we consider is the tangent coordinate system. The origin of this system is coincident with some point on the surface of the earth. In our study this point will always be the physical location of some radar of interest. This localized coordinate system has its z axis opposite in direction to the gravity vector; the x axis points toward North. The y-axis then points West completing the right-handed orthogonal triad. Measurements taken by the radars are first expressed in this coordinate system.

Figure 2 shows these various coordinate systems and their relative orientations.

Since transformations from each of these frames to the others is necessary, Appendix B gives the direction cosine matrices involved.

Dynamics--State Equations

With the description of the vehicle and its environment complete, we now progress to the dynamics and state equations relevant to the current problem.

The States

The states which are chosen to be representative of the orbital determination problem are the three components of the position vector,

x, y, and z and the three components of the velocity vector $\dot{x}$, $\dot{y}$, and $\dot{z}$.

Written in the inertial frame the state equations are:

$$\begin{bmatrix} \dot{X}_1 \\ \dot{X}_2 \\ \dot{X}_3 \\ \dot{X}_4 \\ \dot{X}_5 \\ \dot{X}_6 \end{bmatrix} = \begin{bmatrix} \dot{x} \\ \dot{y} \\ \dot{z} \\ \ddot{x} \\ \ddot{y} \\ \ddot{z} \end{bmatrix} = \begin{bmatrix} X_4 \\ X_5 \\ X_6 \\ a_{gx} + a_{dx} \\ a_{gy} + a_{dy} \\ a_{gz} + a_{dz} \end{bmatrix} \tag{12}$$

where a_{gx}, a_{gy}, a_{gz} are the components of the total derivative of eqn (3) and a_{dx}, a_{dy}, a_{dz} are the components of eqn (10). Expressed in the rotating geocentric frame these state equations become:

$$\begin{bmatrix} \dot{X}_1 \\ \dot{X}_2 \\ \dot{X}_3 \\ \dot{X}_4 \\ \dot{X}_5 \\ \dot{X}_6 \end{bmatrix} = \begin{bmatrix} X_4 \\ X_5 \\ X_6 \\ a_{gx} + a_{dx} + 2\,w\,x_5 + w^2 x_1 \\ a_{gy} + a_{dy} + w^2 x_2 - 2\,w\,x_4 \\ a_{gz} + a_{dz} \end{bmatrix} \tag{13}$$

where ω = earth rotation rate and where the laws of Coriolis have been applied in transferring from the inertial frame to the geocentric frame.

Initial Conditions

Initial conditions will have to be supplied so that the integration of these equations can be begun regardless of what method of filtering is used. Since the vehicle may not enter into its predicted nominal trajectory, the first measurement set must be used to generate the initial conditions. However, the conditions for application of the Kalman filter require that the initial state be uncorrelated with the measurement noise.

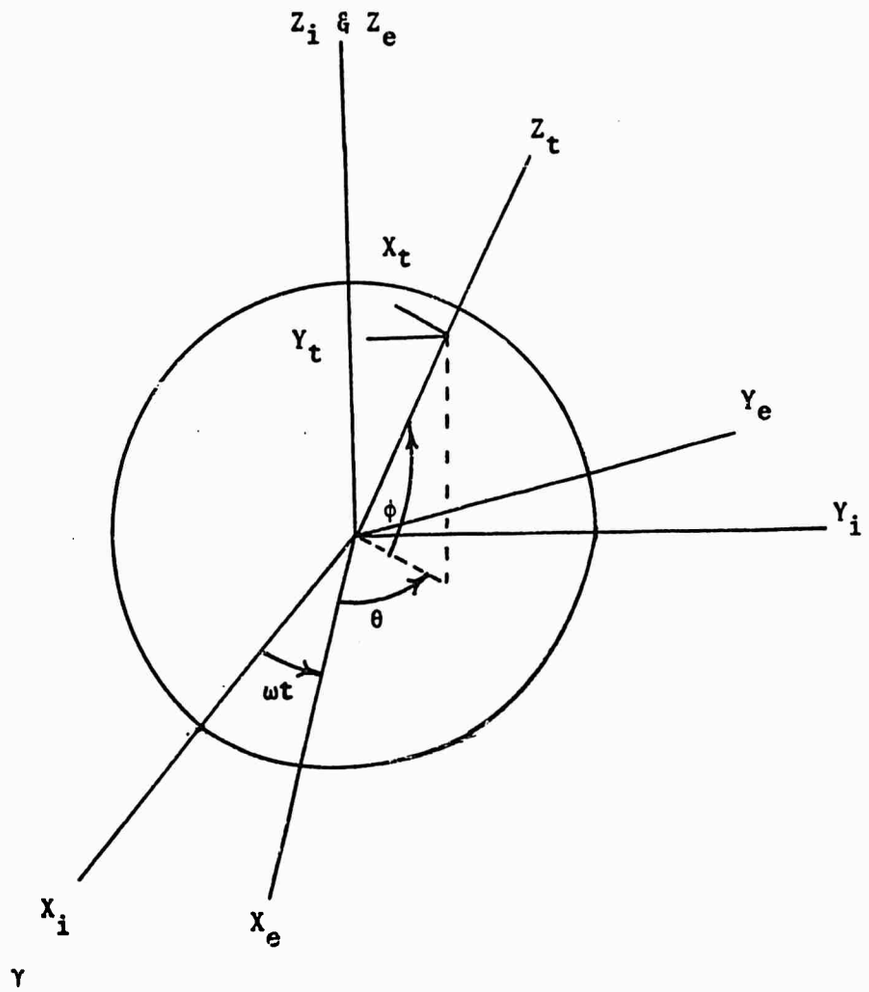

Figure 2. Earth Centered Inertial and Rotating and Station Centered Topocentric Coordinate Systems

To accomplish this the azimuth and elevation angles are rounded to the nearest .25 degree. The range is rounded to the nearest 1000 meters while the range rate is rounded to the nearest 10 meters per second. Although this method may produce a larger error than necessary, initially, the conditions for filter application are met. For application to the Weighted Least Squares filter, the nominal value used is the value determined directly from the first set of measurement data.

To complete the required set of six initial conditions, the azimuth and elevation rates are formed by use of equation (6) with the incremental time equal to the sampling rate of the radar in use and $f(x + \Delta x)$ occurring at the second measurement. Thus six initial conditions, azimuth, azimuth rate, elevation, elevation rate, range and range rate are supplied for initializing the integration of the state equations.

The Measurements

The measurements are related to the state variables through the following equations:

$$\rho = ((x_1 - x_s)^2 + (x_2 - y_s)^2 + (x_3 - z_s)^2)^{1/2} \tag{14}$$

$$\dot{\rho} = \frac{1}{\rho}((x_1 - x_s)x_4 + (x_2 - y_s)y_4 + (x_3 - z_s)x_6) \tag{15}$$

$$a = \tan^{-1}(-y_t/x_t) \tag{16}$$

$$e = \tan^{-1}(x_t/(x_t^2 + y_t^2)^{1/2}) \tag{17}$$

where $x_1, x_2, x_3, x_4, x_5, x_6$ = the vehicle position and velocity expressed in the rotating geocentric frame, the state vector

x_s, y_s, z_s = the coordinates of the tracking sensor in the rotating geocentric frame

x_t, y_t, z_t = the coordinates of the vehicle expressed in the tangent frame by use of the direction cosine matrix found in Appendix B.

III. Kalman Filtering

A Kalman Filter is an algorithm for the determination of the states or parameters of a system using measurements which may not reflect all of the states or parameters directly and are contaminated by white, Gaussian noise. This rather concise statement sums up the intent and purpose of this chapter. Equations will be presented by which the Kalman filtering algorithm can be applied to the orbital determination problem. No rigorous proof of the equations will be presented since they have already been derived and rederived numerous times (Refs: 10:Ch 8 and 14: Ch 4, 5, and 6).

All discussions of Kalman filtering must begin with a discussion of the general state equations descriptive of the system:

$$\dot{\underline{x}} = f\ (\underline{x},t,\underline{u},\underline{w}) \tag{18}$$

$$\underline{z} = h\ (\underline{x},t,\underline{v}) \tag{19}$$

where $\underline{x}$ is the state vector

$\underline{u}$ is a deterministic control vector

$\underline{w}$ is a random noise vector and

$\underline{v}$ is a measurement noise vector.

These are non-linear equations which in general are extremely cumbersome and difficult to handle. As a result a linearization about some nominal path or trajectory is often made leading to equations of the form:

$$\dot{\underline{x}} = F\ \underline{x}(t) \tag{20}$$

$$\underline{z}(k) = M\ \underline{x}(k) + \underline{v}(k) \tag{21}$$

where

$$F = \left.\frac{\partial f(\underline{x})}{\partial \underline{x}}\right|_{\underline{x} = \underline{x}(k+1|k)} \tag{22}$$

and

$$M(\underline{x}) = \left.\frac{\partial h(\underline{x})}{\partial \underline{x}}\right|_{\underline{x} = \underline{x}(k+1|k)} \tag{23}$$

The exact form of F and M pertinent to the orbital determination problem are derived in Appendixes C and D. The matrix F is often referred to as the state sensitivity matrix and the matrix M is called the measurement matrix. Since a linearization was made to obtain equations (20) and (21) we must maintain small perturbations throughout the analysis. To do this, the present state is always determined by the forward integration of equation (13). Thus as the recursive filter begins to take effect all of the linearization assumptions used become more valid.

Prediction

Prediction very simply consists of integrating the state equation forward from the present state to the next state to be considered through use of the state equations.

$$\underline{x}(k+1|k) = \underline{x}(k|k) + \int_{t_o}^{t+\Delta t} f(\underline{x}(k|k))\, dt \tag{24}$$

where k =-1,0,1,2.....

The state error covariance which is defined by

$$P(k+1|k) = E\left((\underline{x}(k+1|k)-\overline{\underline{x}}(k+1|k))\ (\underline{x}(k+1|k)-\overline{\underline{x}}(k+1|k))^T \right) \tag{25}$$

can be projected forward through use of

$$P(k+1|k) = \phi(k+1|k)\ P(k|k)\ \phi^T(k+1|k) \tag{26}$$

Where $\phi(k+1,k)$ is the State Transition Matrix:

$$\phi(k+1,k) = \frac{\partial x(k+1)}{\partial x(k)} \tag{27}$$

$\phi(k+1,k)$ is determined by integrating the linear differential matrix equation

$$\dot{\phi}\ (k+1,k) = F(\underline{x}(k|k))\ \phi(k+1,k) \tag{28}$$

with the initial conditions

$$\phi(k,k) = I \tag{29}$$

Filtering. Filtering is the process of updating the best estimate of the present state through use of an optimal gain matrix, K, and the measurement residuals, Δz. The measurements are predicted by applying the value of the present best estimate of the states to the measurement equation:

$$\hat{\underline{z}} = h(\hat{\underline{x}}(k + 1|k)) \tag{30}$$

remembering that there is zero-mean noise in the measurements. The measurement residuals are then formed by subtracting the best estimate of the measurements from the true measurements.

$$\underline{\Delta z} = \underline{z}(k + 1) - \hat{\underline{z}}(k + 1|k) \tag{31}$$

These residuals are then linearly added to the present best estimate of the state after multiplication by the optimal gain:

$$\underline{x}(k + 1|k + 1) = \underline{x}(k + 1|k) + K(K = 1)\ \underline{\Delta z} \tag{32}$$

where the optimal gain, K, has been determined from

$$K(k + 1) + P(k + 1|k)M^T(MP(k + 1|k)M^T + R)^{-1} \tag{33}$$

We observe that if the noise covariance, R, is large the resulting effect is to diminish K. However, if R is small, then K will be large. This relation could be anticipated for optimal application of the information contained in the residuals. The error covariance of the corrected state estimate $\underline{x}(k + 1|k + 1)$ is determined by the symmetric equation:

$$P(k + 1|k + 1) = (I - K(k + 1)M)P(k + 1|k)(I - K(k \pm 1)M)^T + K(k \pm 1)\ R\ K(k + 1)^T \tag{34}$$

where M is evaluated at time t_{k+1}.

The filter applied in this manner is called the Extended Kalman Filter since the equations are linearized about the current state estimate, $x(k + 1|k)$. The prediction process does not involve any linearity assumptions since the non-linear state equations and the non-linear measurement

matrix, M are used.

Smoothing

Smoothing is the process of conveying information found in later measurements back to the values of states which have been previously determined. There are three basic types of smoothing, (1) fixed interval smoothing, (2) fixed point or single point smoothing, and (3) fixed lag smoothing. These are detailed in Ref 14, chapter 6.

Two types of smoothing were applied to the orbital determination problem in this study, fixed interval and fixed point smoothing.

To perform smoothing requires the storage of many quantities, including the state transition matrix, the error covariance matrix and the states. This is the chief disadvantage from a computational viewpoint.

The fixed interval smoother does its work after the problem has been finished or at least after the number of measurements over which smoothing is desired have been taken. The smoother is basically a "reverse" smoother in the sense that it takes the last measurement and projects it backwards to the previous measurement. This process is repeated until the origin of the problem is reached where theoretically all information learned during the process has been projected back upon the original starting states.

The optimal fixed interval smoothed estimate $x(k|N)$ is governed by the system of equations:

$$\underline{x}(k|N) = \underline{x}(k|k) + A(k)(\underline{x}(K+1|N) - \underline{x}(k+1|k)) \tag{35}$$

where $k = N-1, N-2, \ldots .0$ where $x(N|N)$ is the boundary condition for $k=N-1$. The optimal smoothing gain matrix is given by

$$A(k) = P(k|k)\phi^{T}(k+1,k)P^{-1}(k+1|k) \tag{36}$$

The optimal fixed interval smoothing error covariance matrix is given by

$$P(k|N) = P(k|k) + A(k)(P(k+1|N) - P(k+1|k)A^T(k) \quad (37)$$

where k = N-1, N-2,....0 subject to the boundary condition P(N/N) for k=N-1.

The fixed point smoother is a forward smoother which after it has been given the states and time at which smoothing is desired continually updates the values of the states and covariance errors at that point as new information becomes available.

The system of equations governing the fixed point smoother are:

$$\underline{x}(k|j) = \underline{x}(k|j-1) + B(j)(\underline{x}(j|j)-\underline{x}(j|j-1))$$

for a fixed k and j = k+1, k+2,.... where the initial condition is $\underline{x}(k|k)$.

The gain matrix B is given by

$$B(j) = \prod_{i=k}^{j-1} A(i) \quad (38)$$

and

$$A(i) = P(i|i)\phi^t(i+1;i)P^{-1}(i+1|i) \quad (39)$$

The fixed point smoothing error covariance matrix is given by

$$P(k|j) = P(k|j-1) + B(j)(P(j|j)-P(j|j-1))B^t(j) \quad (40)$$

An alternate formulation of this equation is possible but was not used in this study (Ref 14:231).

Reverse Integration

Once the final filtered estimate has been obtained using the equations (30) to (33), the final state can be reverse integrated using the non-linear state equations (13) so as to obtain the state at any previous time as reflected by the state at the final measurement. A point of special interest is the initial point since reverse integration to this point allows comparison with the results of the Weighted Least Squares filter

presented in chapter IV.

Class I Filter Modification

Class I Filter Modification was employed throughout this study. This subject was first covered in Reference 19. This attempt to account to some extent for computer truncation and round-off error as well as system non-linearities not adequately represented by the system model takes the form:

$$P(k+1|k) = \phi(k+1,k)P(k|k)\phi^T(k+1,k) + q \begin{bmatrix} x_1^2 & & & & & \\ & x_2^2 & & & 0 & \\ & & x_3^2 & & & \\ & & & x_4^2 & & \\ & 0 & & & x_5^2 & \\ & & & & & x_6^2 \end{bmatrix} \quad (41)$$

The value of q is a function of the amount of non-linearity and round-off anticipated. For most of the study a value for

$$q = 1 \times 10^{-12} \quad (42)$$

was used although for purposes of analyses it was varied at certain points. This will be further discussed in Chapter V when the simulated orbit analysis is performed.

IV. Weighted Least Square Error Filtering

Statistical filtering or least square error filtering assumes a cost function (Ref 18:16) indicative of the desired outcome of the problem. The nominal trajectory is to be chosen such that when it is compared to the values of the measured trajectory the difference of the squared error is minimized. If the errors in certain parameters are weighted more than the errors in other parameters than the method is called Weighted Least Squares Filtering. The statistical filter then provides both a smoothed solution and a filter solution simultaneously when the problem is solved since the method is necessarily interested in the errors found along the entire trajectory.

Unlike the probabilistic or Kalman filter, the Least Squares Filter is a batch filter which requires the simultaneous application of all data to be processed. The addition of one new data point under the batch process will require the rerunning of the entire "batch" of data. This is the chief disadvantage of the statistical filter; however, methods are available to transform this batch processor into a recursive processor through changes in the cost function.

A cost function which expresses the least square error concept stated above is given by:

$$J = ||\underline{y} - y(\underline{x}_o)||_W^2 = (\underline{y}-y(\underline{x}_o))^T W(\underline{y}-y(\underline{x}_o)) \tag{43}$$

This quadratic cost function must be convex and therefore has a minimum.

Using minimization techniques common to optimal control and the calculus of variations it can be shown that

$$\Delta\underline{x}_o = (A^T W A)^{-1} A^T W \, \Delta\underline{y} \tag{44}$$

will cause this cost function to be minimized, where

$$\Delta \underline{y} = \underline{y} - \underline{y}(\underline{x}_o)$$

A = the measurement sensitivity matrix

$\Delta \underline{x}_o$ = the required change in the nominal trajectory

and

W = the weighting matrix

The Measurement sensitivity matrix, A, can be determined by use of the measurement matrix M previously discussed in Chapter IV and Appendix D.

$$A = \begin{bmatrix} M_o \phi(t_o, t_o) \\ M_1 \phi(t_1, t_o) \\ M_2 \phi(t_2, t_o) \\ \vdots \\ M_n \phi(t_n, t_o) \end{bmatrix} \tag{45}$$

where ϕ is the state transition matrix found from the solution of the linear matrix differential equation

$$\dot{\phi}(t, t_o) = F\, \phi(t, t_o) \tag{46}$$

Unfortunately due to round-off and truncation error as well as modeling non-linearities the value found for $\Delta \underline{x}_o$ will not cause the cost function, J, to reach its minimum without repeated iteration of this process. Therefore, some criteria must be set for determining convergence to the "true" state x_o.

The criteria chosen involve the residuals. They are forced to be less than some arbitrarily small value. Care must be exercised to make this value realizable since if it is made too small, then many iterations will be required to obtain convergence. If, on the other hand, it is not small enough then the state $\underline{x}_o$ will not be accurately determined.

For this study a value for the epsilon of convergence equal to 2×10^{-4} was found to be suitable.

If we define

$$||\Delta y^P||_W = ||\Delta y_o - A\Delta X||_W \tag{47}$$

then if either

$$C_1 = \frac{||\Delta y||_W - ||\Delta y^P||_W}{||\Delta y||_W} \leq \varepsilon \tag{48}$$

or

$$C_2 = ||\Delta y||_W - ||\Delta y^P|| \leq \varepsilon \tag{49}$$

were true then the data was said to have converged.

V. Simulation Study

To verify filter operations and to provide a basis for analysis of actual radar data, a simulated orbit analysis was first performed using both the WLS and Kalman Filtering methods on an orbit having known orbital parameters.

The Simulated Orbit

The following parameters were chosen for the simulated orbit:

t_o: Day 298 Hour 02 Minute 39 Second 19.466

θ_{g_o}: Day 298 Hour 02 Minute 12 Second 18.503 (Ref Appendix F)

Semi-Major Axis	:	1.161913 earth radii = a_o
Eccentricity	:	.06539071 = e_o
Angle of Inclination	:	54.2538° = i_o
Line of Nodes	:	199.6287° = Ω_o
Argument of Perigee	:	29.9570° = ω_o
Period	:	105.8204 minutes = P_o
Height at Perigee	:	548.174 Kilometers

The period and height at perigee are functions of the other orbital elements and are presented only since they are often parameters of interest.

Care must be exercised to associate the time, t_o, with these orbital parameters since the perturbation effects caused by the oblate earth, non-uniform gravitational field, and the time-varying density models will cause these parameters to vary as the satellite orbits the earth.

Simulated Orbit Data Generation. With the above orbital parameters as the initialization point, a two pass orbit was generated making use of a single simulated radar whose parameters are given in Table I.

Table I

Theoretical Radar Parameters

Position

Latitude = 52.73267°N

Longitude = 174.1023°E

Height = 93. Meters

Measurement Biases

Range = 0.0

Range Rate = 0.0

Azimuth = 0.0

Elevation = 0.0

Measurement Sigmas

Range = 1000 meters

Range Rate = 1 meter/second

Azimuth = .02 degrees

Elevation = .02 degrees

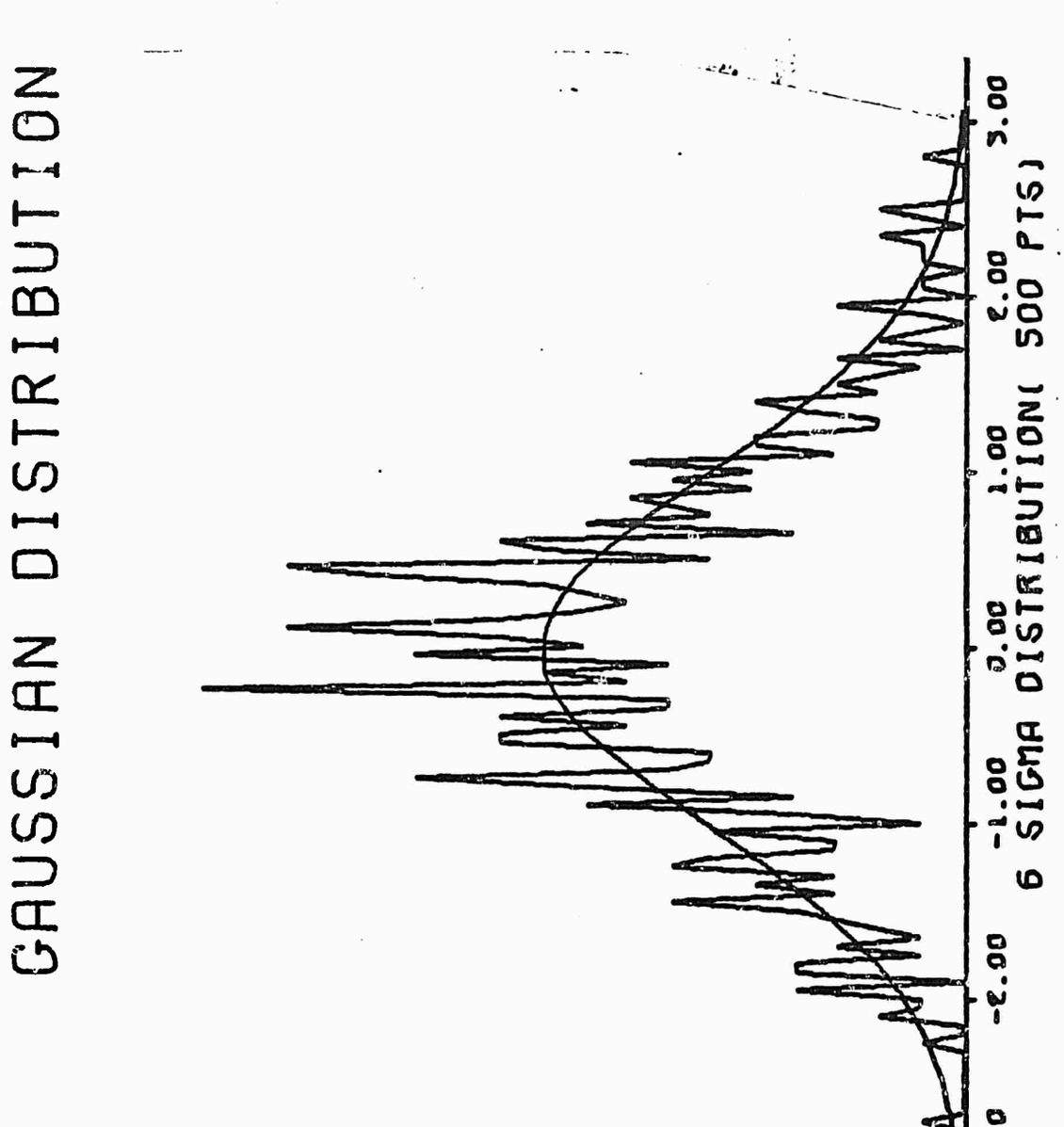

Figure 3. Gaussian Density Distribution 500 Points

Table II

Gaussian Distribution Data Analysis

Sample Size	1st Moment (mean)	2nd Moment	3rd Moment	4th Moment	Variance	Std Dev
N(0,1)	0.00	1.00	0.00	3.00	1.00	1.00
100	0.02	1.07	-0.18	3.13	1.08	1.04
200	-0.02	0.97	-0.06	2.32	0.98	0.99
300	-0.02	0.99	-0.07	2.77	0.99	1.00
400	0.01	0.94	0.10	2.54	0.95	0.97
500	-0.05	0.90	0.01	2.53	0.90	0.95
600	-0.06	0.94	0.11	2.65	0.94	0.97
700	0.03	1.03	-0.08	3.11	1.03	1.01
800	0.05	0.93	0.15	2.41	0.93	0.96
900	0.05	0.98	-0.03	2.76	0.98	0.99
1000	-0.00	0.98	-0.06	2.63	0.98	0.99

The height of the radar is measured with respect to the reference ellipsoid.

In order to obtain a noisy observation, true measurements of azimuth, elevation, range, and range rate were contaminated with computer generated noise. By the repeated addition of points selected from uniform distributions an approximately normal distribution can be obtained from

$$N(0,1) \cong \sum_{i=1}^{12} x_i - 6 \qquad (50)$$

where the x_i are randomly selected from a uniform distribution between 0 and 1. This distribution is known to be a truncated distribution having at best a variance of six sigma. However, for the orbital problem at hand variations outside this range are unlikely and the distribution is therefore accepted as adequate.

A study of the generated noise distributions was made using the shape of the generated distribution curve as a rough measure of the density of the distribution. Figure 3 shows a plot of a distribution composed of 500 sample points. Other plots of various numbers of points are presented in Appendix E. Other basic statistical descriptors of the samples are shown in Table II. The non-zero mean shown in Table II presents a small problem to the filters since the versions of both which are programmed for this study expect zero mean noises as would be anticipated in the actual orbital determination problem. Small biasing effects should therefore be anticipated in the results. The samples indicated were also subjected to Kolomogorov-Smirnov Test with a significance level of .20, and all of the samples were accepted as possibly being from a N(0,1) distribution.

On the basis of the distributions studied, it was determined that a single run consisting of two sets of fifty-five measurements each of azimuth, elevation, range, and range rate could not present a truly Gaussian

noise to the filters. Therefore, a series of 25 runs against the same theoretical parameters but contaminated with different sequences of noise were studied with the statistical average of the parameters determined being accepted as the final determination of the filters in the theoretical study.

Orbital Perturbations. Figures 2 through 6 show the true orbital parameters as determined using the previously described models of the oblate earth, non-uniform gravitational field, and time-varying atmosphere. The large tick on the abscissa indicates the passage of one revolution. Table III summarizes the effects noted on these graphs. Generally, these perturbations can be divided into two types, secular and those due to the oblate earth effects (Ref 21:208-241). Appendix G notes how the state vector may be transformed into the classical orbital elements graphed.

Secular Perturbations. Only two of the orbital elements considered are subject to secular perturbations, the line of nodes and the argument of perigee. From Reference 21 first order approximations to these perturbations can be obtained by using

$$\Delta\Omega = \frac{-3\pi J_2 a_e^2 \cos i_o}{a_o^2(1-e_o^2)^2} \text{ deg/rev} \tag{51}$$

and

$$\Delta\omega = \frac{6\pi J_2 a_e^2 (1-5/4\sin^2 i_o}{a_o^2(1-e_o^2)^2} \text{ deg/rev} \tag{52}$$

When the values of the true orbital parameters at t_o are substituted in these equations, the following values for the secular changes are determined:

$$\Delta\Omega = -.255160 \text{ deg/rev} \tag{53}$$

$$\Delta\omega = .154332 \text{ deg/rev} \tag{54}$$

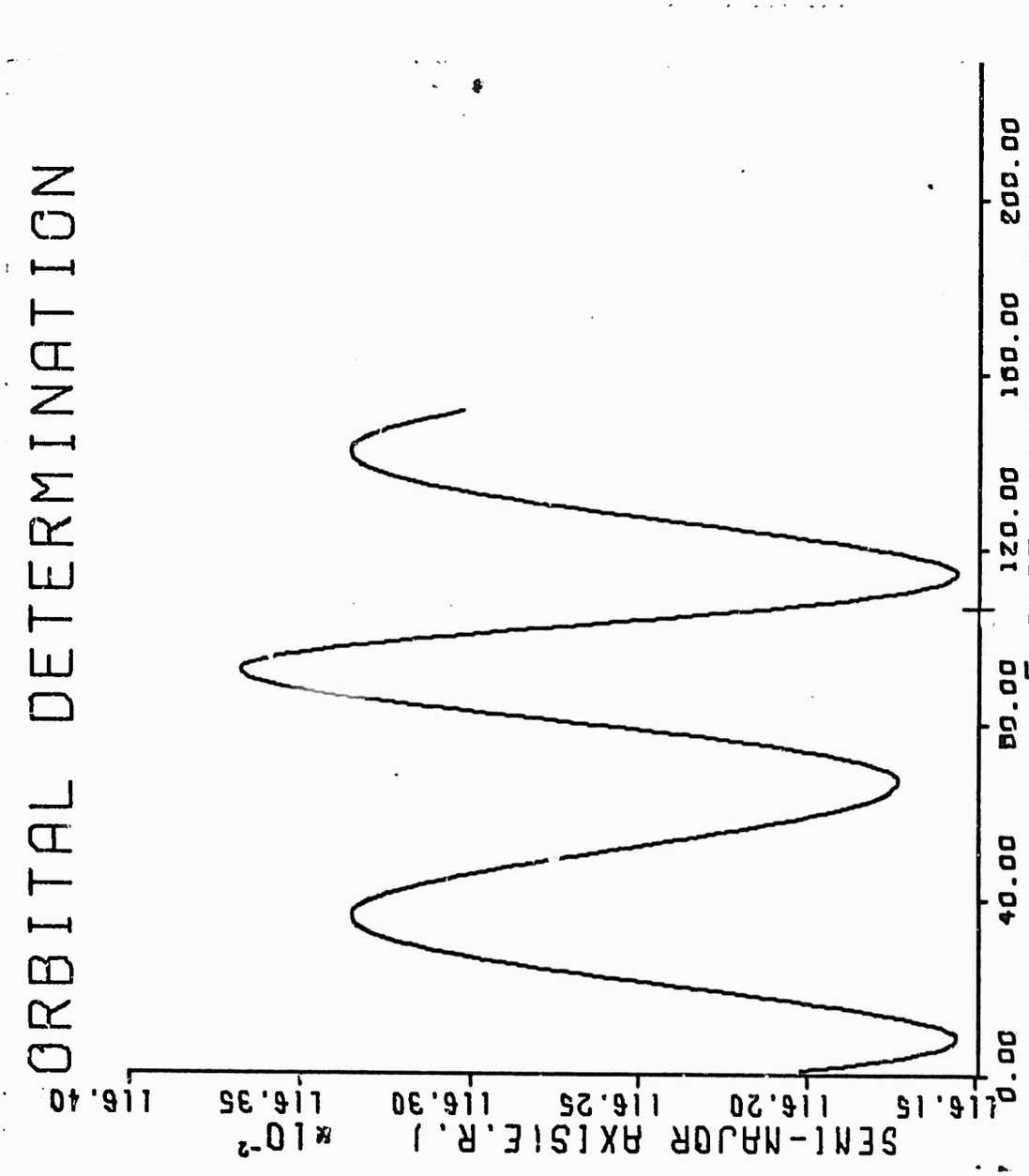

Figure 4. True Simulated Semi-Major Axis

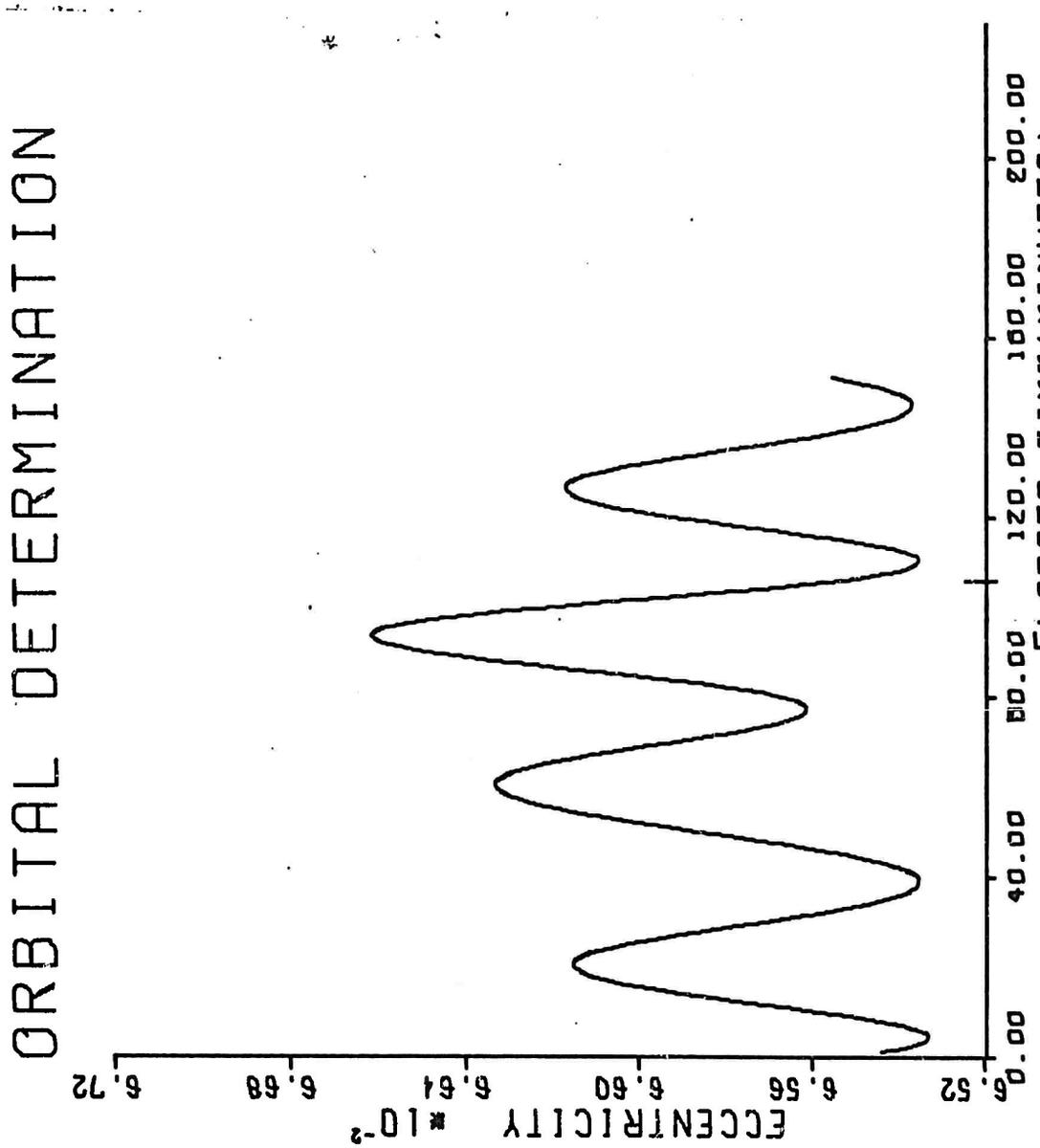

Figure 5. True Simulated Eccentricity

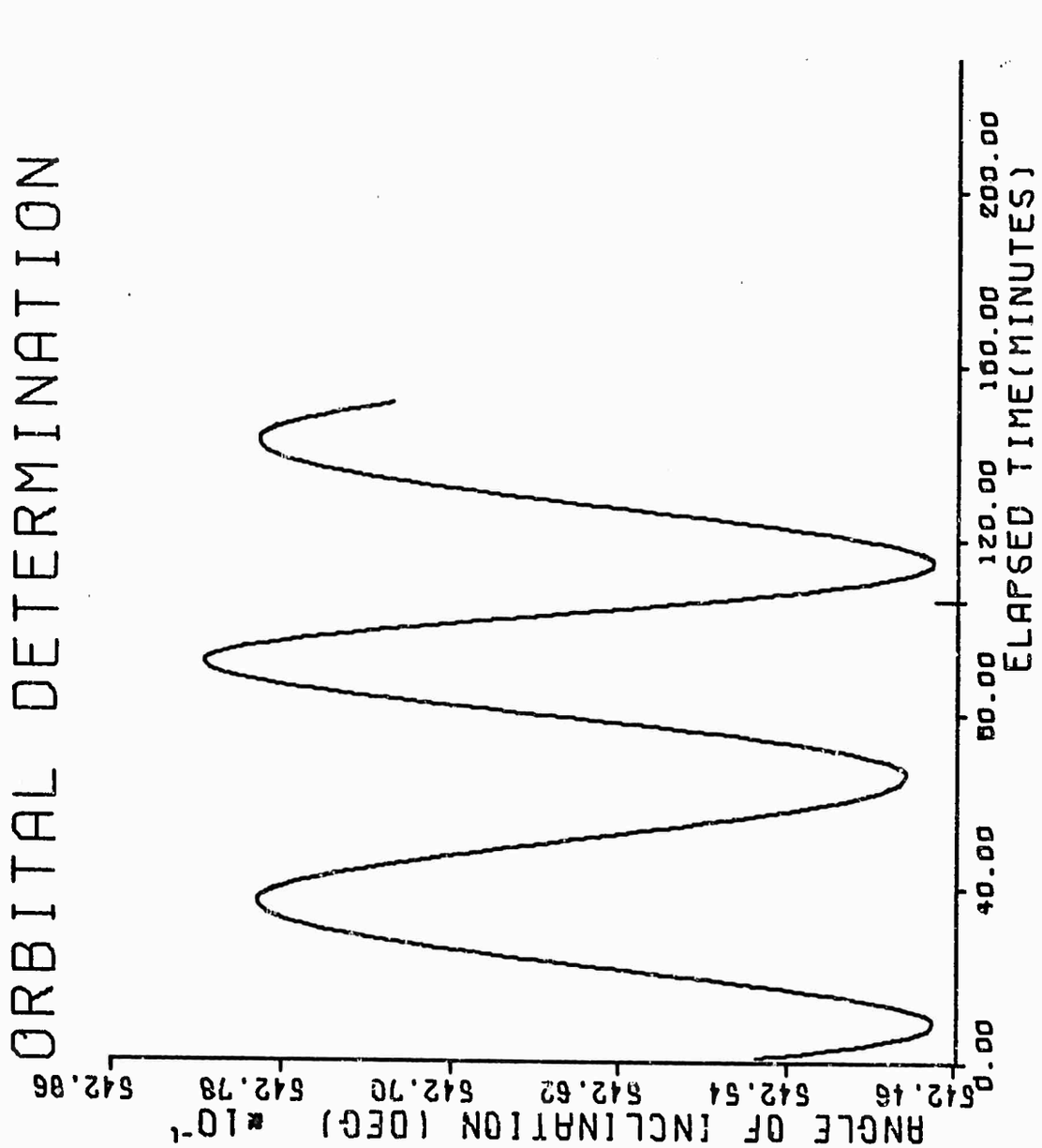

Figure 6. True Simulated Angle of Inclination

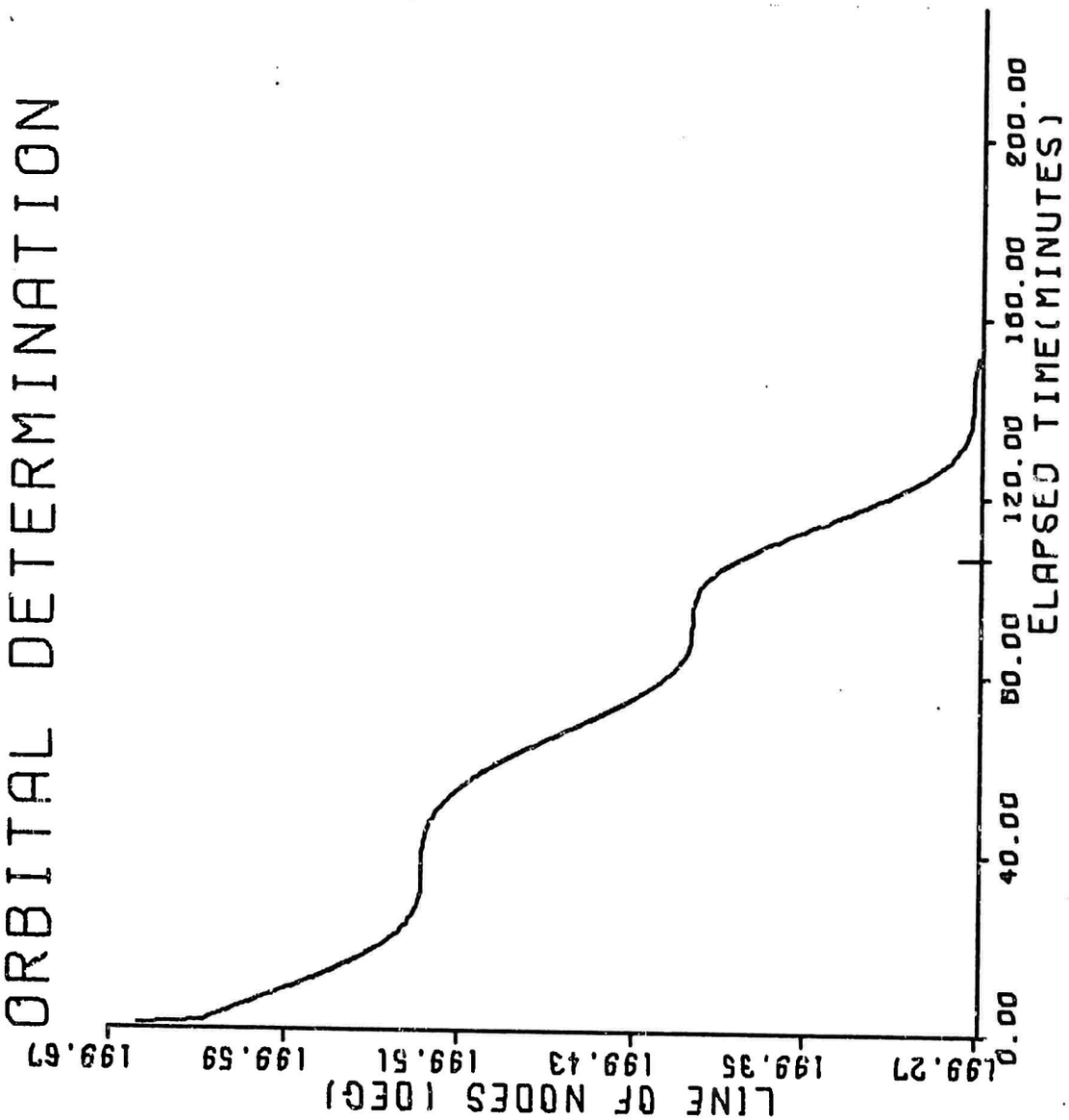

Figure 7. True Simulated Line of Nodes

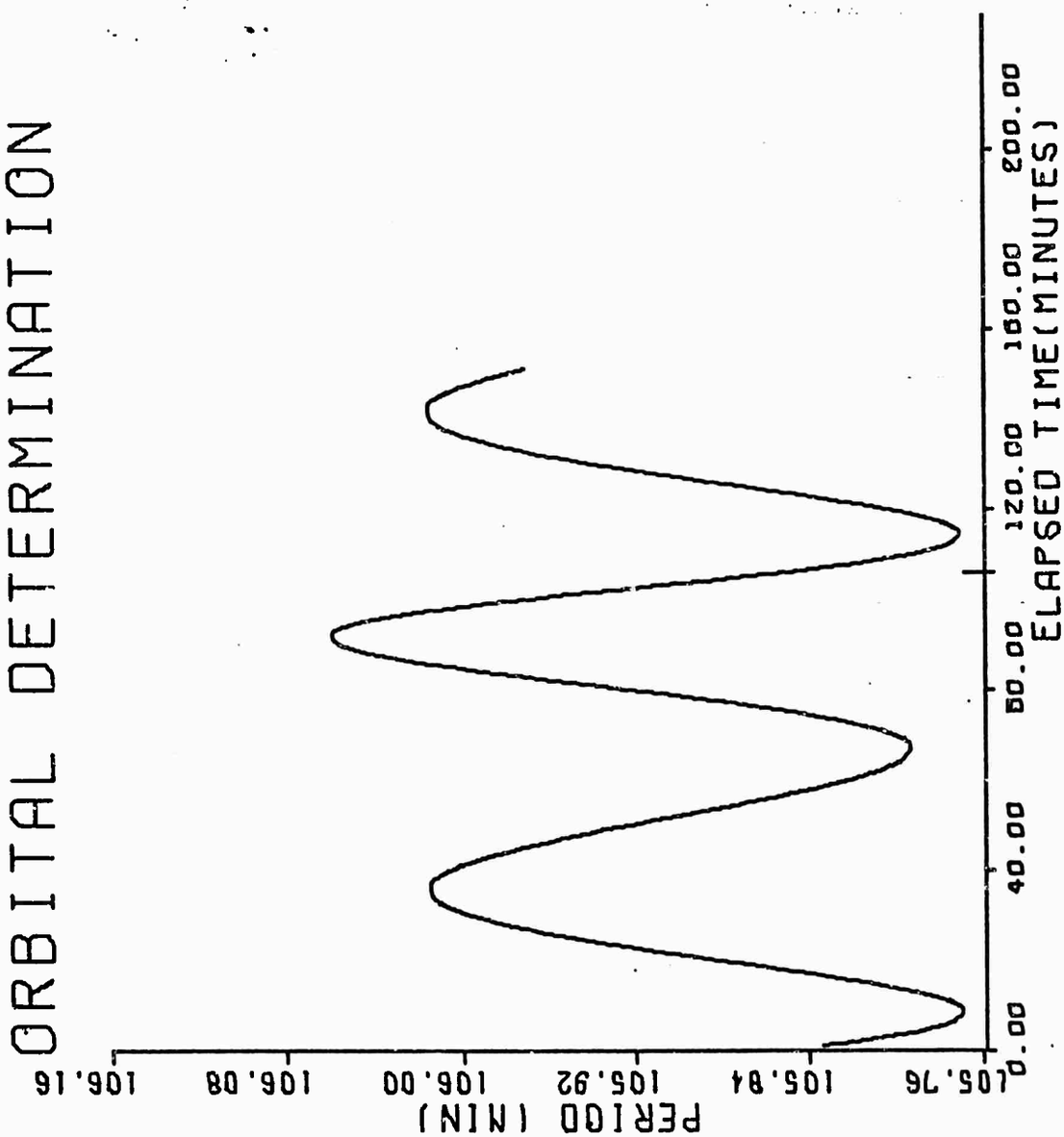

Figure 8. True Simulated Period

Table III

Orbital Perturbation Analysis

Parameter	Max	Min	Cycles	Secular Change (Deg/Rev)
Semi-Major Axis (E.R.)	1.1637	1.1616	2	none
Eccentricity	.0667	.0654	3	none
Period (Min)	105.78	106.07	2	none
Angle of Inclination (Deg)	54.282	54.247	2	none
Line of Nodes (Deg)	199.65	199.40	2	-.25°
Arg. of Perigee (Deg)	30.435	29.443	3	+.15°

The graphs and analytic results from the integration of the state equations yield the following compatible results:

$$\Delta\Omega = 199.347° - 199.602° = - .255 \text{ deg/rev} \tag{55}$$

$$\Delta\omega = + 29.700° - 29.551° = .149 \text{ deg/rev} \tag{56}$$

Oblate Earth Perturbations. Since this study is confined to low eccentricity orbits ranging from approximately circular (0) to a value of about .124, certain approximations to the general equations given in Reference 21, page 220, can be made. Basically all terms which contain the eccentricity at t_o and powers of it are deleted as being small with respect to 1. Thus these equations can be reduced to:

$$a \cong K_a + \frac{3J_2 a_e^2}{2a_o(1-e_o^2)^3} \sin^2 i_o \cos 2u_o \tag{57}$$

$$e \cong K_e + \frac{3J_2 a_e^2}{2a_o^2(1-e_o^2)^2}\left((1-3/2\sin^2 i_o)\cos f^0 + \frac{1}{4}\sin^2 i_o \cos(2\omega_o + f^0) + 7/12 \sin^2 i_o \cos(2\omega_o + 3f^0)\right) \tag{58}$$

$$i \cong K_i + \frac{3J_2 a_e^2 \sin 2i_o}{8a_o^2(1-e_o^2)^2}\left(\cos 2u_o\right) \tag{59}$$

$$\Omega \cong K_\Omega - \frac{3J_2 a_e^2 \cos i_o}{4a_o^2(1-e_o^2)^2}\left(2f^0 - \sin 2u_o\right) \tag{60}$$

$$\omega \cong K_\omega + \frac{3J_2 a_e^2}{4a_o^2(1-e_o^2)^2}\left((4-5\sin^2 i_o)f^0 + \frac{1}{e_o}(2-3\sin^2 i_o)\sin f^0 - \frac{1}{2e_o}\sin^2 i_o \sin(2\omega_o + f^0) + \frac{7}{6e_o}\sin^2 i_o \sin(2\omega_o + 3f^0)\right) \tag{61}$$

where secular perturbation terms have been included in Ω and ω and where $u_o = \omega_o + f^o$ and

$$\frac{df^0}{dt} = \sqrt{\frac{\mu}{a_o^3(1-e^2)^3}}(1 + e_o \cos f^0)^2 \text{ and } f^0 \tag{62}$$

is the true anomaly at t_o.

Since the true anamaly, f, must progress through 360 physical degrees per revolution or one cycle, the number of cycles in the predominant frequency component of the perturbations can be predicted from the preceeding equations. Thus it can be anticipated that the semi-major axis, period, angle of inclination, height at perigee, and the line of nodes will experience two cycles per revolution while the eccentricity and the argument of perigee will experience three cycles. These conclusions are borne out by the figures in this chapter. It should also be anticipated that the argument of perigee will becomo extremely difficult to determine as the eccentricity of the orbit approaches zero. If the eccentricity and argument of perigee become extremely difficult to calculate, a change in orbital parameters can be made as detailed in Reference 21, page 194. However, in this study no change in parameters will be made since the Ent analyses are based on parameters of the type determined in Appendix G.

Filter Operation. Both the Kalman Filter and WLS filter presented highly accurate estimates of the orbital parameters. Comparison of the estimated parameters occurs in Tables IV and V. The errors in the outputs of the Kalman filter as a function of the number of measurements are presented in Figures 7 through 20. It must be noted that the points plotted in these figures are at observations 1,2,3,4,5,10, and every fifth observation thereafter during the first pass and at observations 56,57,58, 59,60,65 and every fifth observation thereafter in the second pass. Thus general trends are being displayed with a change of scale usually occurring on the second graph in each set so that the data may be more accurately presented. Generally, the data converges toward a zero-mean error. However, a bias of .02° is seen in the line of nodes parameter. Previous discussion of the noise distribution involved may account for this bias.

Non-linearity due to initial condition errors in the early phases of the filtering processes also undoubtedly contributed to all of the residual errors. Both the values shown and the errors graphed are the results of the 25 run statistical averages discussed previously. All parameters determined are considered sufficiently accurate to enable future position prediction. The values determined for the orbital elements by the Kalman filter are shown in figures 21 through 25.

Table IV

Kalman Filter Analysis*

Number of Observations	20	30	40	55	75	110
Error In						
Semi-Major Axis (E.R.)	-.000078	.000014	.000008	-.000021	.000073	.000051
Eccentricity	-.0000463	.0000205	.0000156	.0000130	.0000597	.0000287
Angle of Inclination (Deg)	-.0004	-.0003	-.0002	-.0002	-.0005	.0001
Line of Nodes (Deg)	.232	.0246	.0246	.0248	.0347	.0246
Angle at Perigee (Deg)	-.0380	-.0171	-.0169	-.0128	.0048	.0188
Height at Perigee (Km)	-.124	-.072	-.070	-.044	-.007	-.069
Period	-.010	.002	.001	.001	.010	.007

*This data is also presented graphically in figures 7 through 20.

Table V

WLS Filter Analysis

Epoch time = t_o = 0.0 seconds

Number of Observations	20	30	40	55	75*
Error In					
Semi-Major Axis (E.R.)	.000014	.000046	.000018	.000009	.000049
Eccentricity	.0000146	.0000438	.0000260	.0000180	.0000836
Angle of Inclination (Deg)	.0000	.0002	.0002	.0001	.0044
Line of Nodes (Deg)	-.0047	-.0038	-.0040	-.0041	-.0015
Angle at Perigee (Deg)	.0003	-.0038	-.0125	-.0139	-.0570
Height at Perigee (Km)	-.024	-.030	-.084	-.078	.323
Period (Min)	.0019	.0063	.0025	.0012	.0067
Iterations	3	3	3	3	7

*The 75 point run is a single run and not the average of 25 runs as are the others. This was necessitated by the large amount of machine time required by repeated integrating the state equations around the orbit with different starting conditions. (CP Time, Single Run 75 Points = 484 sec). However, convergence on pass two was achieved after 7 iterations.

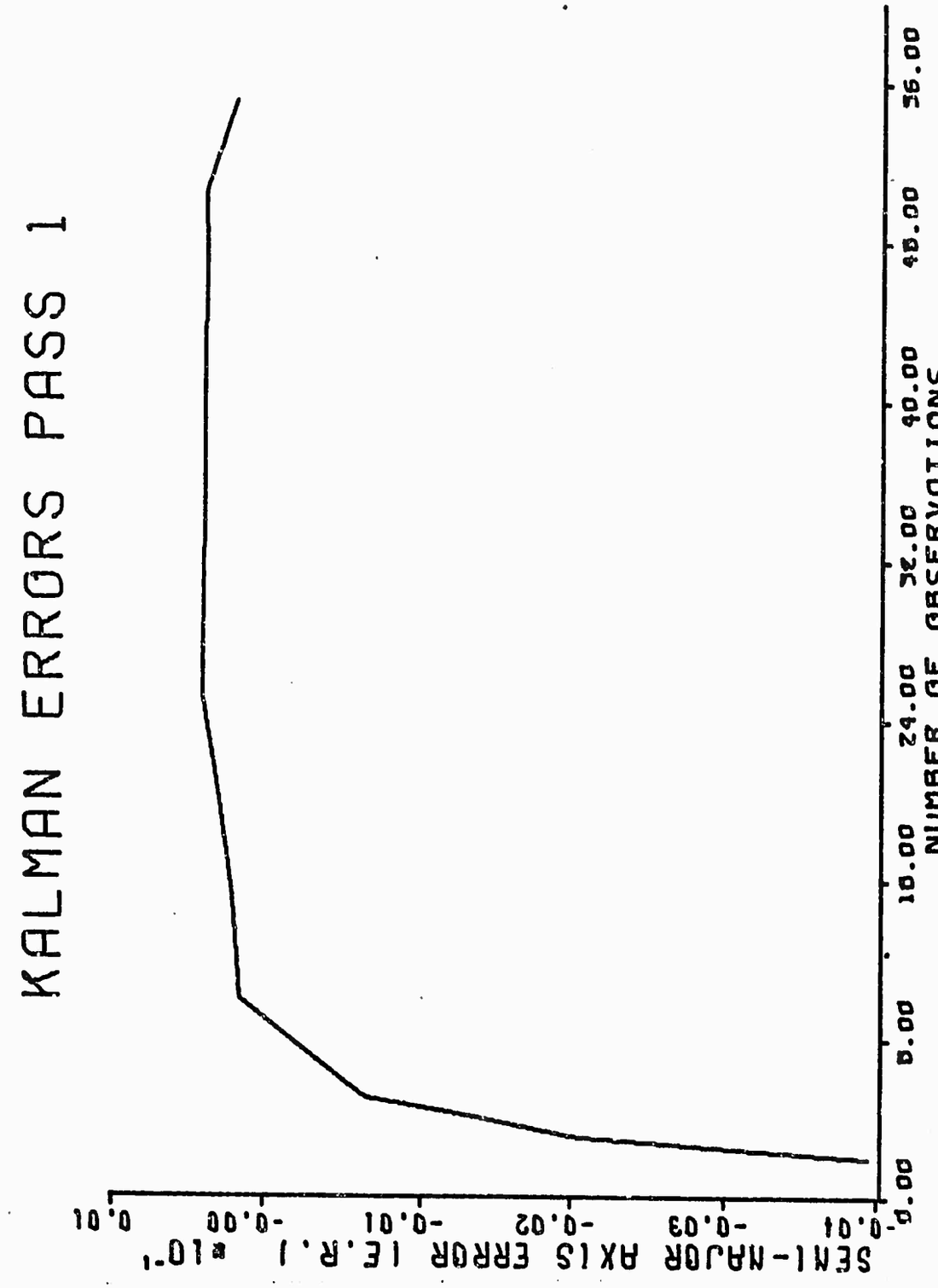

Figure 9. Semi-Major Axis Error Pass 1

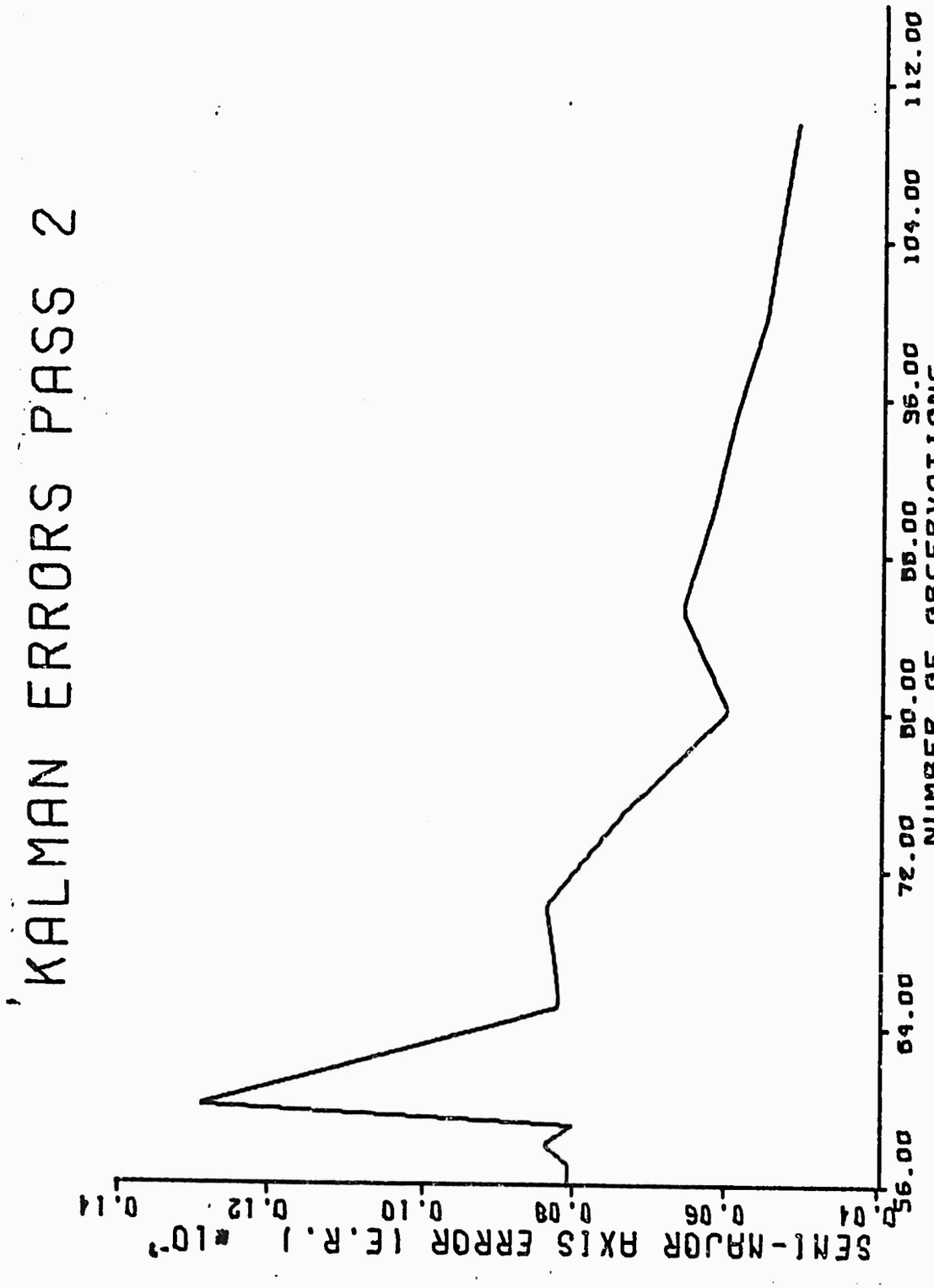

Figure 10. Semi-Major Axis Error Pass 2

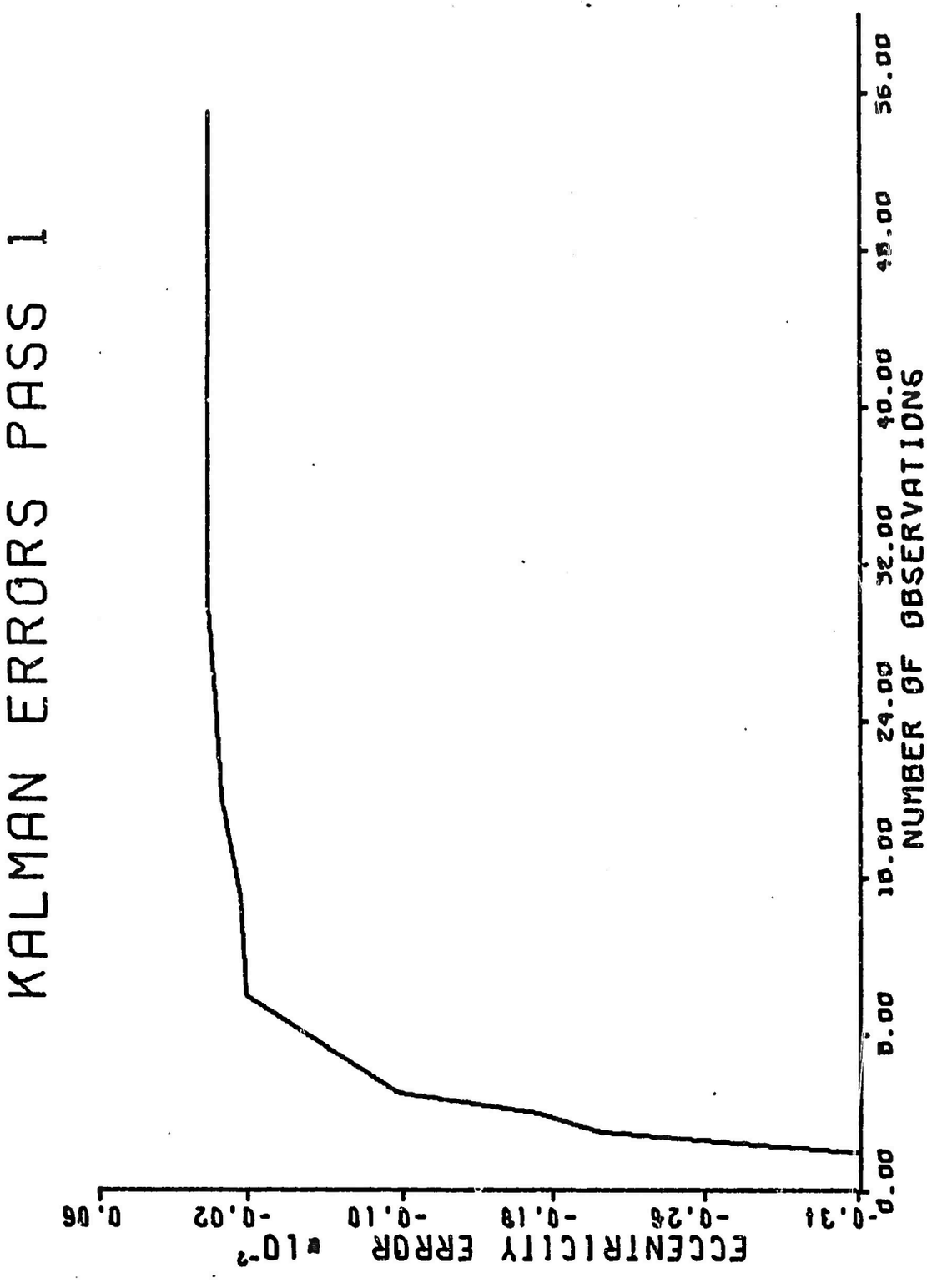

Figure 11. Eccentricity Error Pass 1

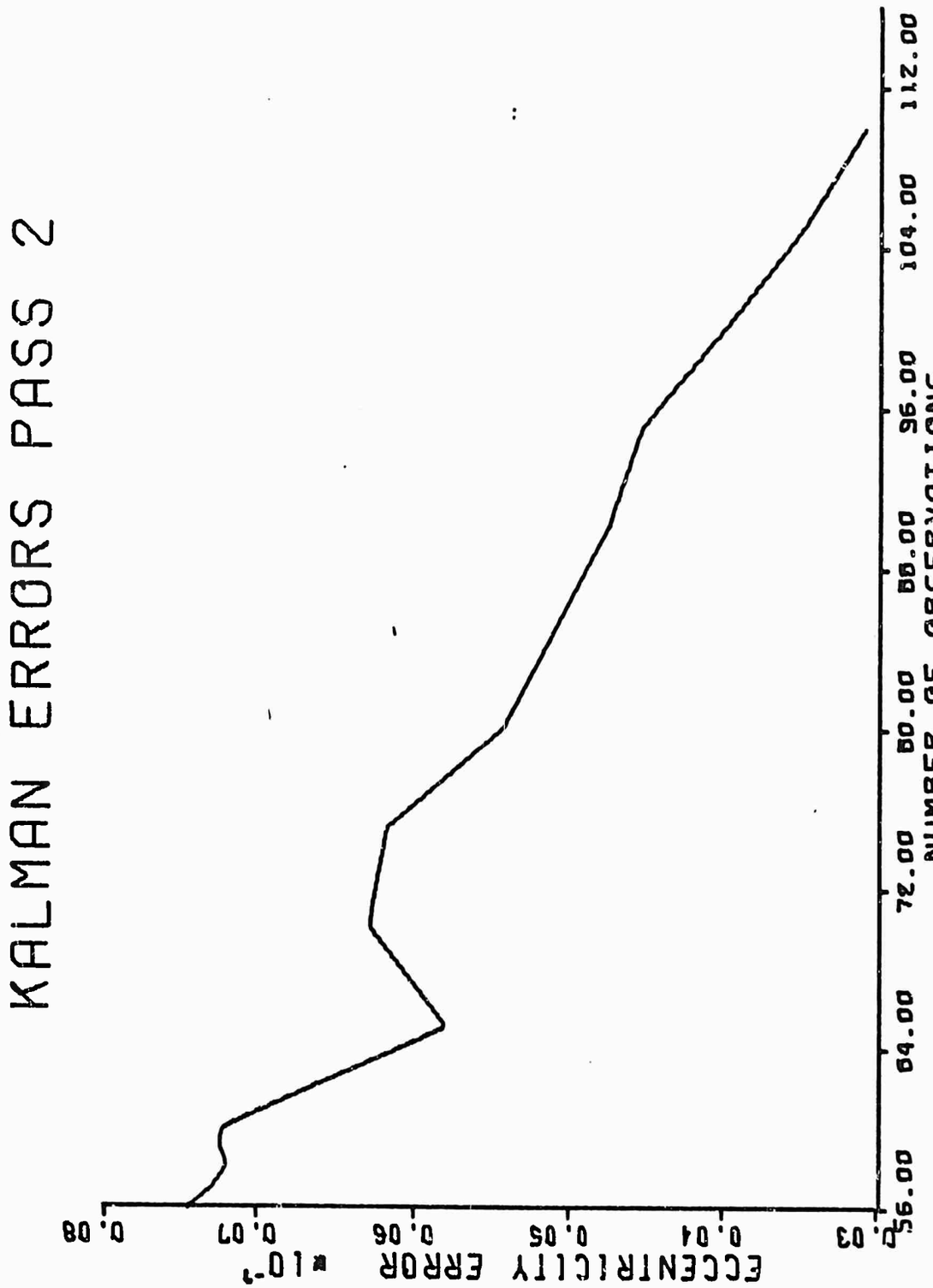

Figure 12. Eccentricity Error Pass 2

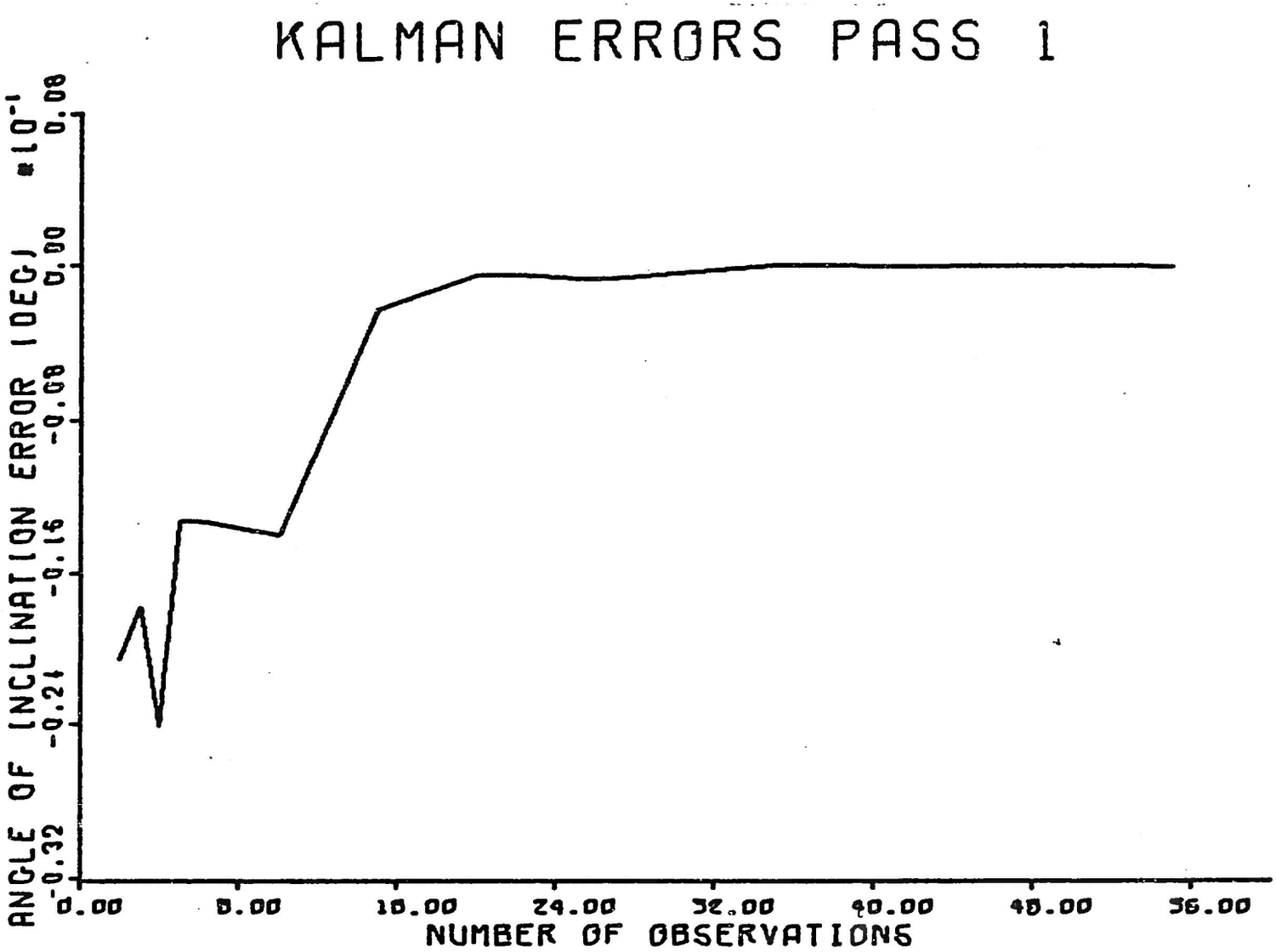

Figure 13. Angle of Inclination Error Pass 1

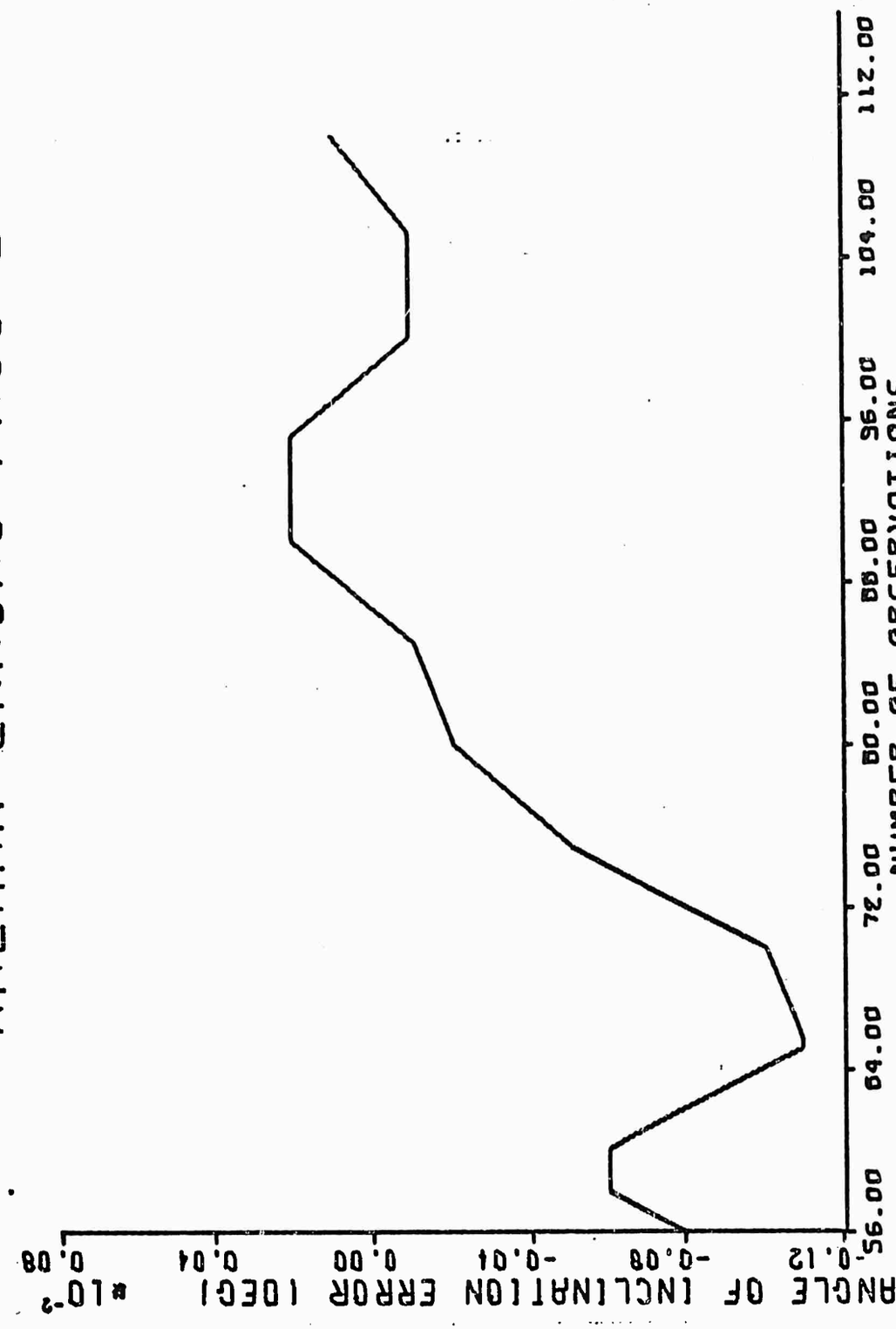

Figure 14. Angle of Inclination Error Pass 2

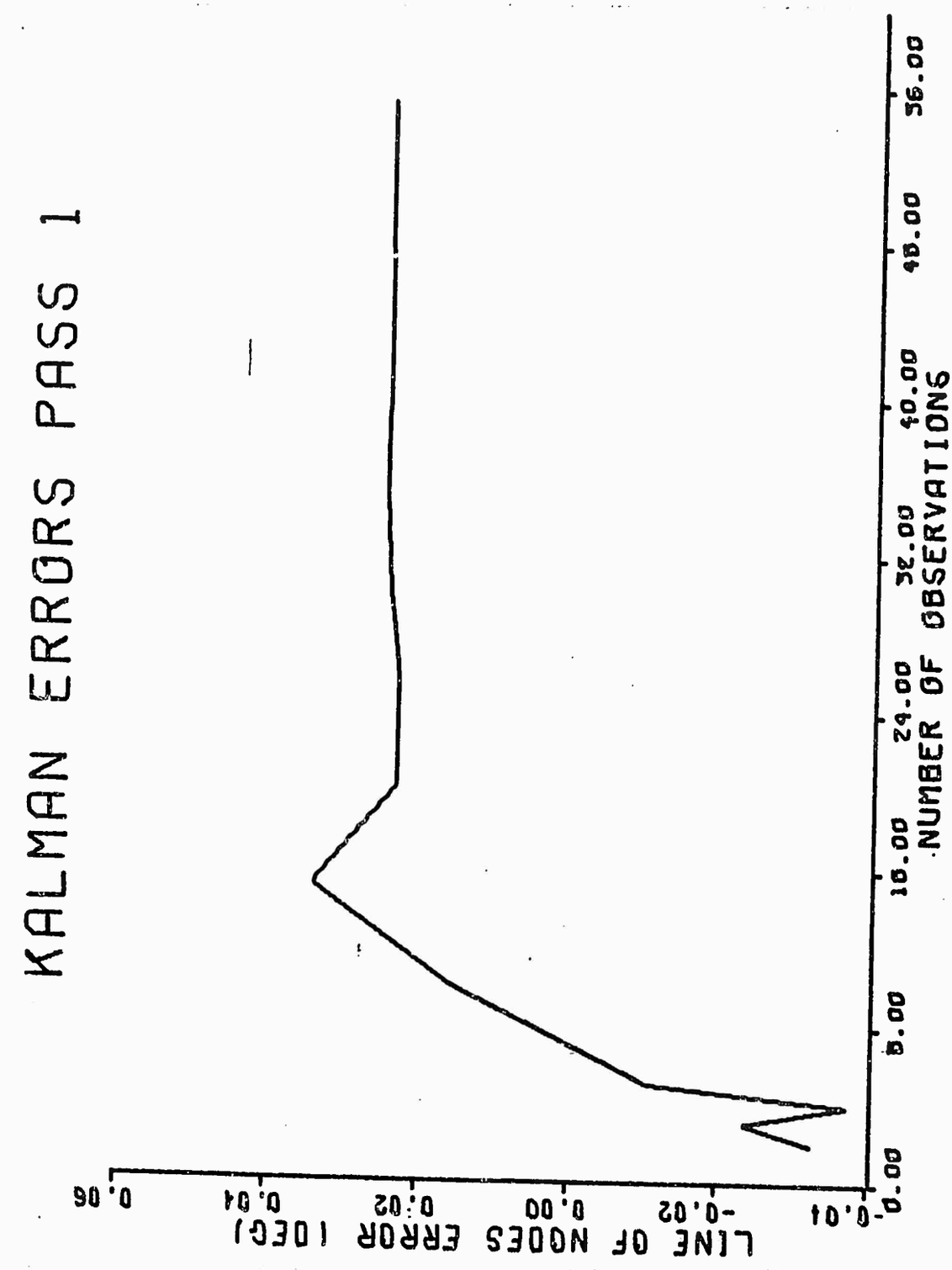

Figure 15. Line of Nodes Error Pass 1

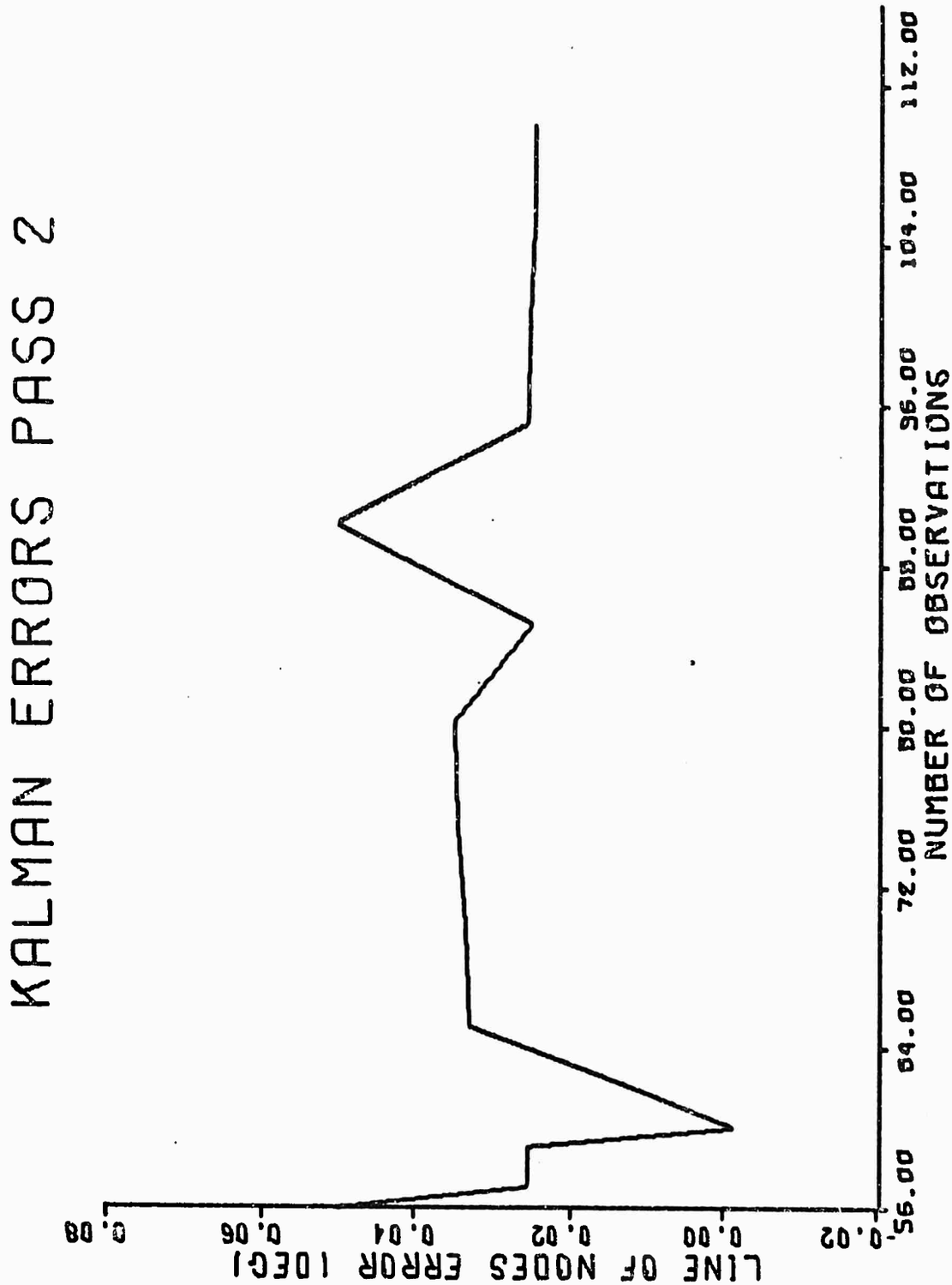

Figure 16. Line of Nodes Error Pass 2

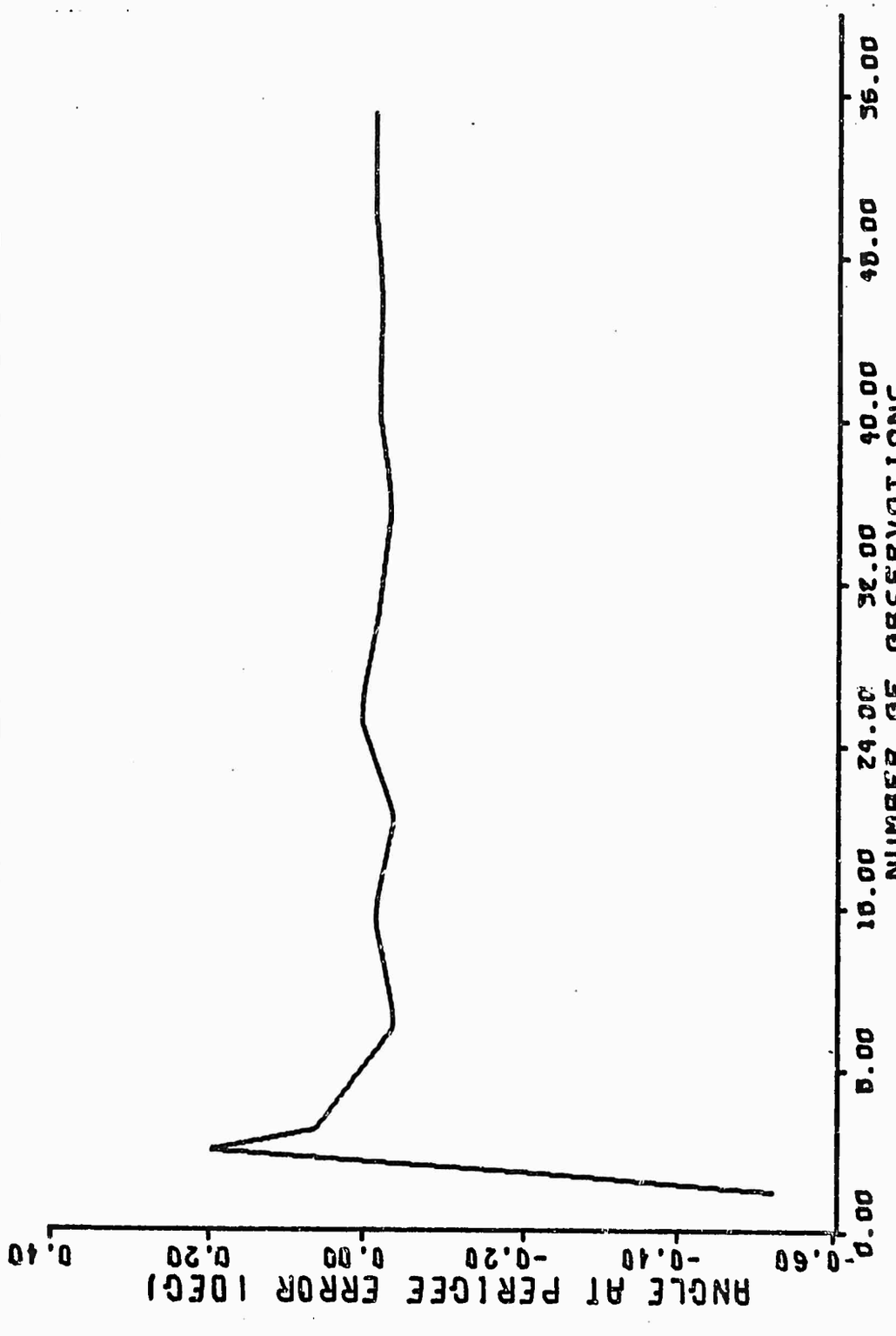

Figure 17. Angle at Perigee Error Pass 1

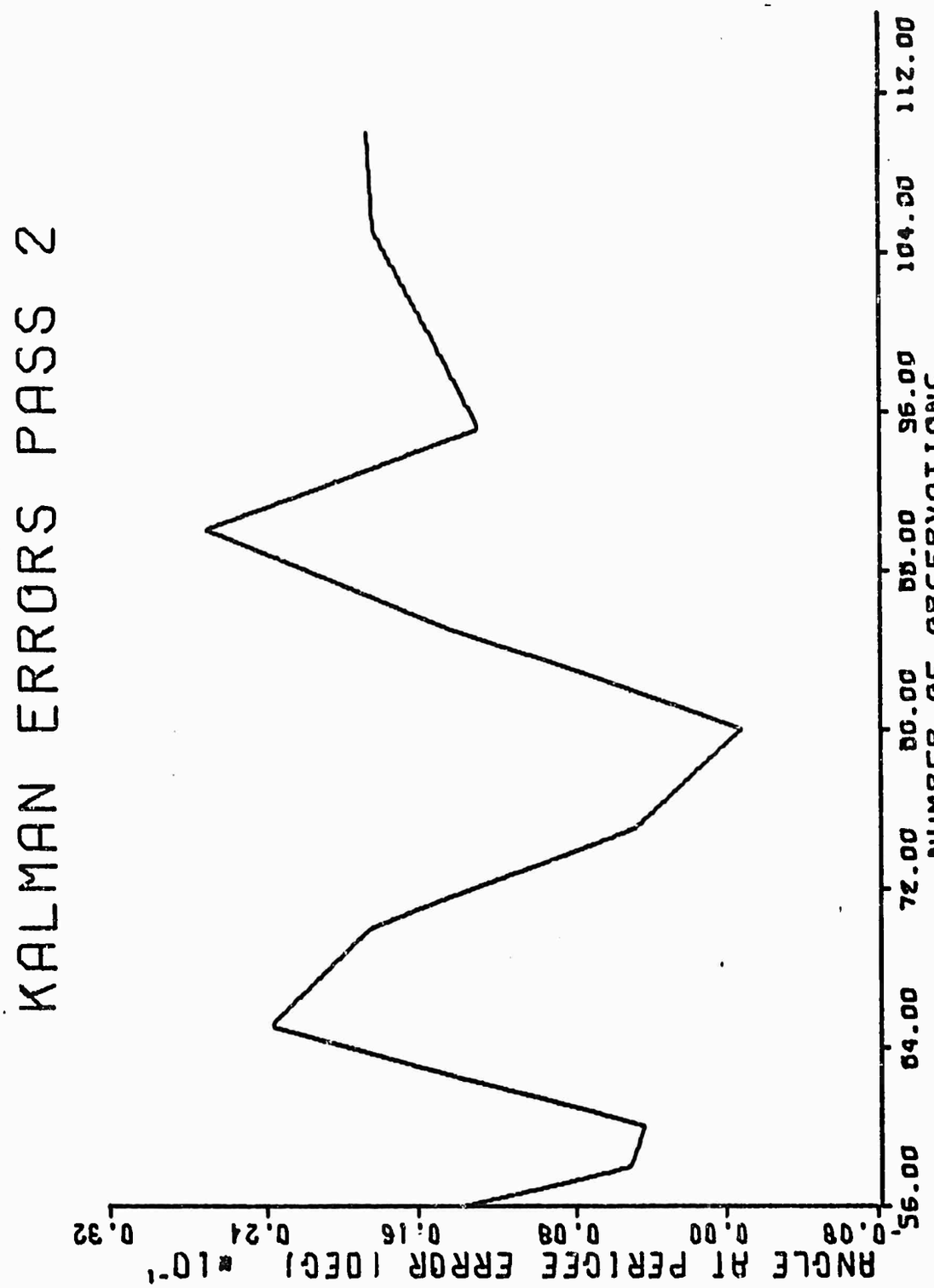

Figure 18. Angle at Perigee Error Pass 2

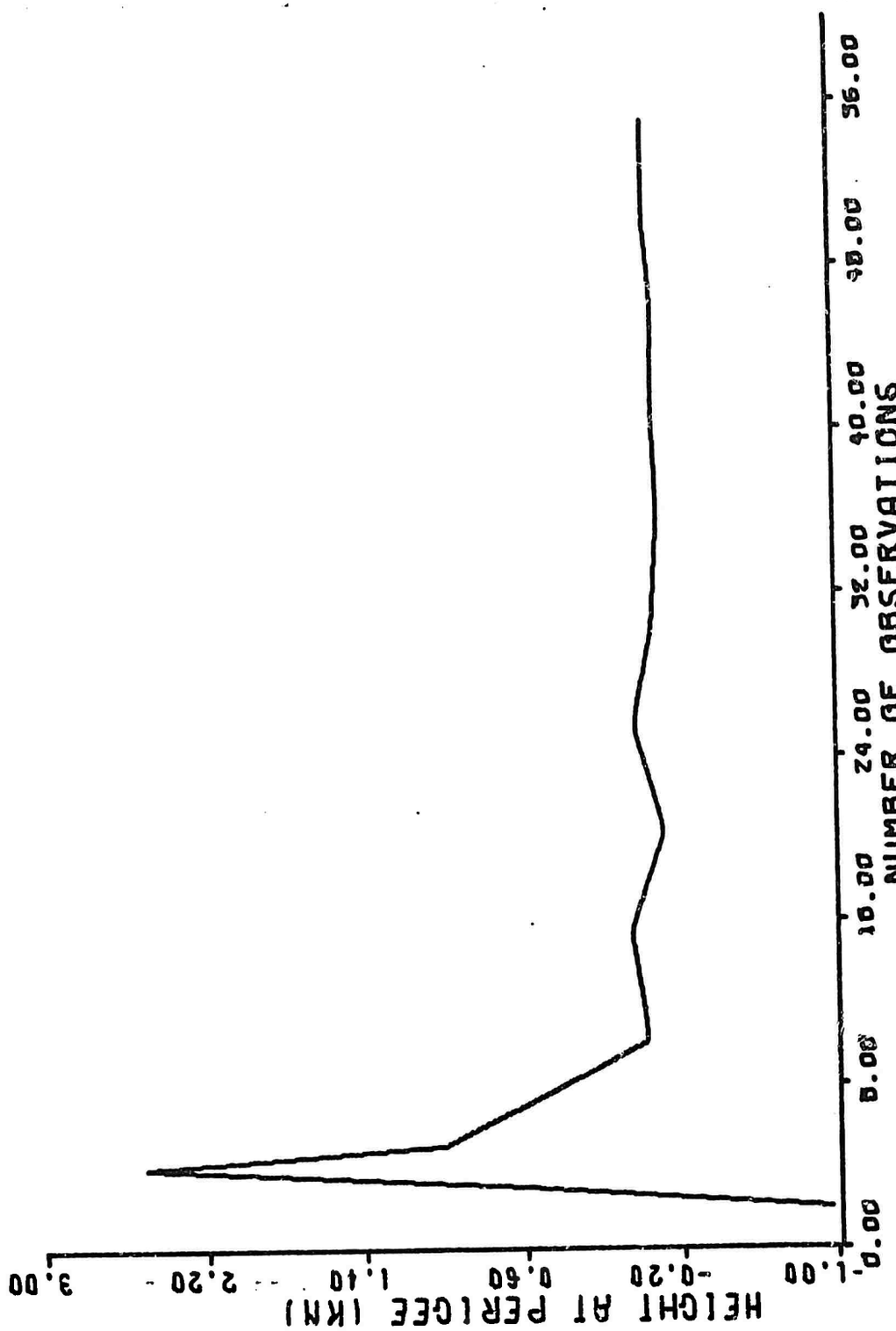

Figure 19. Height at Perigee Error Pass 1

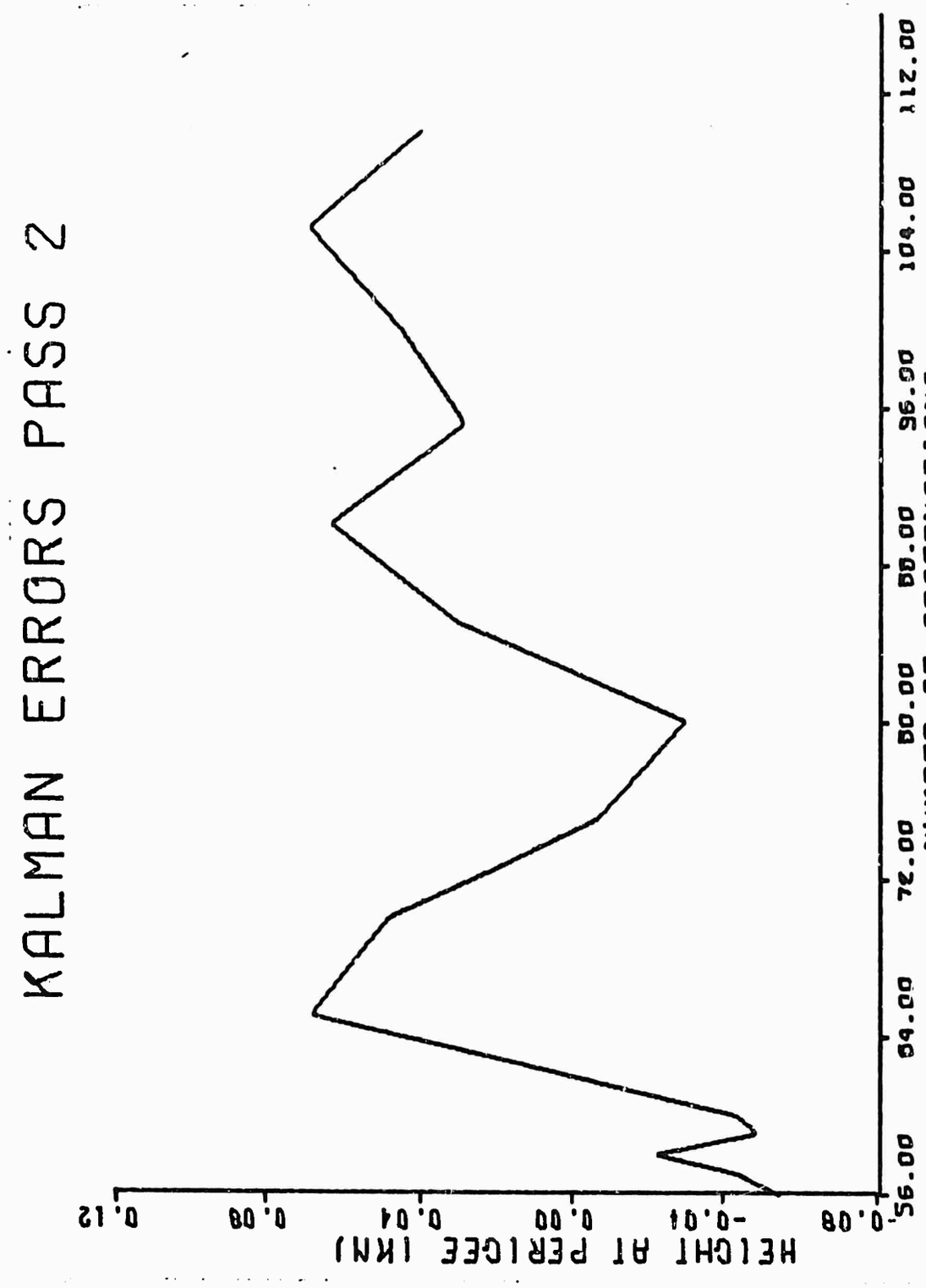

Figure 20. Height at Perigee Pass 2

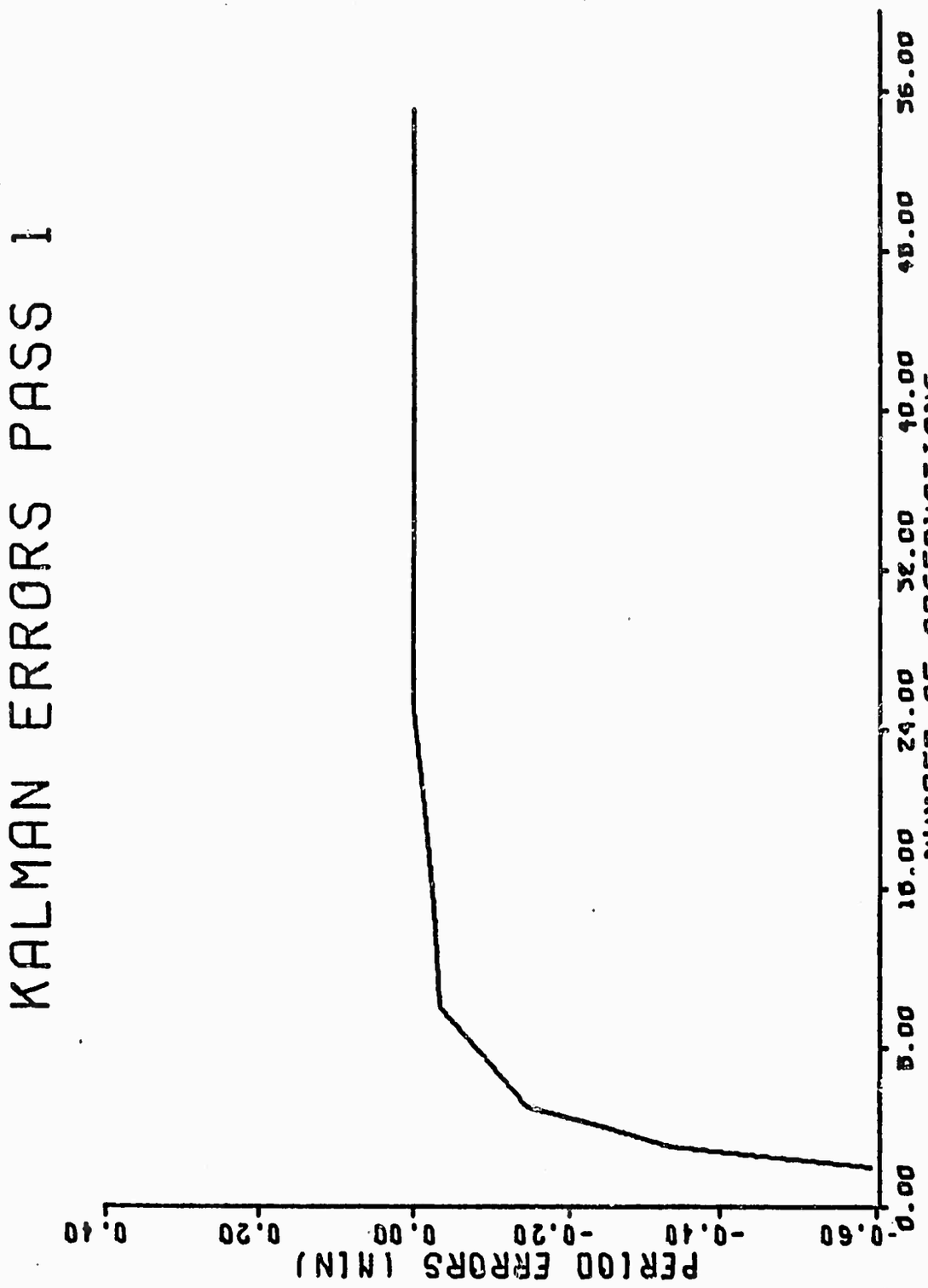

Figure 21. Period Error Pass 1

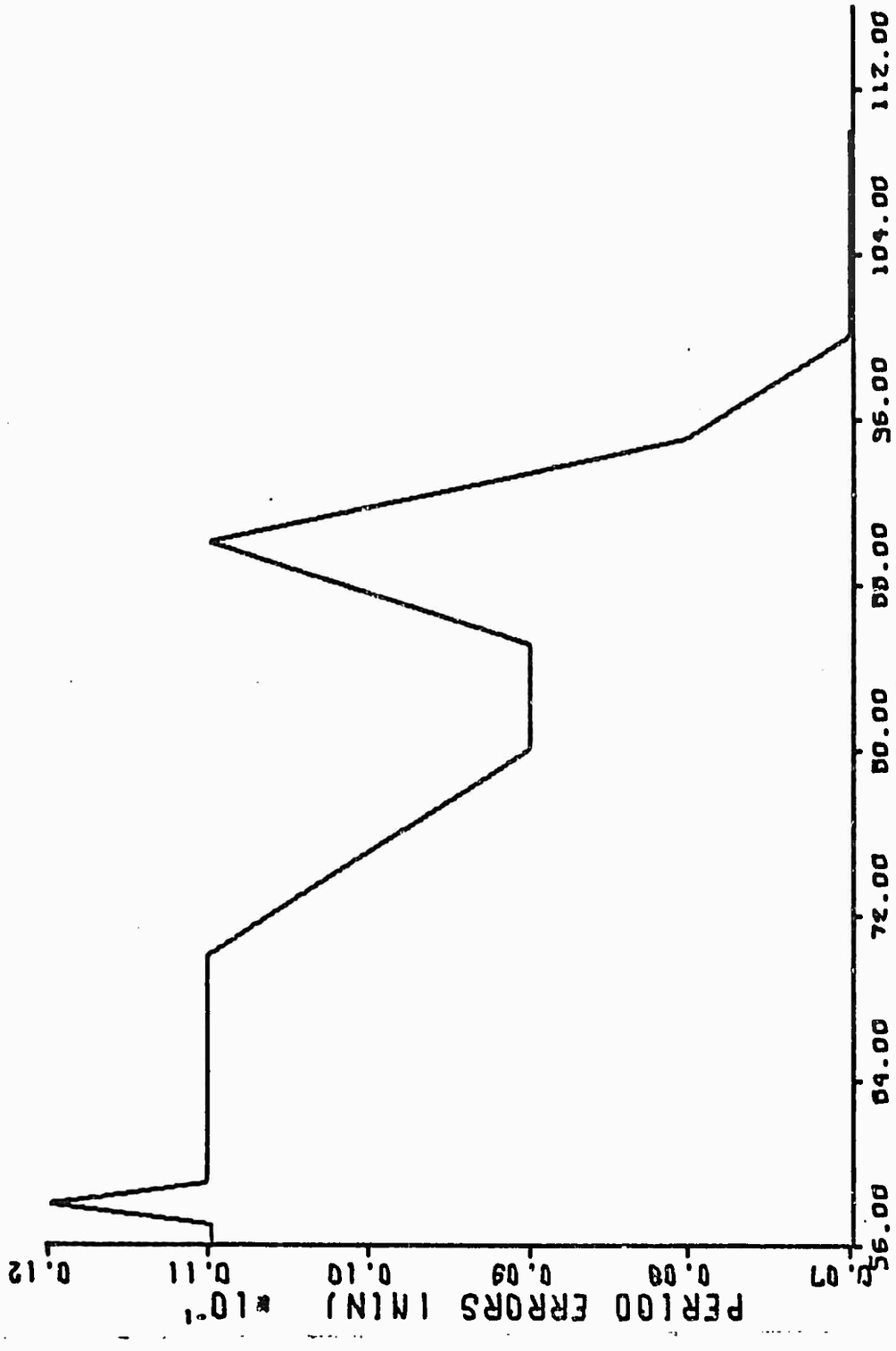

Figure 22. Period Error Pass 2

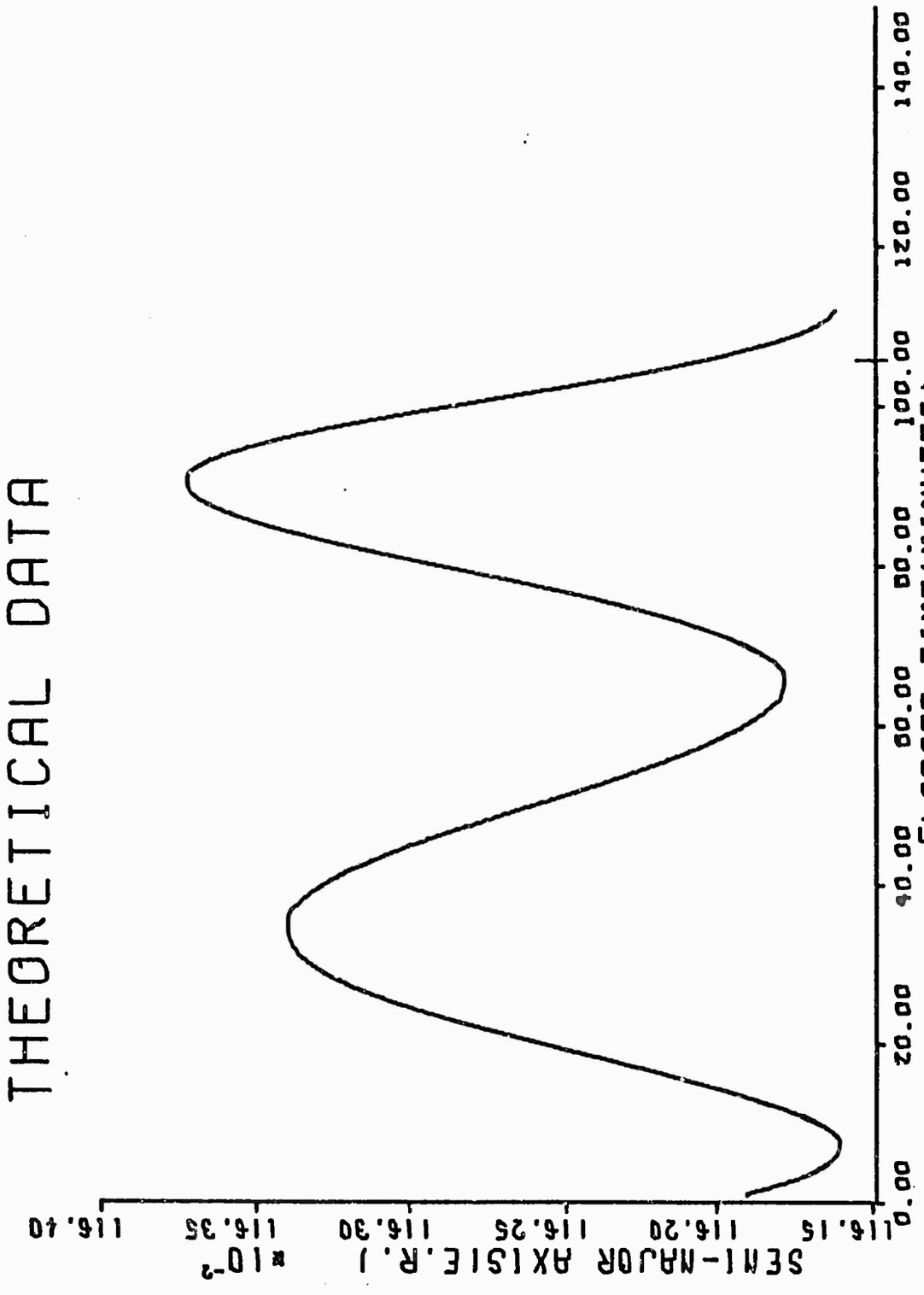

Figure 23. Kalman Determined Semi-Major Axis, Simulated Orbit

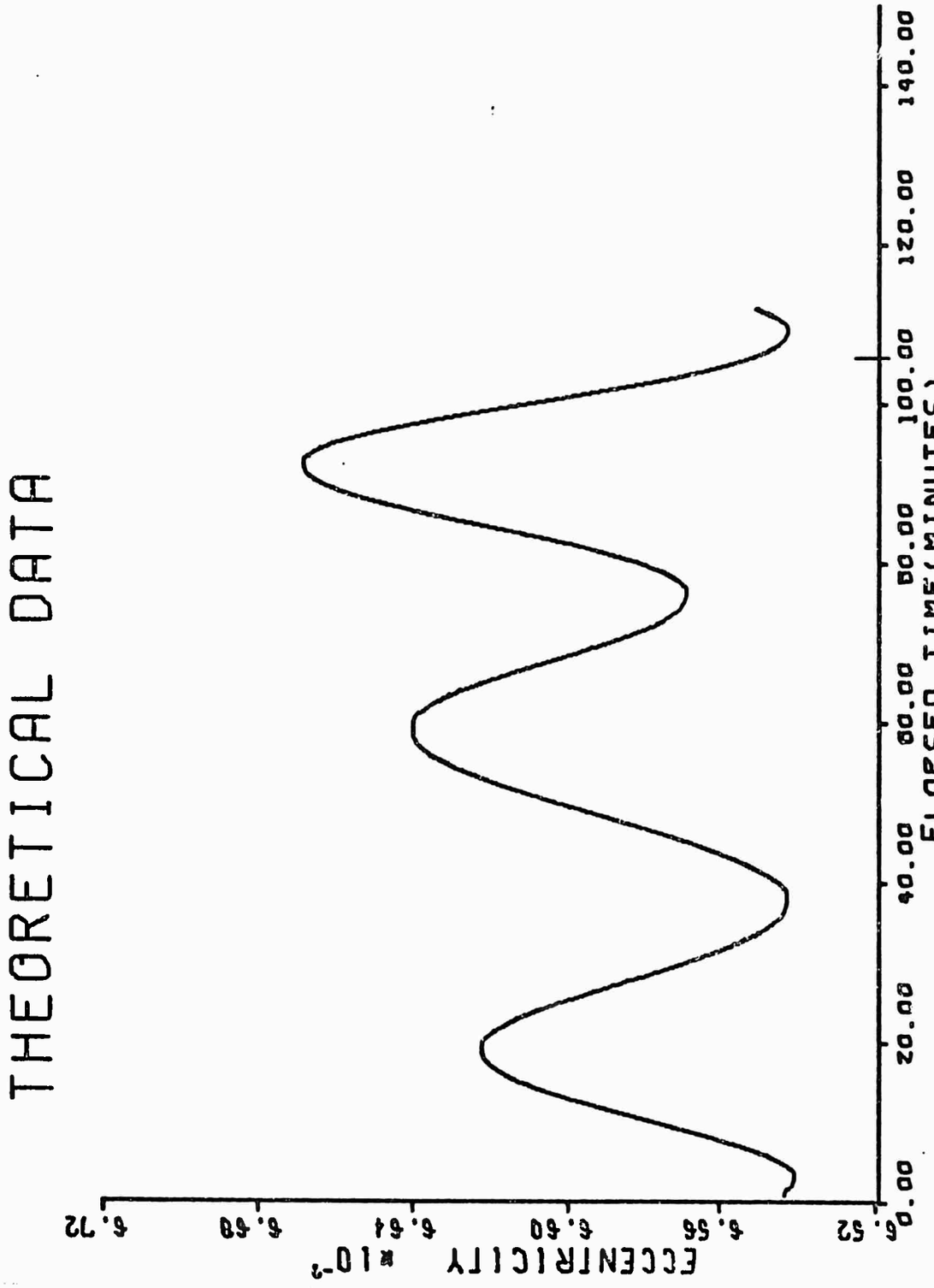

Figure 24. Kalman Determined Eccentricity, Simulated Orbit

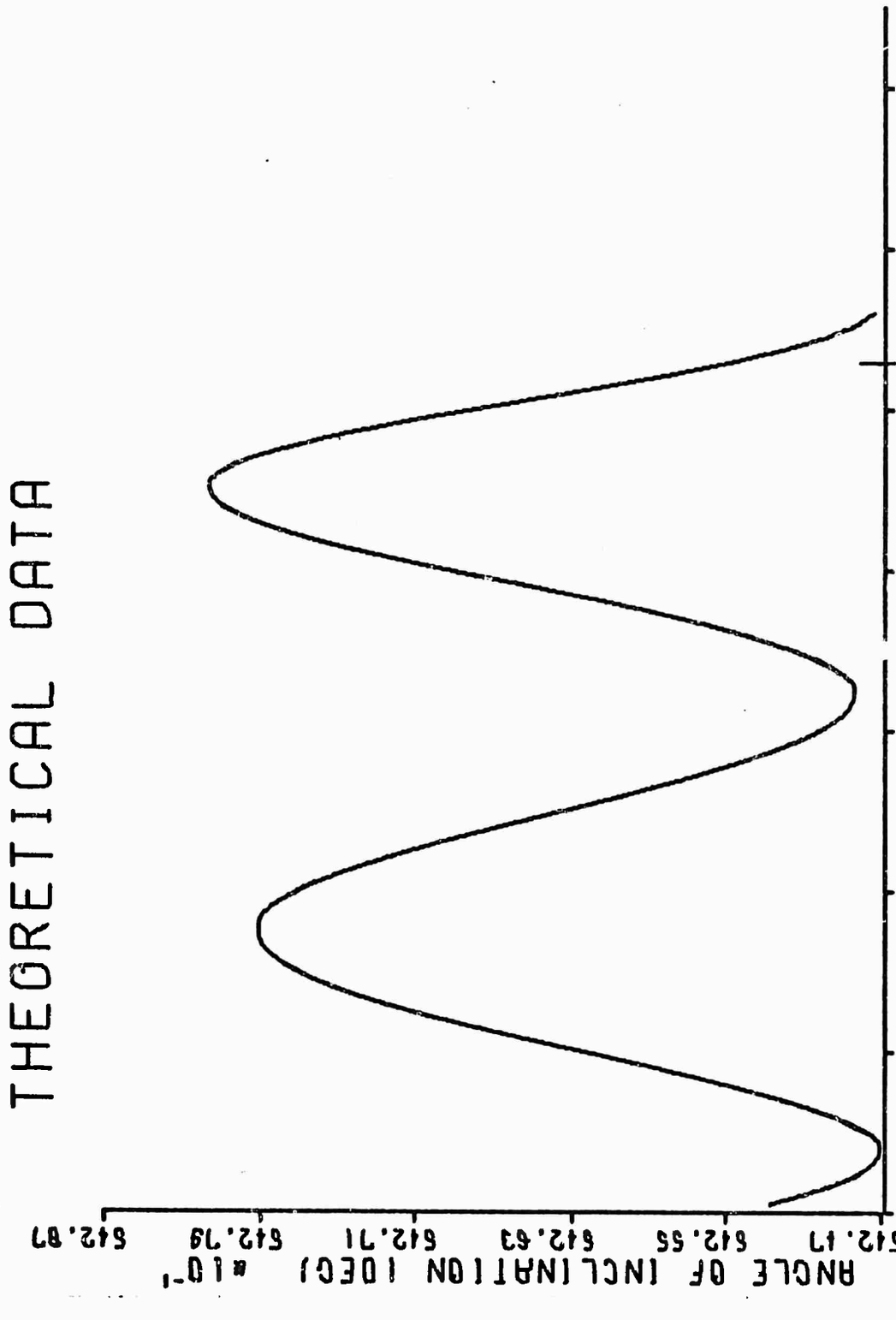

Figure 25. Kalman Determined Angle of Inclination, Simulated Orbit

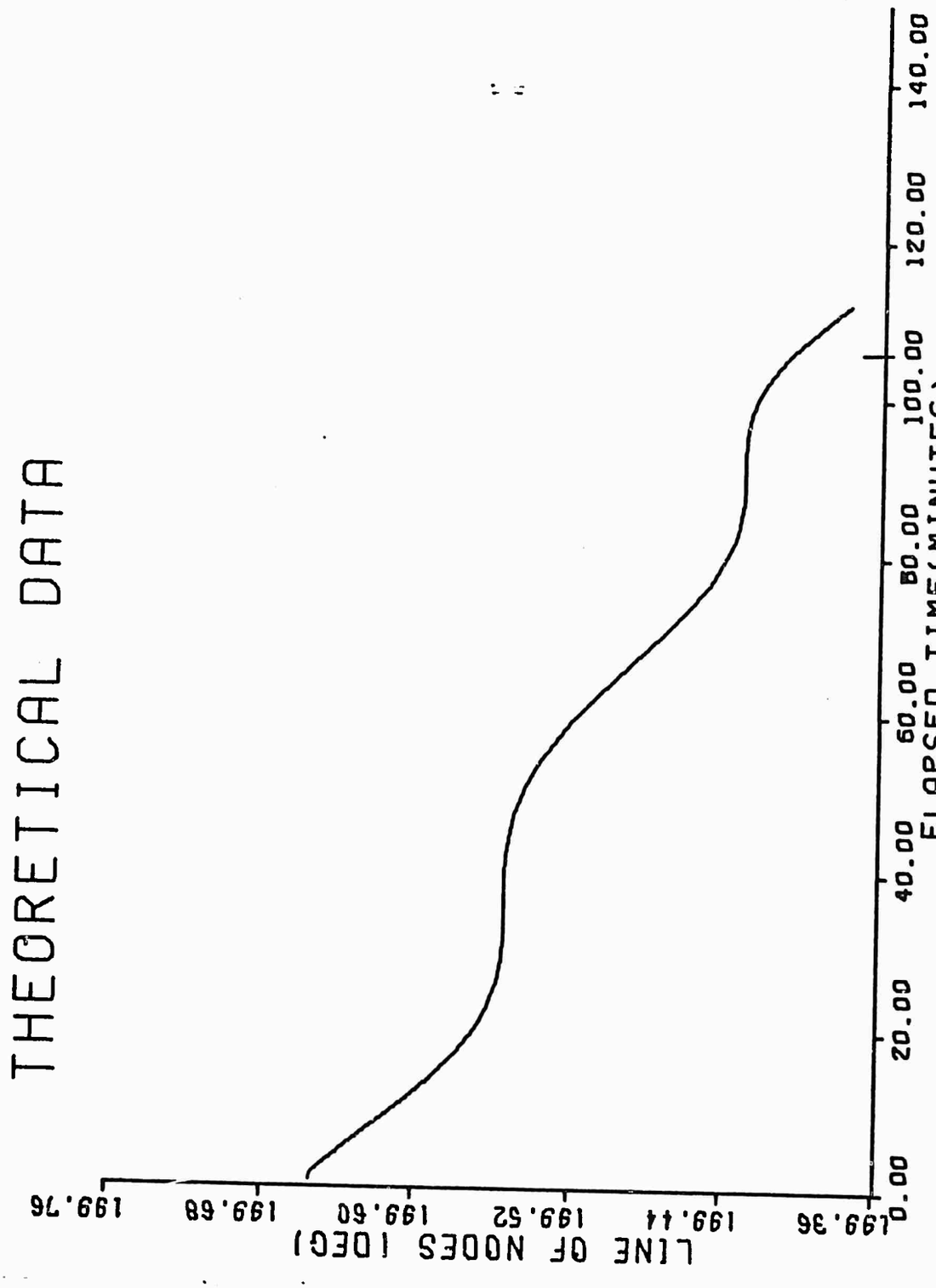

Figure 26. Kalman Determined Line of Nodes, Simulated Orbit

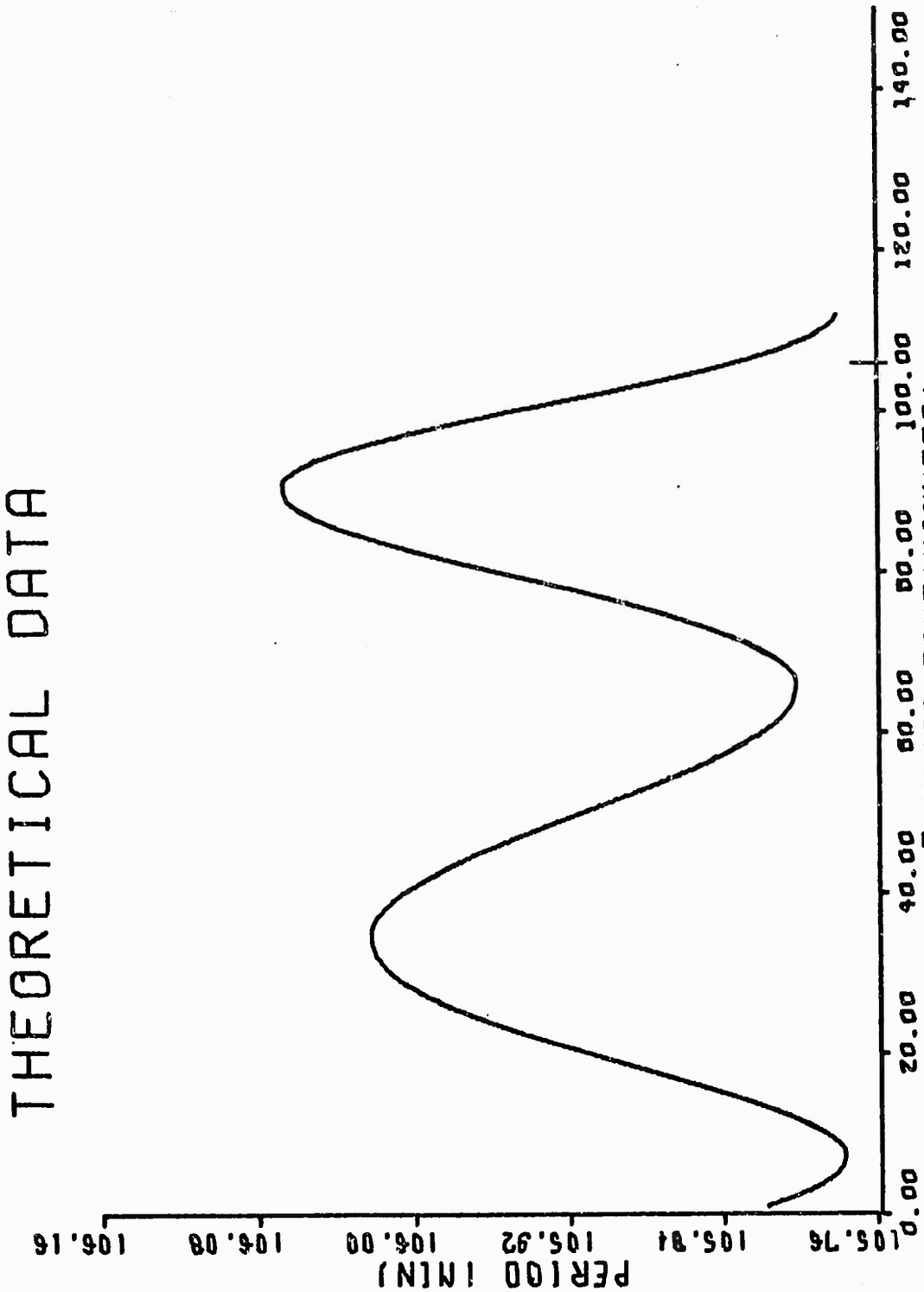

Figure 27. Kalman Determined Period, Simulated Orbit

Kalman Smoothing. Both types of smoothing discussed in Chapter III were applied to the theoretical data.

Fixed Interval Smoothing. Fixed interval smoothing failed when applied to the simulated orbit data. After processing all data points in the first pass with the filtering algorithm, the smoother was applied to attempt to smooth back to point #15. However, at point #47 the smoothing covariance matrix lost symmetry and soon thereafter, negative terms began to appear on the diagonal. Because of these effects, this method of smoothing was abandoned.

Fixed Point Smoothing. The fixed point smoother performed extremely well when applied during the first pass of the theoretical data. Table VI shows some comparative results. As can be seen some of the best and some of the worst errors occur with this smoother. For those terms which do not experience secular variations, the smoother works with extreme accuracy. However, for the line of nodes and the argument of perigee large errors occur.

Less successful results were obtained from this smoother during second pass applications. The probable cause for this change in performance was the change in the behavior of the filtering covariance matrix in the second pass. This point will be discussed thoroughly in the following section concerning the covariances encountered using the simulated orbit data. No problems were encountered with loss of symmetry or negative diagonal terms while using the fixed point smoother.

All smoothing performed during the simulated orbit study was done at point #15 or with respect to it. The choice of this point was arbitrary although it was chosen with the intention of allowing the filtering algorithm

Table VI

Kalman Smoother Analysis

Point # 15 is being smoothed. t=84 seconds.

Number of Observations	20	30	40	55
Errors In				
Semi-Major Axis (E.R.)	-.000086	.000005	.000001	.000000
Eccentricity	.0000479	-.0000196	.0000149	.0000121
Angle of Inclination (Deg)	.0007	.0004	.0003	.0002
Line of Nodes (Deg)	.1229	.3749	.6257	1.0020
Angle at Perigee (Deg)	.0462	.0248	.0245	.0203
Height at Perigee (Km)	.193	.113	.063	.090
Period (Min)	.012	.001	.000	.000

to have a chance to settle towards a steady state before the smoother was applied.

Covariance Matrix Behavior. The behavior of the covariance matrix during this study was typical of those matrices described in theory (Ref 15). Starting with an intentionally large and diagonal covariance at t_o the covariance matrix continues a rapid constant descent until a "steady state" is achieved. Figures 26 through 29 show the behavior of the P_{xx} or P_{11} element, the $P_{\dot{x}\dot{x}}$ or P_{44} element, as well as the Position and Velocity Standard Deviation which are the square root of the sum of the squares of the appropriate covariance elements:

$$\text{Position Standard Deviation} = (P_{xx}^2 + P_{yy}^2 + P_{zz}^2)^{1/2} \quad (63)$$

$$\text{Velocity Standard Deviation} = (P_{\dot{x}\dot{x}}^2 + P_{\dot{y}\dot{y}}^2 + P_{\dot{z}\dot{z}}^2)^{1/2} \quad (64)$$

Initial Covariance Matrix, P(0). The initial covariance matrix was chosen after experimentation with various values. Values as large as 10^{30} for position variance and 10^{15} for velocity covariance were tried. These values converged rapidly to the same steady state values as those obtained with the values actually used, 10^{10} and 10^6. Values between these limits were also tried with convergence to the same values occurring. However, it was determined that if small values were chosen, 10^5 and 10^3, for example, then convergence to the same values did not occur and in fact a steady state was never achieved during the allowed observation period of 110 measurements. Additionally, physical significance can be attributed to values of 10^{10} for position and 10^6 for velocity. These values represent one sigma values of 10^5 and 10^3 for position and velocity respectively. Because of the manner in which the initial state x(0) is chosen, little

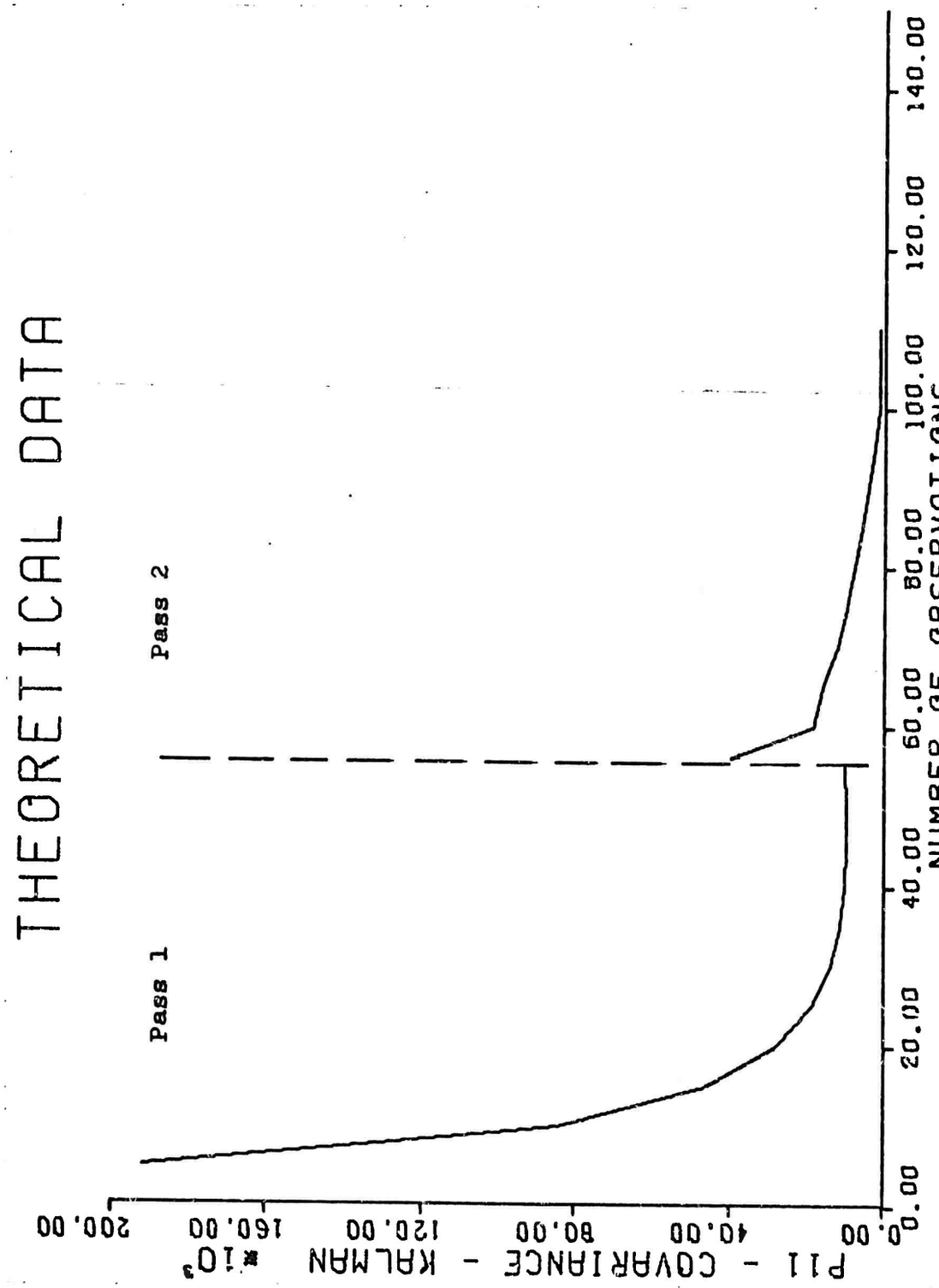

Figure 28. Covariance Data P_{xx}, Simulated Orbit

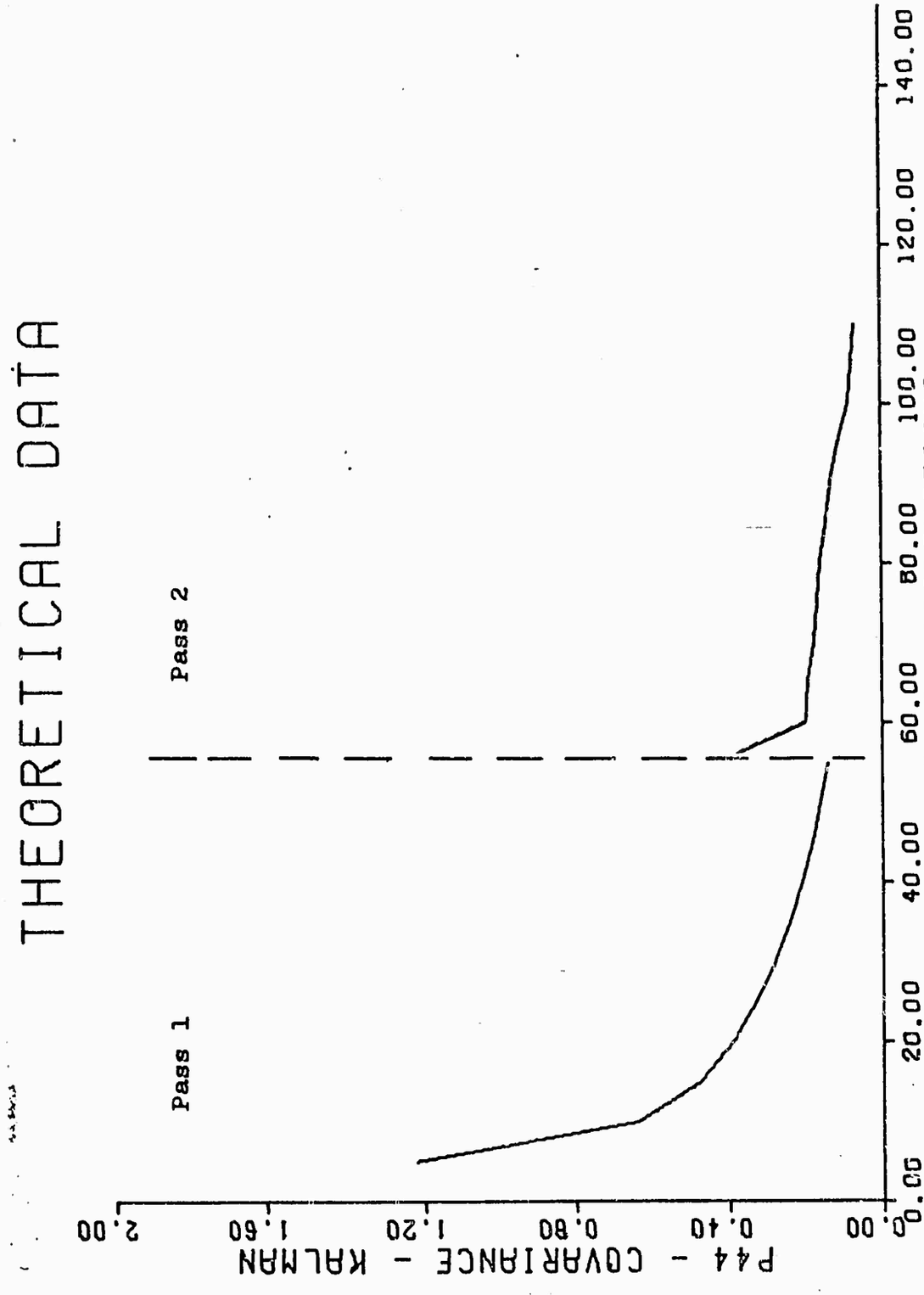

Figure 29. Covariance Data $P_{\dot{x}\dot{x}}$, Simulated Orbit

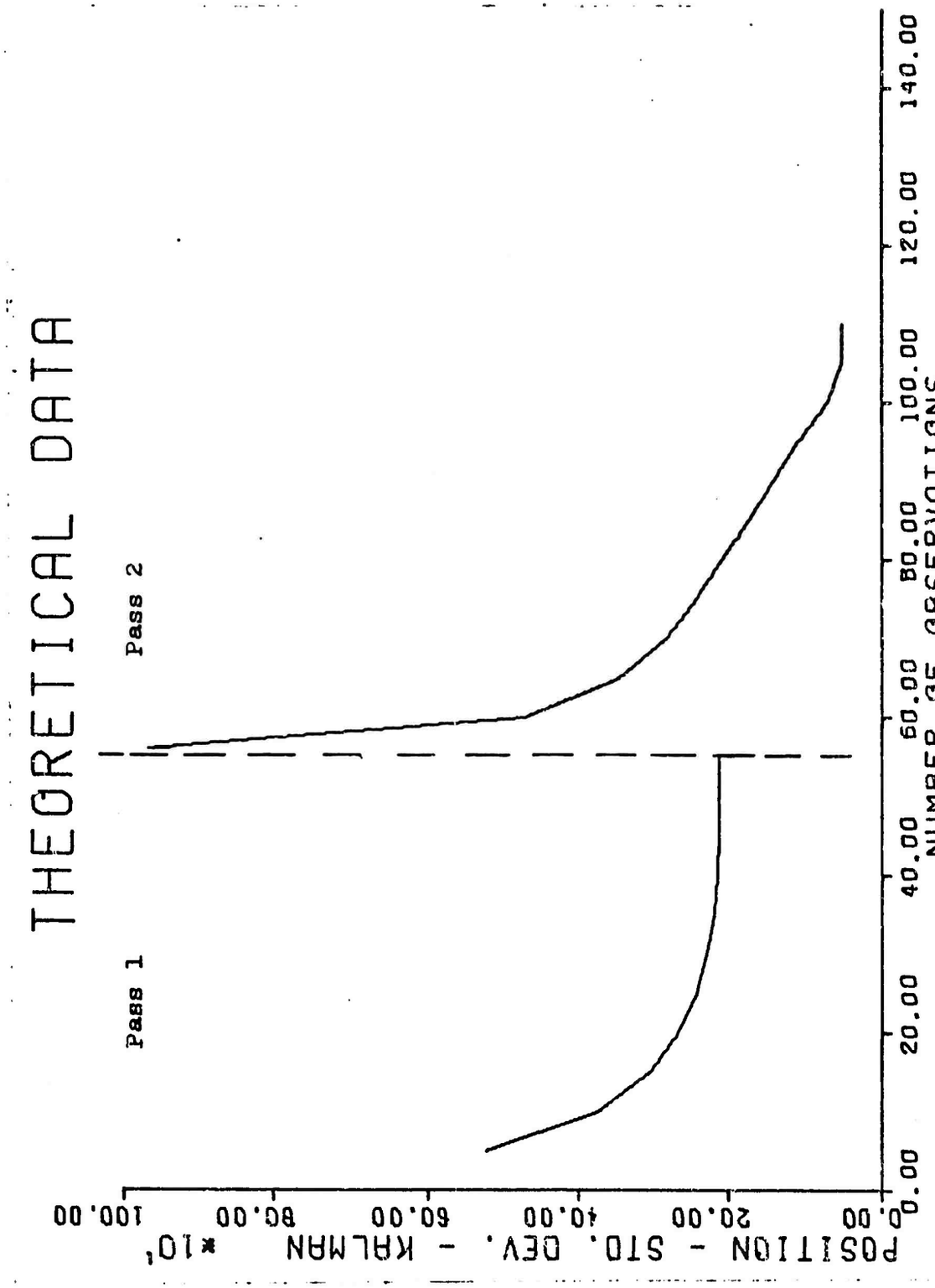

Figure 30. Standard Deviation of Position, Simulated Orbit

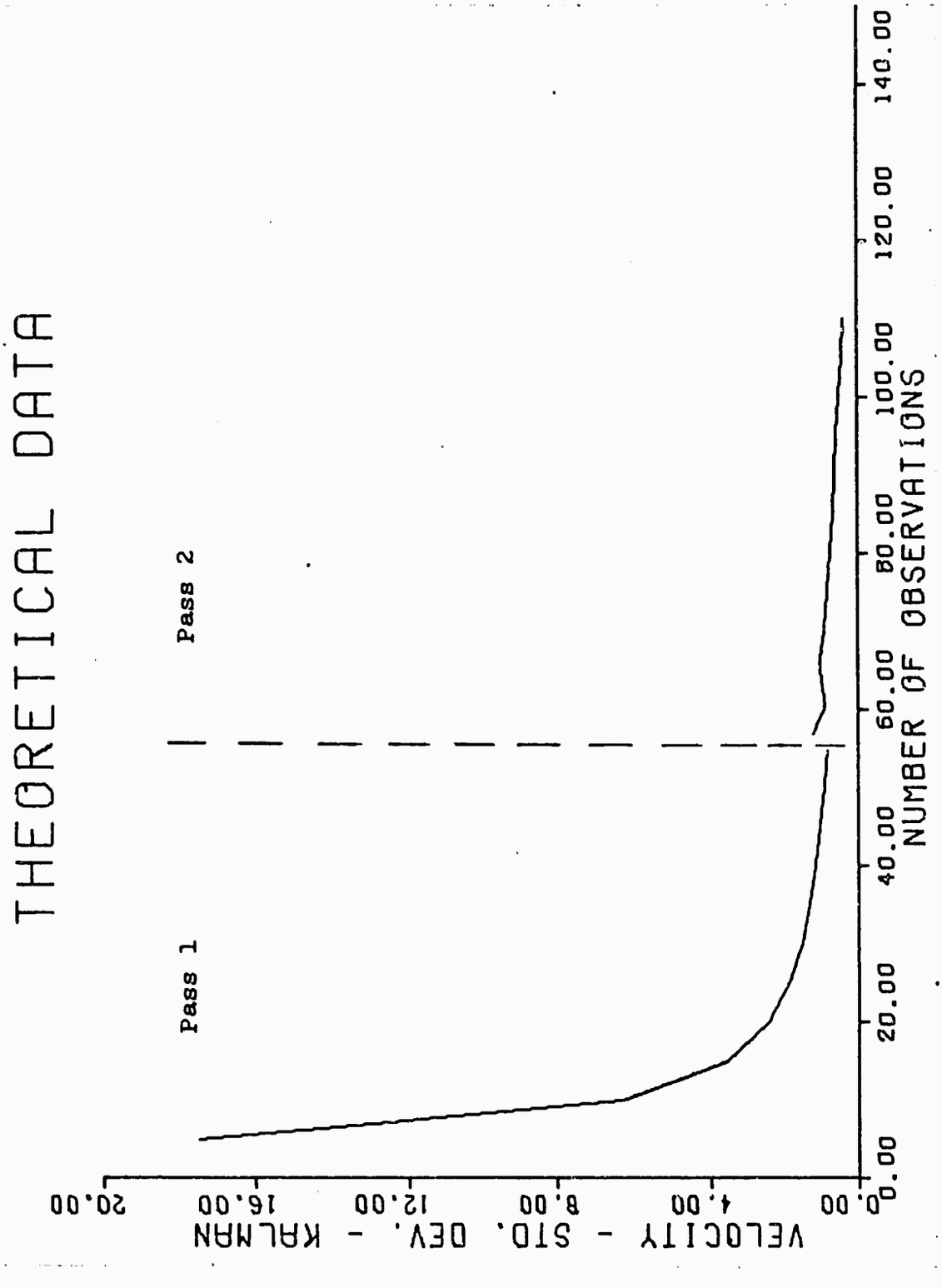

Figure 31. Standard Deviation of Velocity, Simulated Orbit

can truly be said about the position and velocity of the vehicle other than that orbital speed was attained. Since the position and velocity are of the order of magnitude of 10^5 and 10^3 meters and meters/second respectively, this choice of sigma implies that very little statistical confidence should be placed in the initial values.

Experimentation with the Kalman Gain, K. During the study the Kalman matrix was varied by premultiplication by a constant and by premultiplication of columns of elements by different constants. Theory shows that the Kalman matrix as derived by Kalman is the optimal which can be applied to a set of data to obtain estimates of the states. Experimentation confirms this result and, in fact, indicated that the Kalman matrix is extremely sensitive to manipulation.

Multiplication by constants varying from .8 to 3. was attempted. Multiplication by a constant less than one provided slower convergence to the values achieved than when the unaltered K matrix is used. Multiplication by a constant greater than one tended to induce oscilations in the values of the elements until when the constant was increased greater than 2, filter divergence occured.

Premultiplication by different patterns of constants produced no acceptable effects for the orbital determination problem.

Experimentation with the value of P. The value of the covariance matrix P was varied by the addition of a constant term to the values for the velocity covariances at every measurement update in accordance with recommendations for compensation for non-linearity and covariances which approach zero (Ref 10:305-307). This effective noise addition produced no desirable results over the number of observations used. Oscillations

about the value obtained using the unaltered covariance matrix tended to occur.

Experimentation with the value of Q. The value of Q chosen for use with Level One Modification (Ref 19) was $1. \times 10^{-12}$. The number of significant digits carried by the CDC 6600 in single precision arithmetic is 14. Thus to be exact theory requires a value of $1. \times 10^{-28}$. The lower value of 10^{-12} assists in accounting for additional non-linearities in the system. However, it should be noted that changes to values of 10^{-20} and zero were made to the modification with little noticeable effect. The large capacity and capability of the CDC 6600 probably precludes necessity for this type of modification. The between pass covariance matrix reached a maximum of 10^5 for the diagonal position terms and 10^3 for the diagonal velocity terms prior to update using the first measurement of the second pass. No tendency toward divergence was observed.

Pointing Information from Prediction

The use of prediction capabilities of the filters is of key importance in the pointing of downrange radars in order to obtain additional tracking data for orbital refinement and also to enable possible rendezvous or interception. Table VII shows the capability of the Kalman filter to predict future measurements. Two items are important when comparing these numbers. First the time of observation and prediction may vary slightly and second the measurement is, of course, corrupted by noise while the filter parameters are best estimates.

Table VII

Theoretical Interpass Pointing Data Kalman Filter

Single Run (randomly chosen)

Pass	Range (meters)	Range Rate (meters/second)	Azimuth (Deg)	Elevation (Deg)
1-2 Calculated*	1986441	-6530	259.437	10.327
1-2 Measured	1982343	-6526	259.437	10.384

*Calculations are performed using the equations found in Appendix C.

VI. Actual Data: Ent Set 1

Data. Data for approximately three days of the orbit of satellite 6096 was supplied for this study by the 1st Aerospace CON Squadron, Ent AFB, Colorado. This data was processed at Ent using a special perturbational analysis and the results were provided for comparison in this study. The Ent analysis used approximately 660 observations of the vehicle, rejecting about 40 observations for failure to fit the predicted statistics of the problem. The spiral decay differential correction program converged providing orbital elements at an epoch time corresponding to the final measurement on the third day.

From the supplied data, 115 observations were selected to be processed by the Kalman Filtering program. These observations were chosen because they represent a three orbit two radar problem. Nothing was known of the characteristics of any particular observation at the time of selection. The Kalman program produced orbital elements at the time of its final measurement which occurred early in the first day of orbit. To obtain values of the orbital elements at other times a reverse integration to the beginning was accomplished. To predict values, the fact that the elements remain periodic and have known secular variations was used. This allows comparison of the determined elements with elements generated by the other programs at any time.

The first 80 of the same 115 data points were used to run the WLS filter. A forward integration was performed to project the determined elements to other times for comparison with ENT and Kalman filtering data. Table VIII shows the specifics of the data used.

Table VIII

Orbit Data

Satellite # 6096 Day 190 Year 72

θ_{g_o} = 19 hr 4 min 23.4378 sec (Ref Appendix F)

Start GMT = 20 hr 41 min 8.839 sec

Pass	Observation Interval	Number of Observations	Duration Pass Min Sec	Station	Duratic of Gap Min Sec
1a	10 sec	22	3:30	359	
					1:15.7
1b*	10 sec	25	4:10	359	
					85:29.5
2	10 sec	33	5:30	359	
					91:30.3
3	6 sec	35	3:30	345	

*Pass 1b is a continuation of pass 1a which occurred due to a radar dropout of 1 minute/15 seconds.

Radar Characteristics. The parameters or characteristics of the radars used are shown in Table IX. The similarities between these properties and those of the simulated radar discussed in Chapter V are noted. Passes 1a, 1b, and 2 are obtained from radar 359 while pass 3 comes from radar 345.

Comparison of Orbital Parameters. The results of the Kalman filter and the WLS filter projected forward to the epoch time of the ENT data are compared in Table X. From this table a high degree of compatibility is noted in all parameters except the argument of perigee. Since this orbit is extremely circular in nature, the very term perigee tends to lose meaning and thus so does the parameter argument of perigee. As a result this parameter is seen to vary from 290° to 355°. The eccentricity appears to have a larger error than the other parameters but again it is noted that an eccentricity such as those obtained merely indicates that the orbit is circular. A maximum difference of .007 minutes is noted between the WLS period and the ENT period. This comes to .42 seconds which is certainly an acceptable error considering the small amount of data processed. Graphs of the Kalman determined orbital elements are found in figures 30 through 34. These graphs exhibit the same characteristics noted in the theoretical study although the parameters have assumed a more symmetric shape due to the polar circular nature of the orbit.

Table IX

Radar Parameters Ent Set 1

	Position	
	Sensor # 359	345
Latitude	64.291 N	52.73267 N
Longitude	149.19318 W	185.8976 E
Height	199.	86. meters
	Sensor Biases	
Range	105.9	218.3 meters
Range Rate	1.0	1.0 meters/second
Azimuth	-.037	-.067 degrees
Elevation	.023	.054 degrees
	Sensor Sigmas	
Range	819.	929. meters
Range Rate	24.	18. meters/second
Azimuth	.474	.259 degrees
Elevation	.331	.268 degrees

Table X

Ent Data Set I Results

Epoch Time: Day: 192 Hour: 20 Min: 01 Sec: 23.325

Element	ENT	Kalman Predicted	WLS Predicted
Semi-Major Axis	1.076376	1.076902	1.076808
Eccentricity	.000915	.00160	.00141
Angle of Inclination	96.149°	96.152°	96.154°
Line of Nodes	N/A*	248.367°	248.369°
Arg. of Perigee	290.2294°	354.889°	345.234°
Period	94.415 min	94.420 min	94.408 min
Height at Perigee	480 km	480 km	480 km
# of Observations Used to Obtain Results	660	115	80
Radius (m)	6871522	6873301	6873552
Velocity (m/sec)	7612.8	7612.7	7612.1

*Not Available

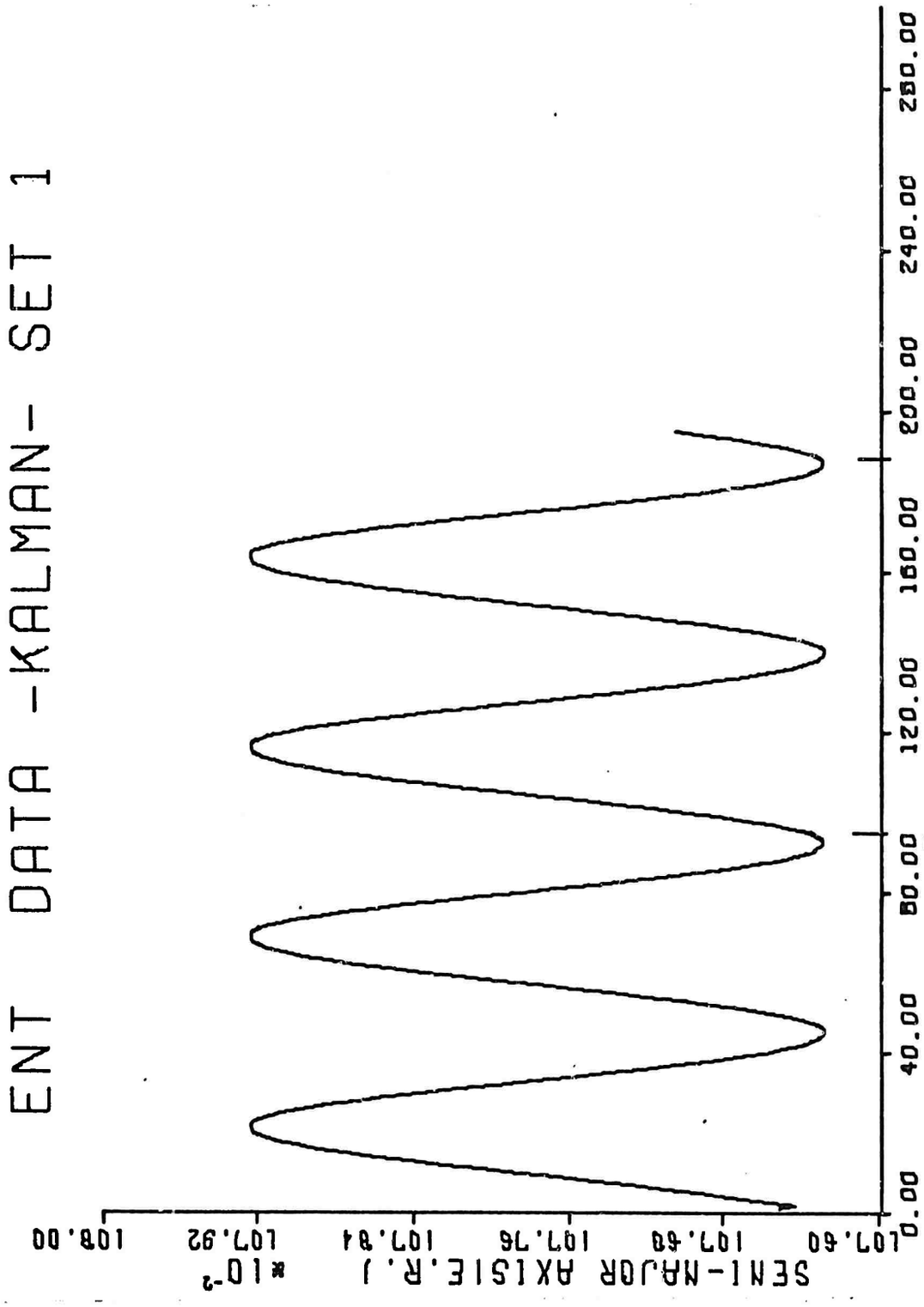

Figure 32. Semi-Major Axis Ent Set 1

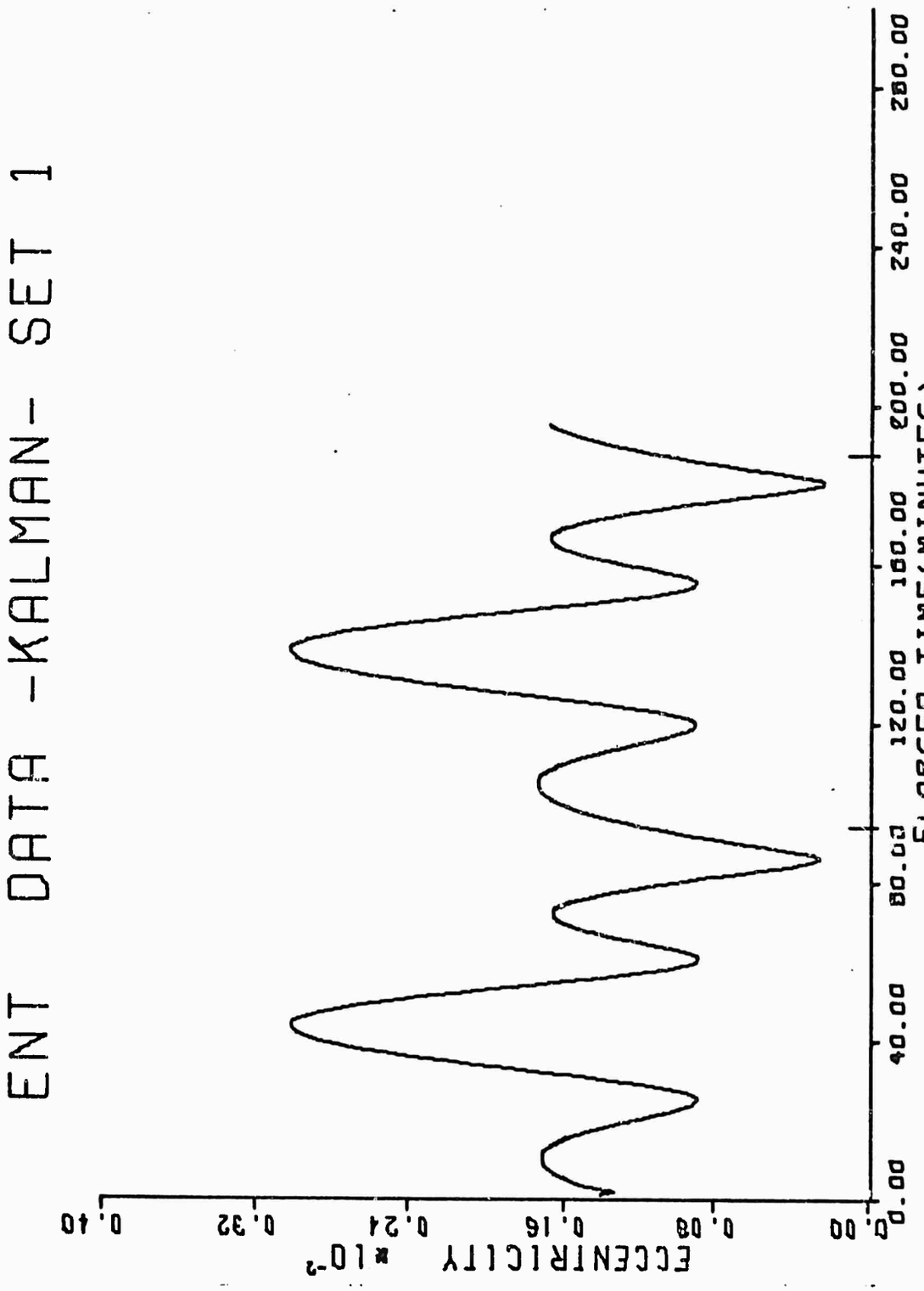

Figure 33. Eccentricity Ent Set 1

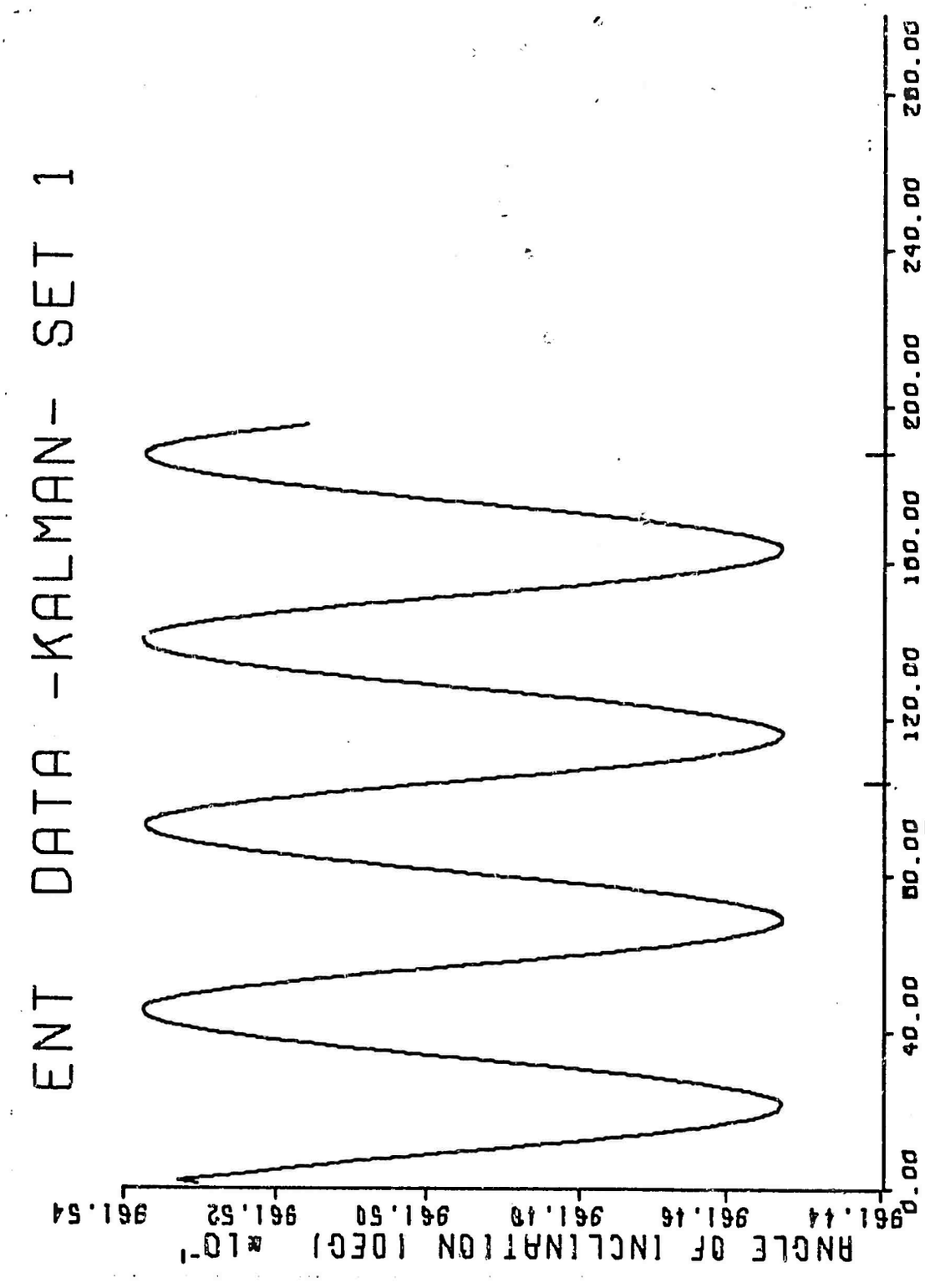

Figure 34. Angle of Inclination Ent Set 1

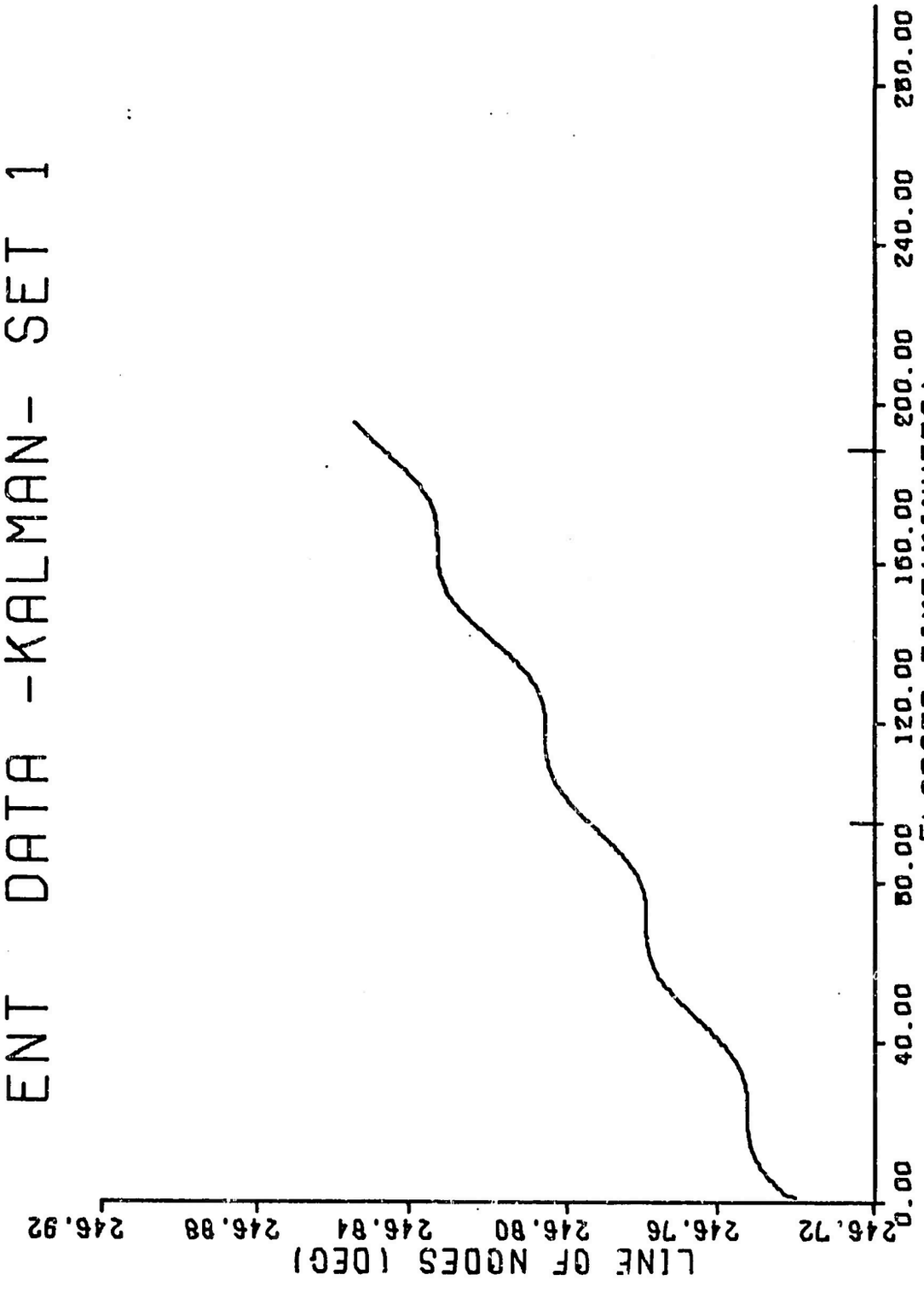

Figure 35. Line of Nodes Ent Set 1

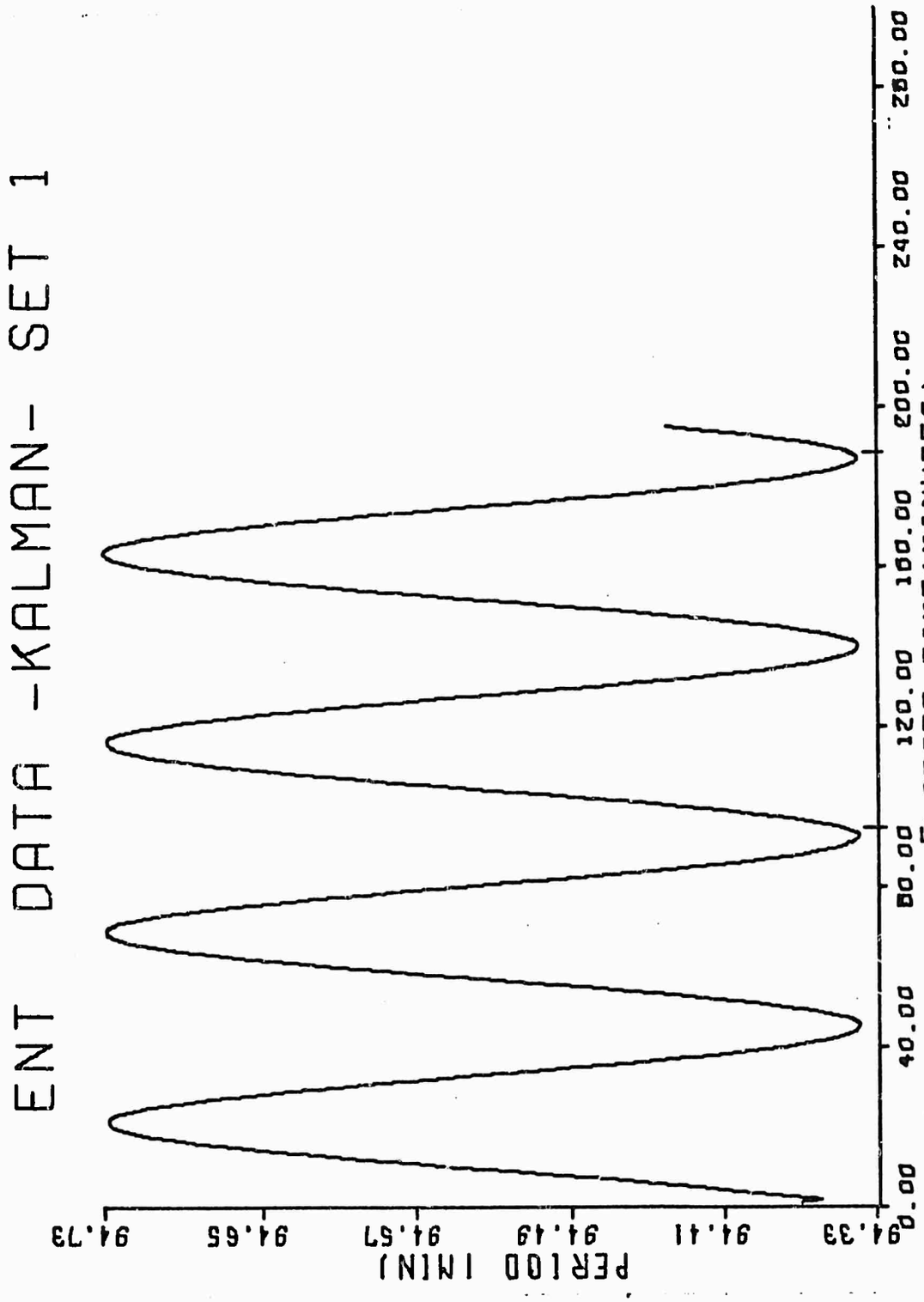

Figure 36. Period Ent Set 1

Kalman Smoothing. The smoothing capability exhibited by the fixed point smoother using simulated orbit data was not as effective when applied to true data. Primary causes for this are the loss of a white Gaussian distribution due to a smaller number of observations applied to the smoothing algorithm as well as the inability of the filter to stabilize the orbital parameters as quickly using the real data. However, stability was achieved during passes 2 & 3 with the results comparing favorably with the Kalman reverse integration as shown in Table XI. In order to obtain a maximum number of measurements the point being smoothed was the first observation point for each set of data. This was done at the risk and with the understanding that the desired stability obtained by waiting till the fifteenth point as in the theoretical study would be lost. Although satisfactory results were not obtained for first pass data, no extremely adverse effects were noted and the smoother was gradually bringing the unstable first observation parameters toward the actual parameters although hampered severely by a lack of measurements in each of the first two data sets (1a and 1b). The secular varying terms, line of nodes and argument of perigee, are again noted as failing in all cases to reach an acceptable value. Smoothing at points five and fifteen was also performed with no appreciable difference in the results.

Table XI

Smoothing Data at First Observations

Ent Set 1

	Kalman Reversed	WLS	Smoother
Pass 1a			
t=0., 22 observations used for smoothing.			
Semi-Major Axis (E.R.)	1.07638	1.07629	1.07342
Eccentricity	.00128	.00126	.00374
Angle of Inclination (Deg)	96.153	96.155	96.160
Line of Nodes (Deg)	246.739	246.745	247.619
Arg. of Perigee (Deg)	332.050	246.745	288.591
Period (Min)	94.352	94.340	93.963
Pass 1b			
t=285.7. 25 observations used for smoothing.			
Semi-Major Axis (E.R.)	1.07695	1.07676	1.07701
Eccentricity	.00162	.00141	.00171
Angle of Inclination (Deg)	96.151	96.153	96.162
Line of Nodes (Deg)	246.746	246.749	247.733
Arg. of Perigee (Deg)	3.711	347.809	6.378
Period (Min)	94.429	94.395	94.541

Smoothing Data at First Observations (Cont.)

Pass 2

t=5655.2. 33 observations used for smoothing.*

Semi-Major Axis (E.R.)	1.07636	1.07627	1.07639
Eccentricity	.00126	.00119	.00116
Angle of Inclination (Deg)	96.153	96.156	96.154
Line of Nodes (Deg)	246.795	246.799	248.136
Arg. of Perigee (Deg)	336.732	315.589	313.768
Period (Min)	94.348	94.336	94.353

Pass 3

t=11465.5. 35 observations used for smoothing.*

Semi-Major Axis (E.R.)	1.07655	1.07645	1.07655
Eccentricity	.00149	.00139	.00150
Angle of Inclination (Deg)	96.153	96.155	96.153
Line of Nodes (Deg)	246.851	246.855	247.704
Arg. of Perigee (Deg)	344.000	332.569	344.984
Period (Min)	94.374	94.361	94.371

*A steady state was achieved.

Interpass Pointing Data. Table XII shows the values for the measurements and the predicted values of the range, range rate, azimuth and elevation. These results are extremely similar to those obtained in the theoretical case and certainly are adequate to provide pointing information.

Filter Covariance. Graphs of the position and velocity covariance of the x parameter are shown in figures 35 and 36. These graphs exhibit only slightly differing characteristics from those found in the theoretical case. The time lag between pass 1a and 1b is seen to be small enough that the covariance does not increase significantly. However, Figure 39 shows a graph of the total position standard deviation as defined by equation 63. The standard deviation is seen to rise during pass 1b. Although this diverging tendency is not sufficient to cause filtering problems, the smoothing algorithm as seen in equations 38 through 40 is hampered by this behavior. Figure 40 shows the velocity standard deviation. Covariances generated by each of the filters are comparable.

Filter Effectiveness. Both the WLS and the Kalman filters showed a high degree of capability in processing the selected data for a polar circular orbit. Despite known limitations the models provided accurate pointing information. The smoothing algorithm provided no useful additional information during pass 1 but functioned as expected during passes 2 and 3.

Table XII

Interpass Pointing Data Ent Set 1

Pass	Source	Range (meters)	Range Rate (meters/second)	Elevation (deg)	Azimuth (deg)
1a-1b	WLS	856125	4784	33.59	239.59
1a-1b	Kalman	856136	4790	33.55	239.59
1a-1b	Measure	859086	4785	32.50	239.52
1b-2	WLS	1726472	-3848	10.05	348.06
1b-2	Kalman	1829049	-4353	8.55	353.03
1b-2	Measure	1822414	-4333	8.70	352.48
2-3	Kalman	2338937	-5107	2.58	348.35
2-3	Measure	2334897	-5099	2.72	348.12

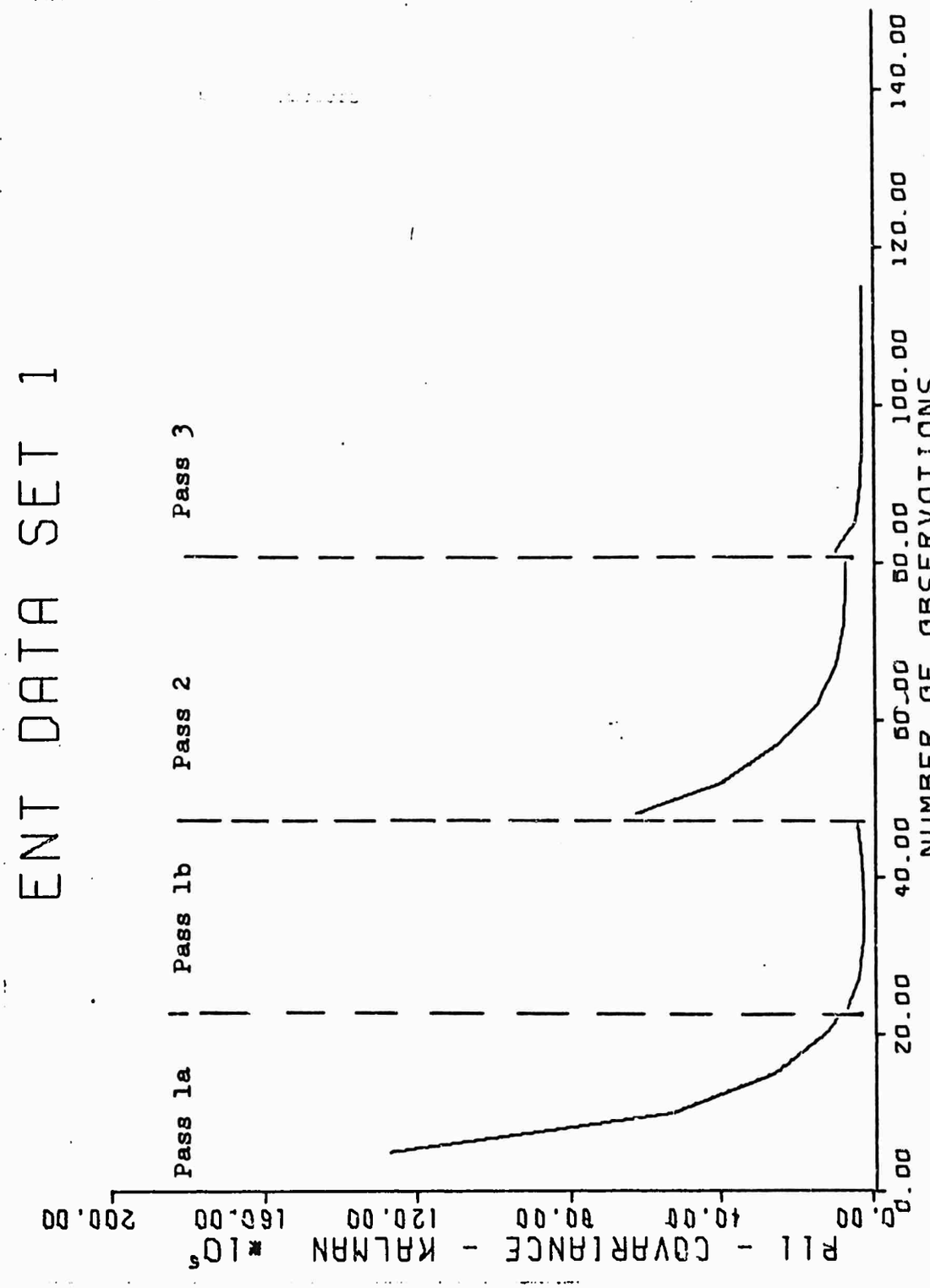

Figure 37. Covariance of P_{xx}, Ent Set 1

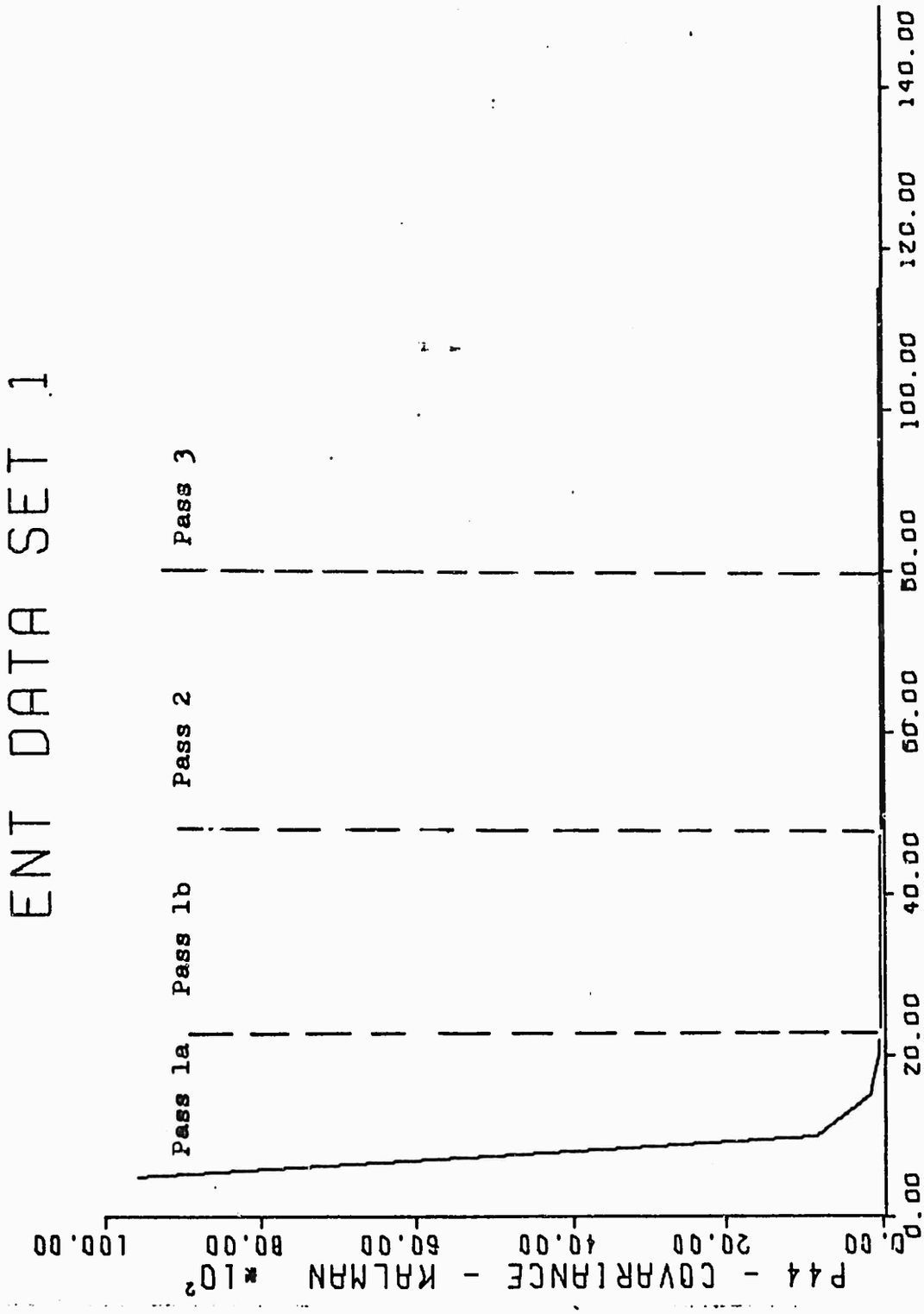

Figure 38. Covariance of P_{xx}, Ent Set 1

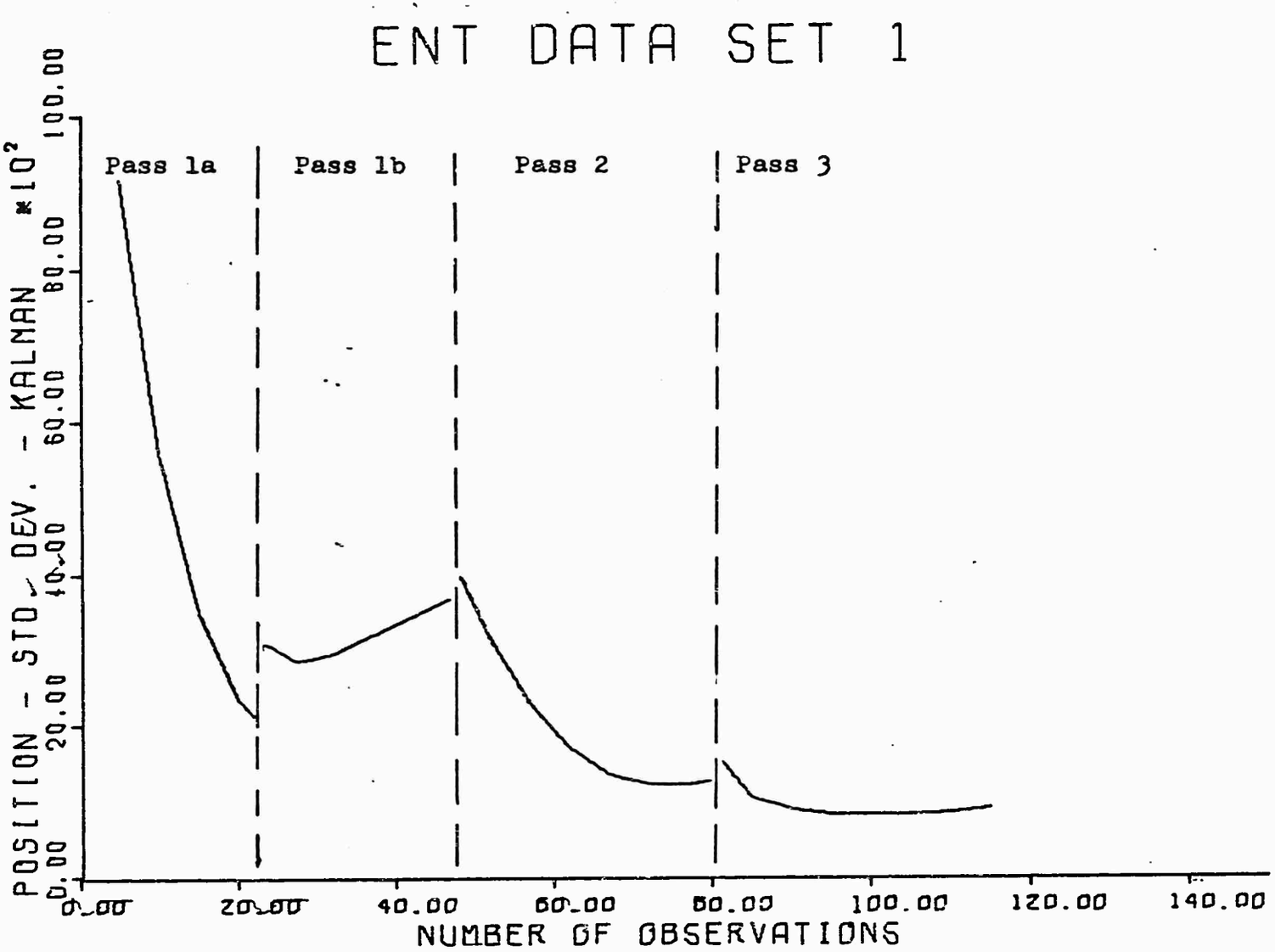

Figure 39. Standard Deviation of Position, Ent Set 1

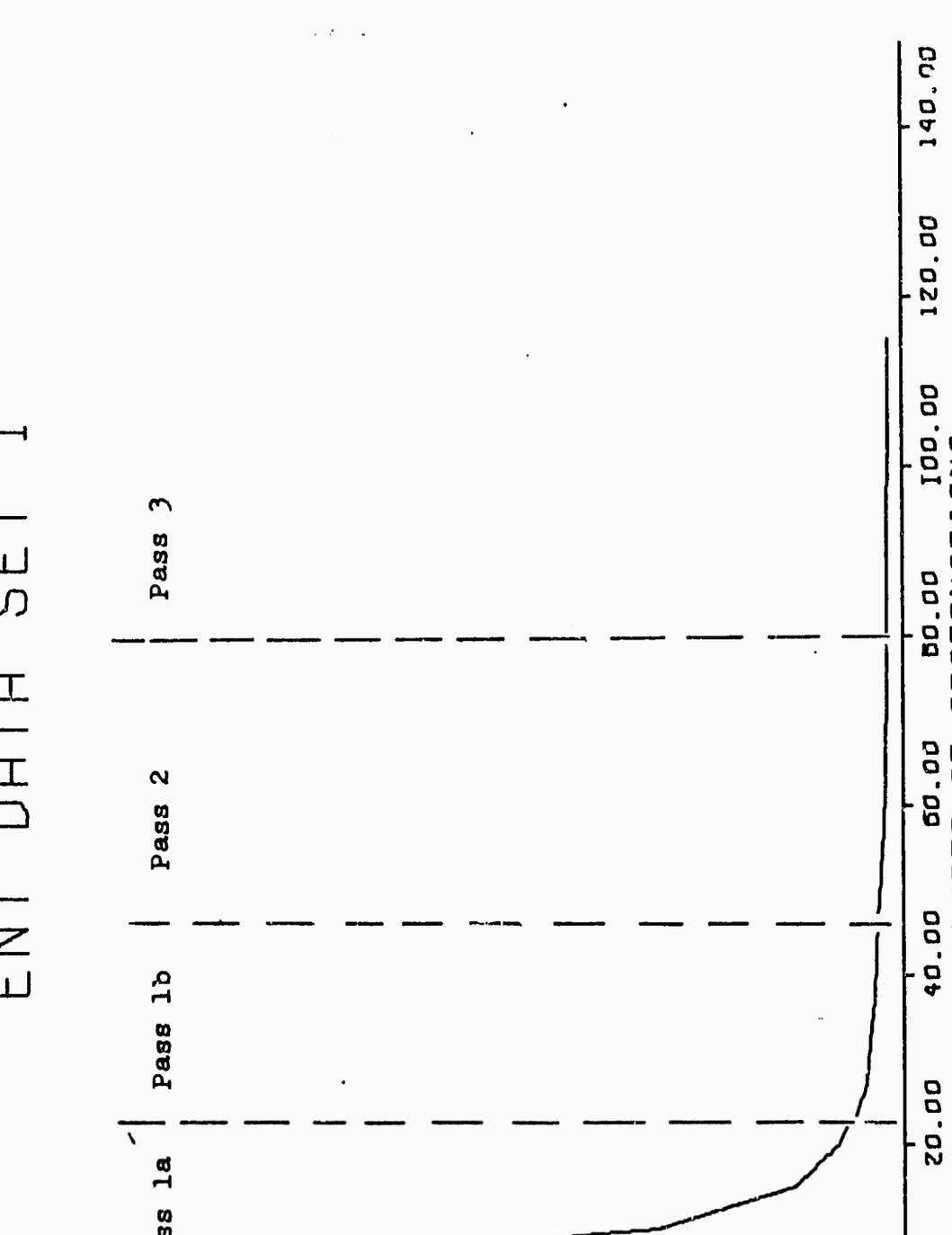

Figure 40. Standard Deviation of Velocity, Ent Set 1

Chapter VII

Actual Data: Ent Set 2

Data. Data for the orbit of satellite 6100 was supplied by the 1st Aerospace CON Squadron, Ent AFB, Colorado for use in this study. This data was processed at Ent using a general perturbations least square error processor (SQEPRI3C). The Ent data consisted of 74 observations of range, range rate, azimuth, and elevation. The results were presented at an epoch time corresponding to the time at which the vehicle crossed the equitorial plane ascending in a northerly direction. The details of the data are presented in Table XIII.

Radar Characteristics. Sensor 344 was used exclusively for this study. The parameters of this radar are given by Table XIV as they were supplied by Ent. The sigmas given are actually extremely high for the data of this study and more attention wi-l be given this problem later in this chapter.

Comparison of Orbital Parameters. The orbital parameters supplied by Ent were of the mean or general perturbations type (Ref 21:231). To compare these parameters with those obtained by the filters, a graphical analysis of the orbital parameters is presented in figures 39 through 48. The results of this analysis are presented in Table XV. It should be noted at this point that the processor used by Ent found the data divergent although it obtained an orbit where the residuals were extremely small and therefore the orbital parameters approximately truly determined. The parameters found by the WLS filter are comparable to those obtained by the Ent processor when the divergence of the Ent processor is considered.

Table XIII

Orbit Data Ent Set 2

Satellite #6100 Day 215 Year 72

g_o = 20 hr 42 min 57.365 sec (Ref Appendix F)

Start GMT = 9 hr 25 min 39.134 sec

Pass	Obs Int	No. of Observations	Duration Pass Min Sec	Station	Duration Gap Min Sec
1	6 sec	30	3:00	344	
					104:34
2	6 sec	44	4:24	344	

Table XIV

Sensor #344 Ent Set 2 Parameters

Position

Longitude:	185.89769°W
Latitude:	52.73267°N
Height:	86. meters

Measurement Biases

Range:	+160 m
Range Rate:	1 m/sec
Elevation:	.063°
Azimuth:	-.019°

Measurement Sigmas

Range:	852 m
Range Rate:	12.8 m/sec
Azimuth:	.426 deg
Elevation:	.304 deg

Table XV

Ent Data Set 2 General Perturbations

Epoch Time: Day 215 Hour 10 Min 55 Sec 19.920

Elements	Ent**	Kalman	WLS***
Semi-Major Axis (E.R.)	1.178309	1.1793	1.1783
Eccentricity	.122512	.1236	.1245
Angle of Inclination (Deg)	48.4313°	48.453°	48.422°
Line of Nodes (Deg)	255.6498°	255.3691°	255.3046°
Arg. of Perigee (Deg)	172.2760°	171.4976°	171.9439°
Period (Min)	108.0	108.20	108.05
Height at Perigee (Km)	216 Km	216	205

**Failed Convergence

***Converged in 5 iterations

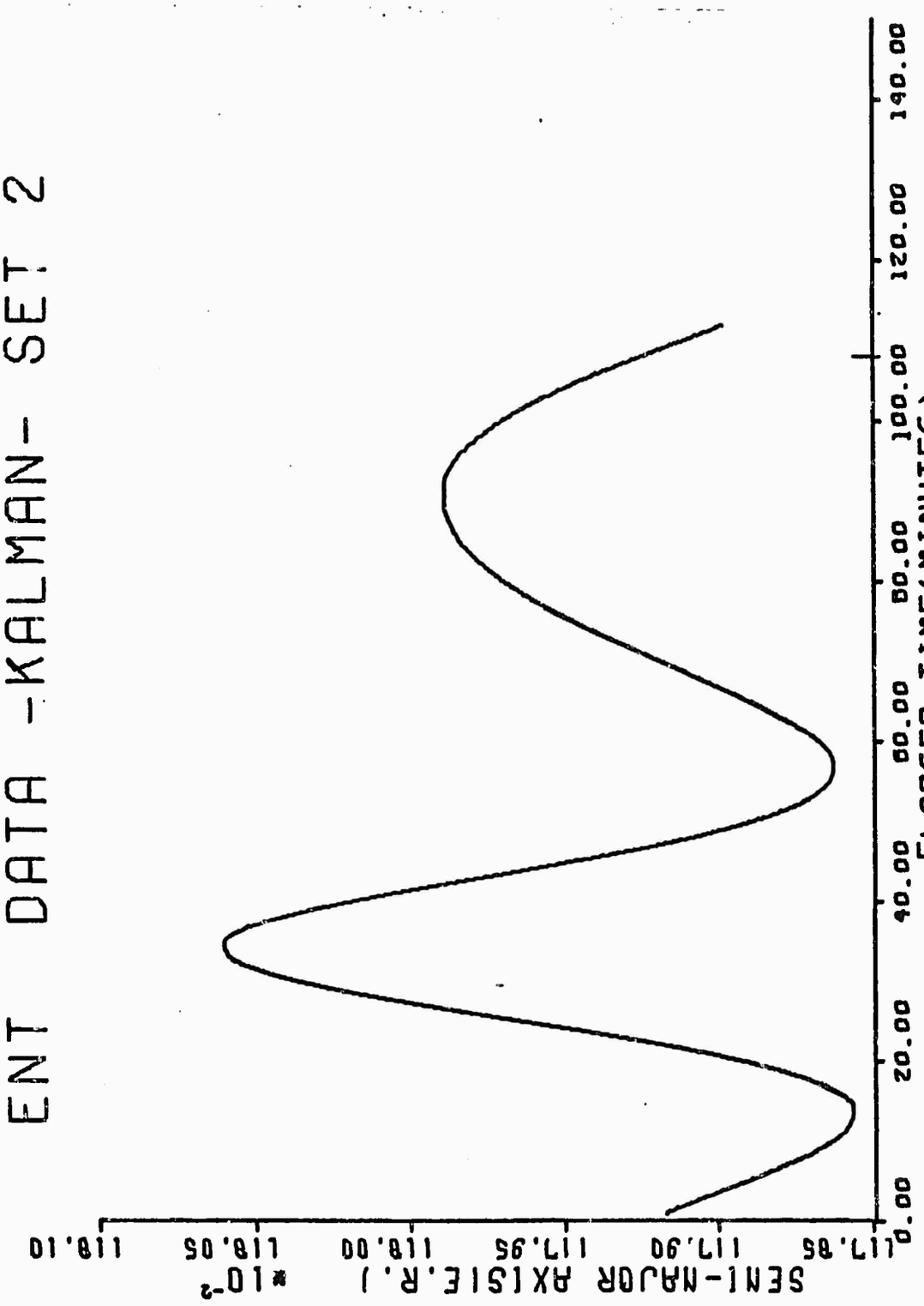

Figure 41. Semi-Major Axis, Kalman, Ent Set 2

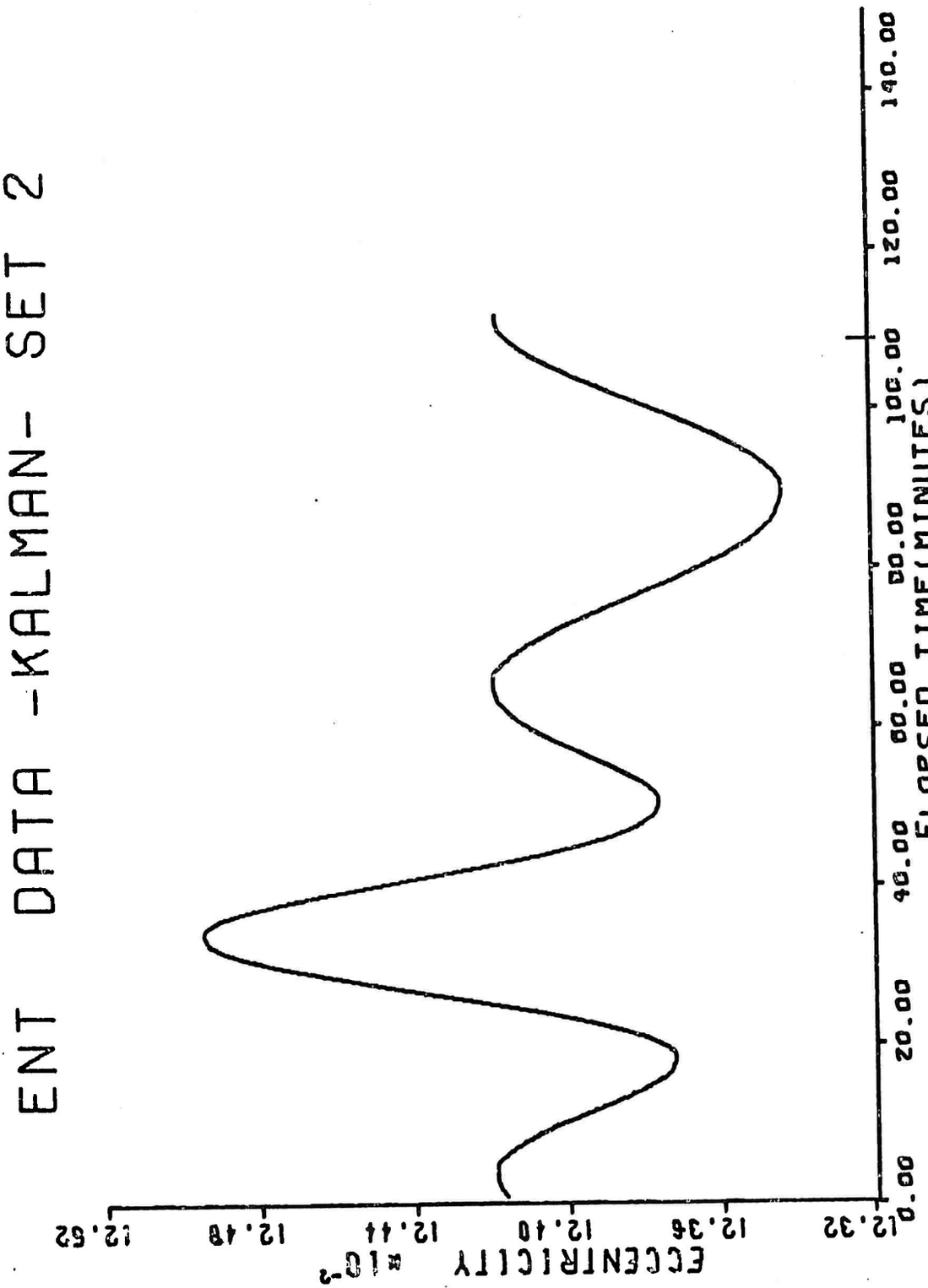

Figure 42. Eccentricity, Kalman, Ent Set 2

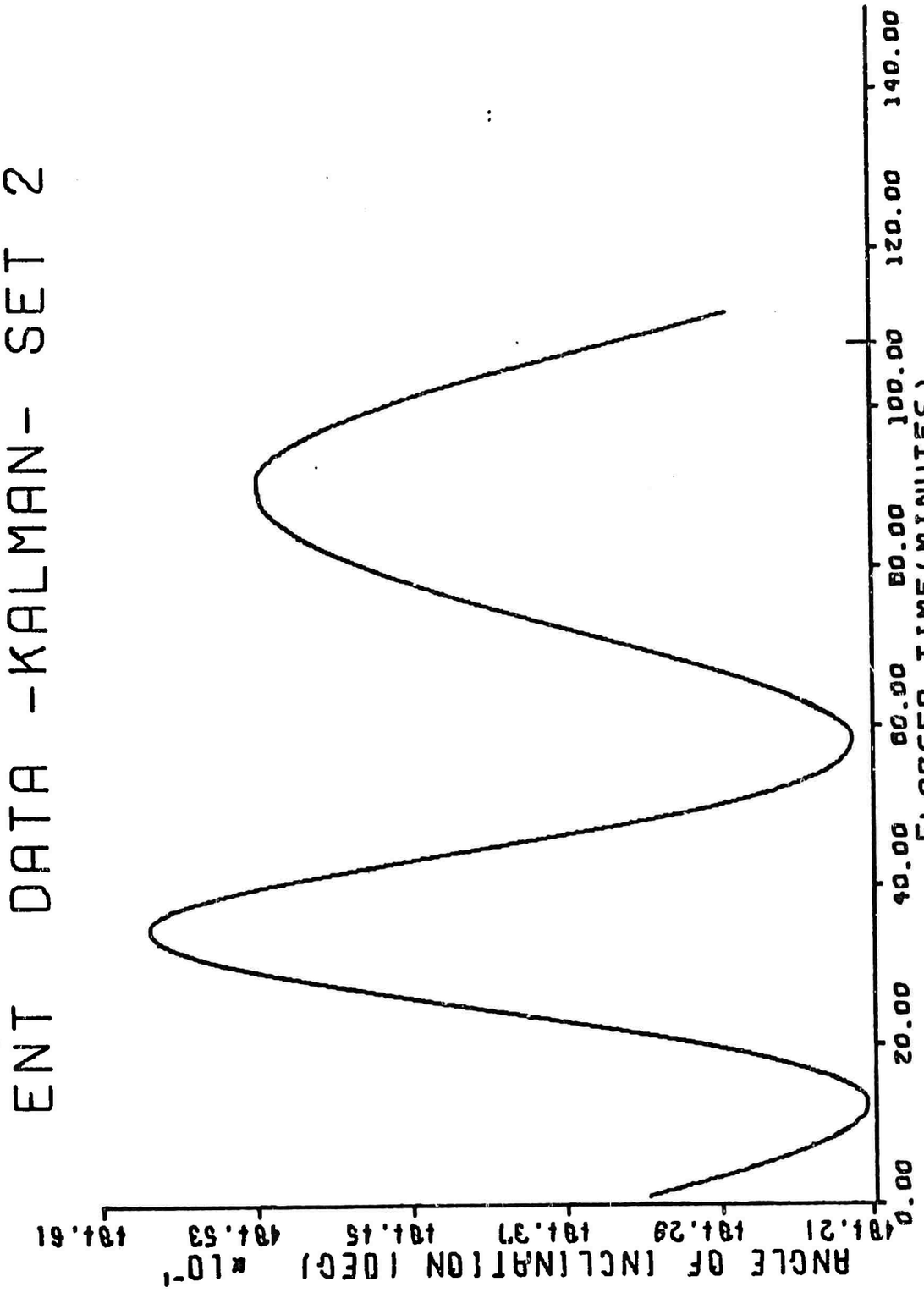

Figure 43. Angle of Inclination, Kalman, Ent Set 2

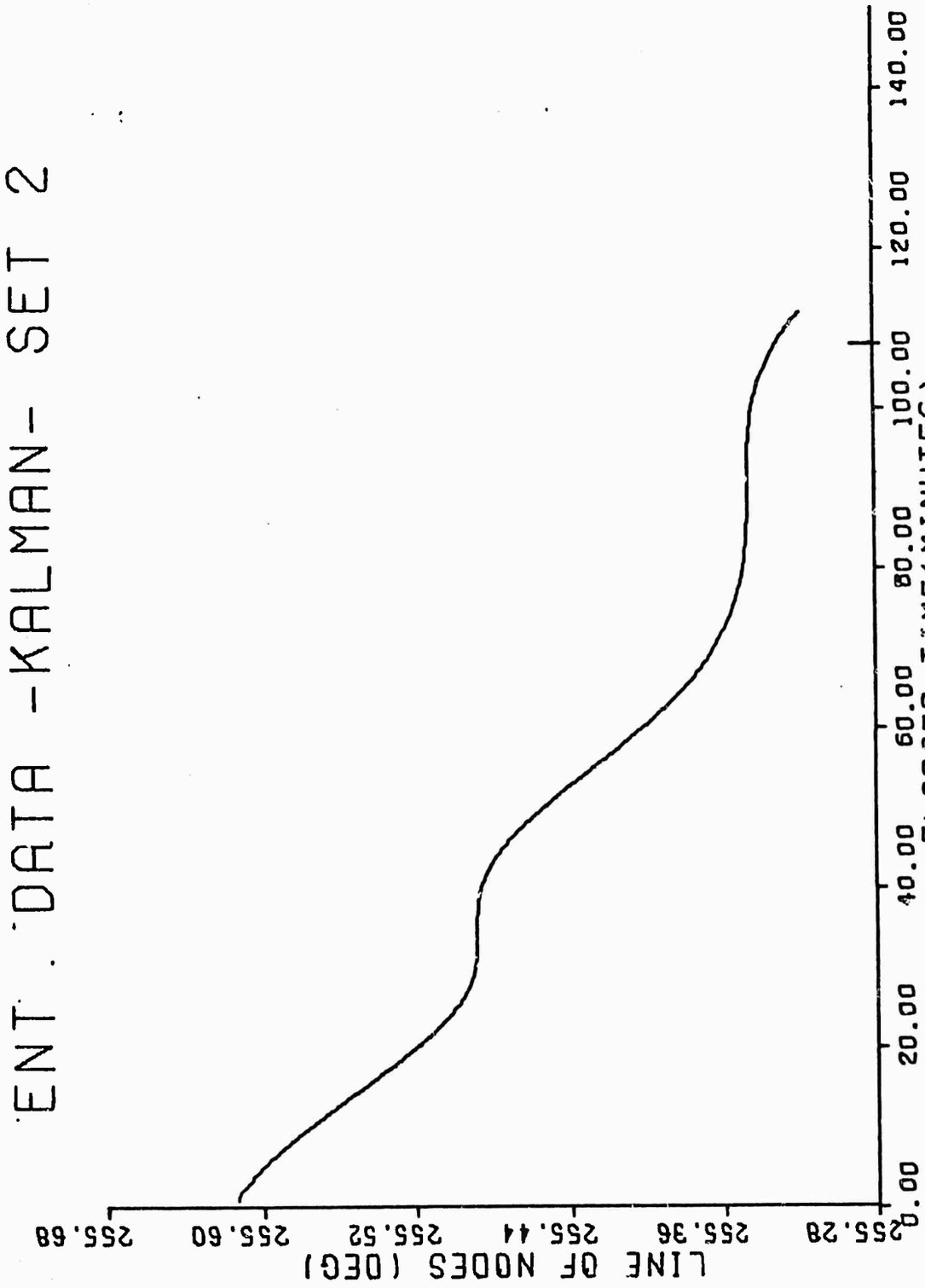

Figure 44. Line of Nodes, Kalman, Ent Set 2

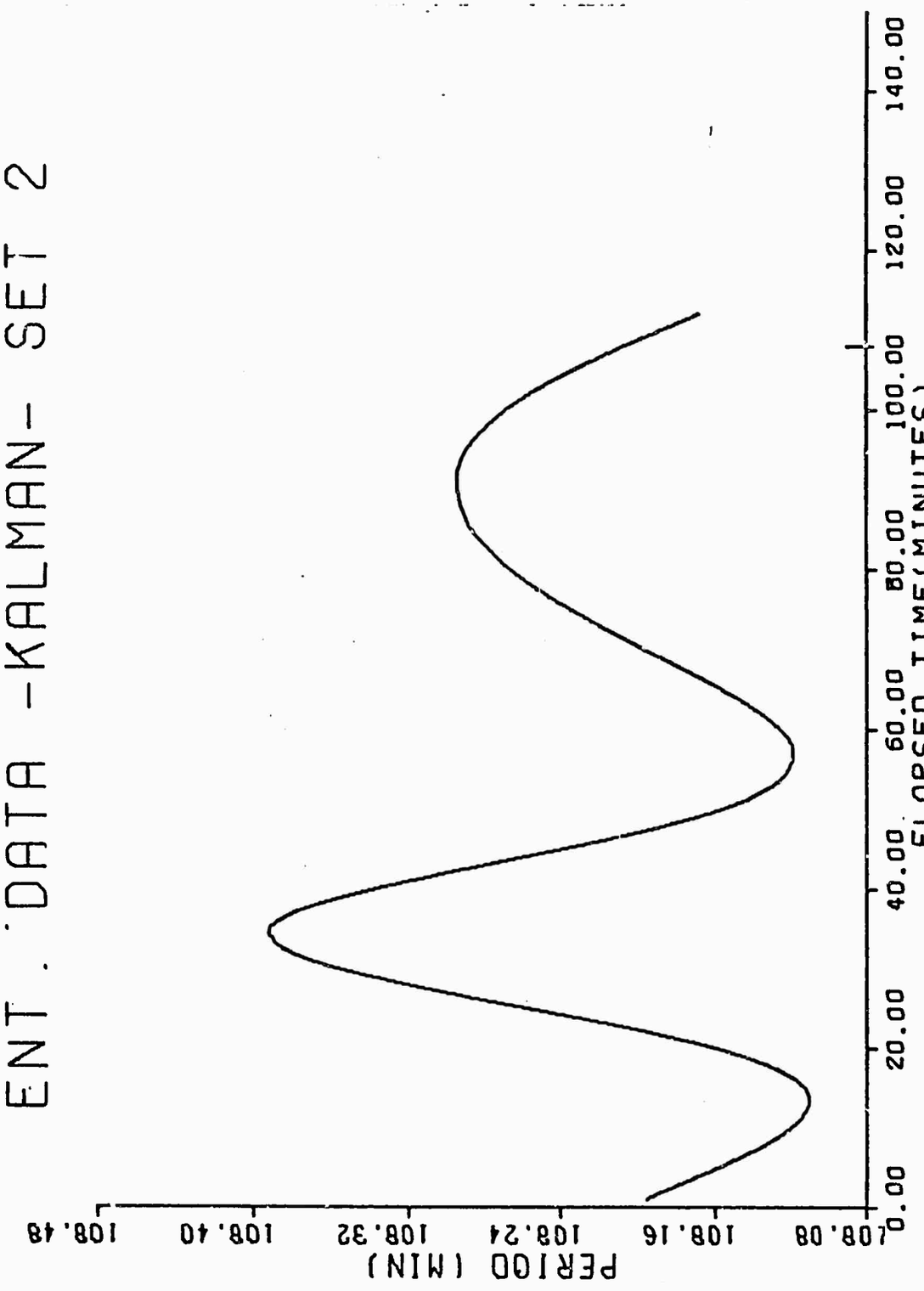

Figure 45. Period, Kalman, Ent Set 2

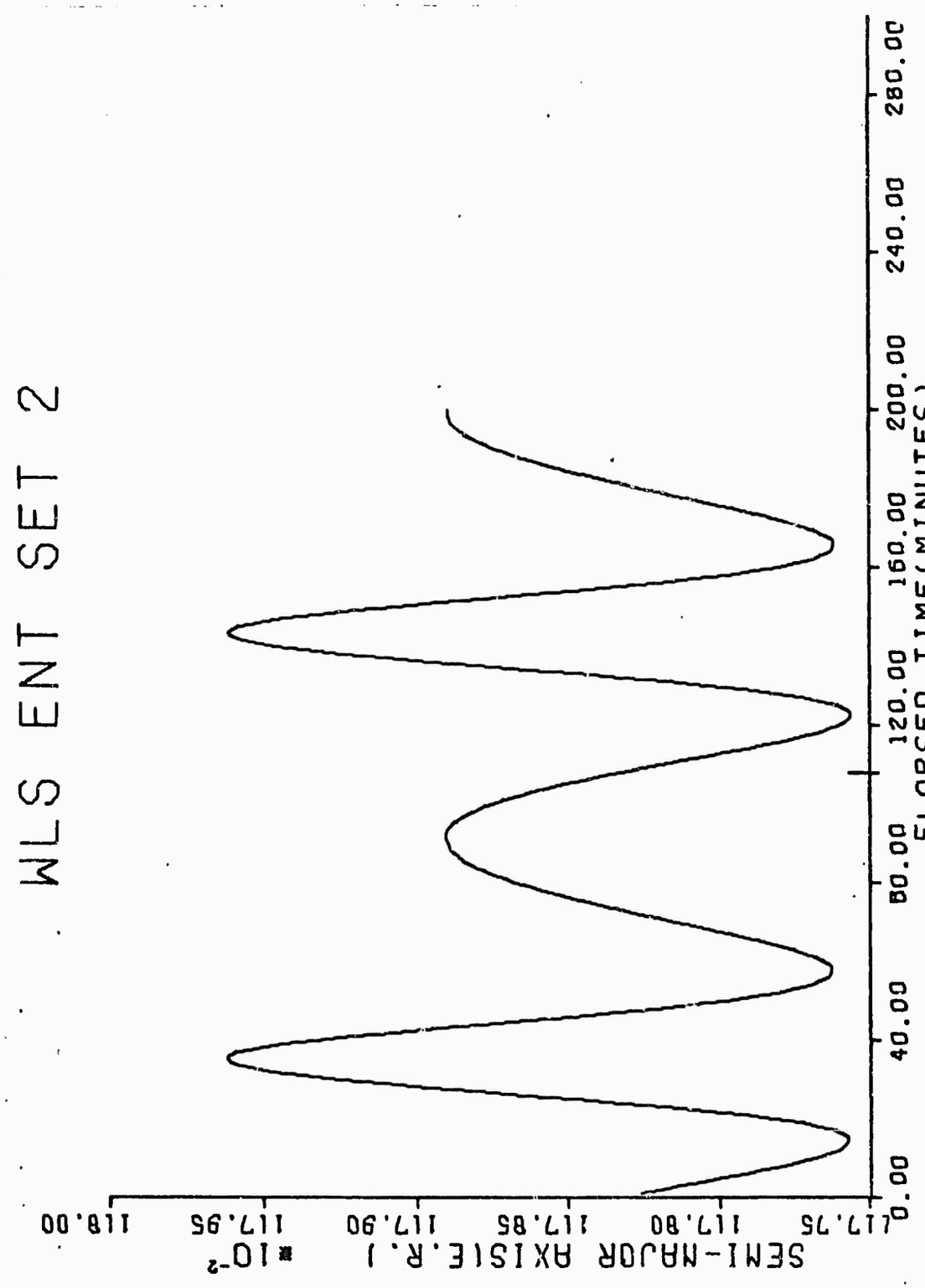

Figure 46. Semi-Major Axis, WLS, Ent Set 2

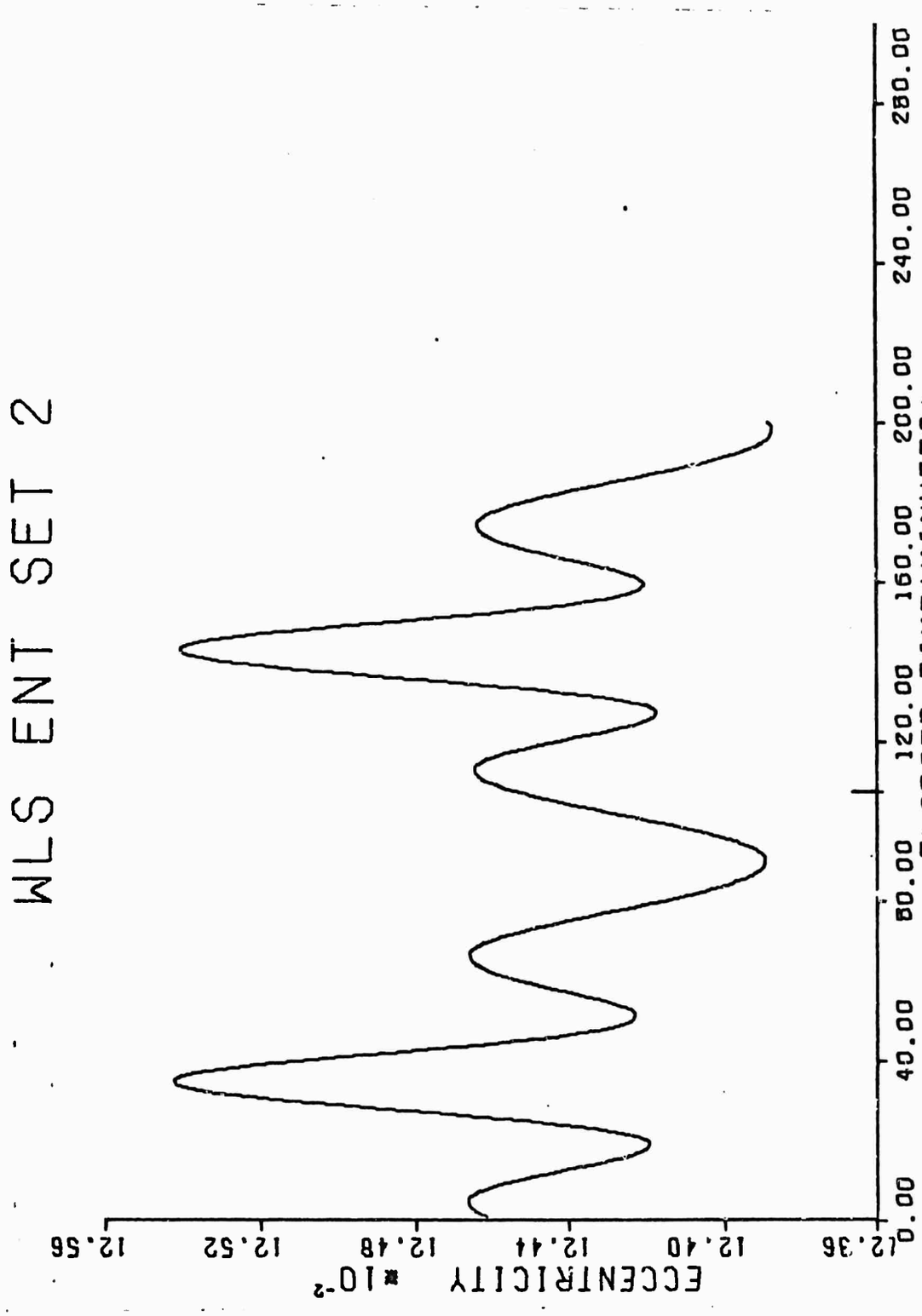

Figure 47. Eccentricity, WLS, Ent Set 2

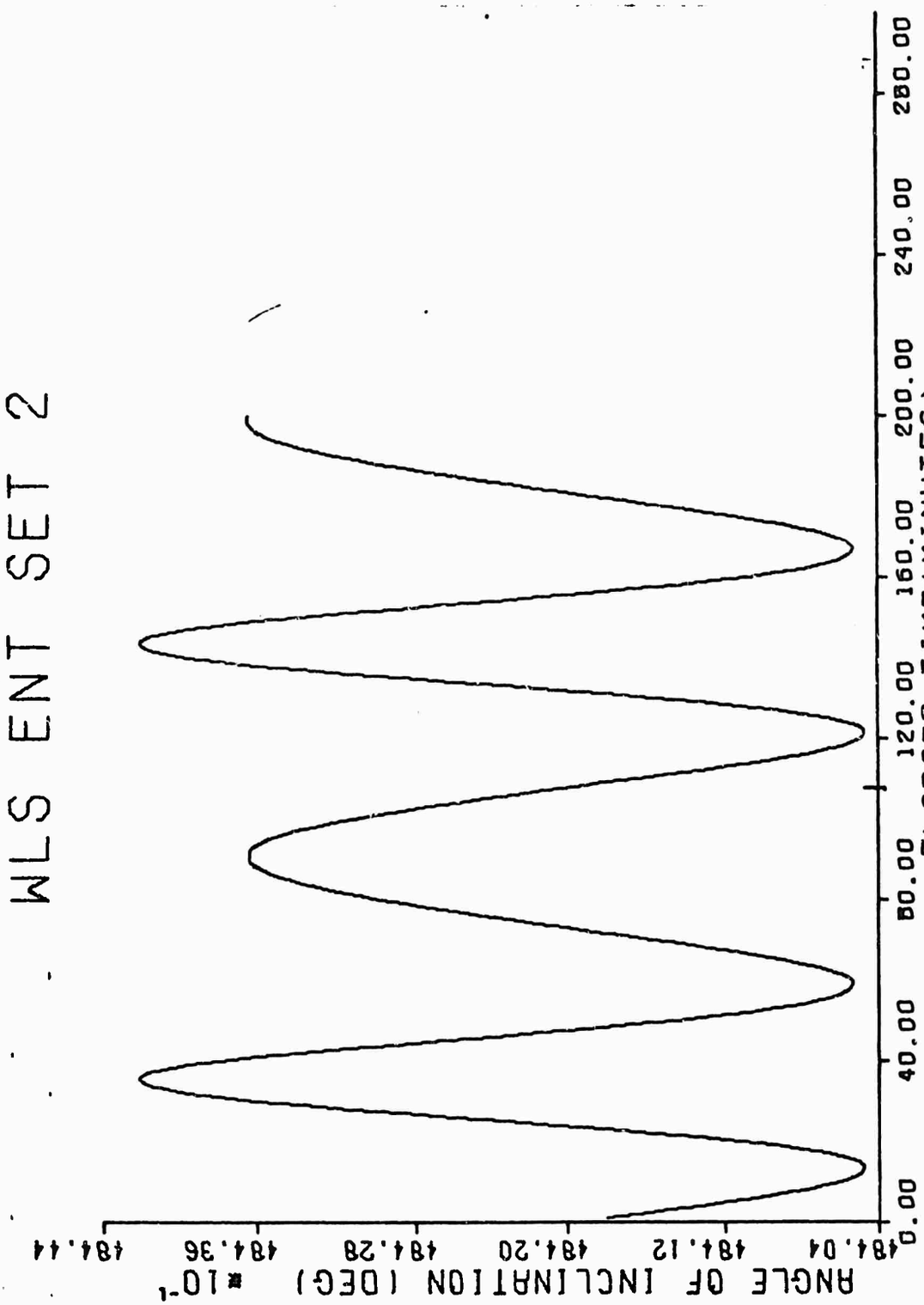

Figure 48. Angle of Inclination, WLS, Ent Set 2

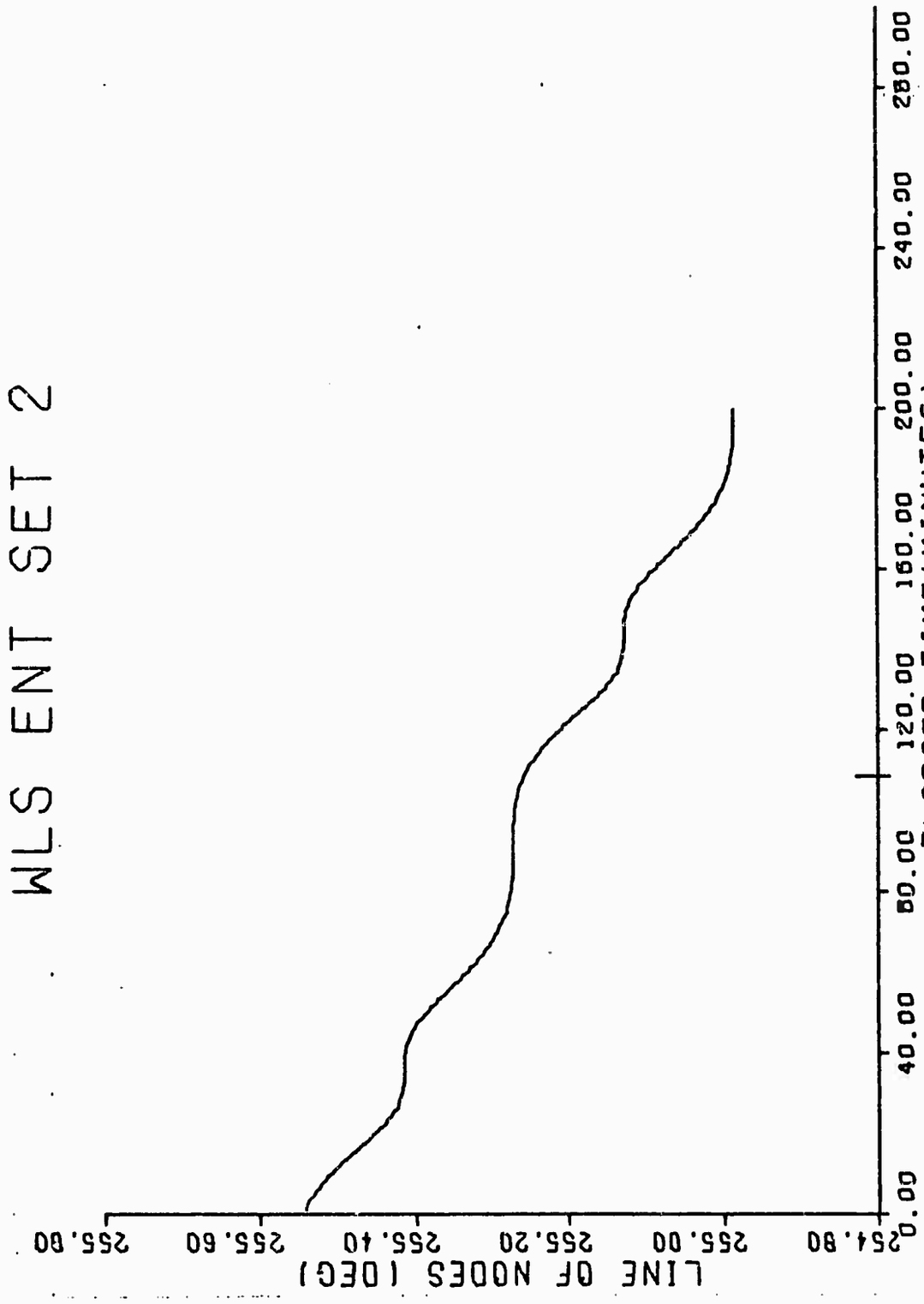

Figure 49. Line of Nodes, WLS, Ent Set 2

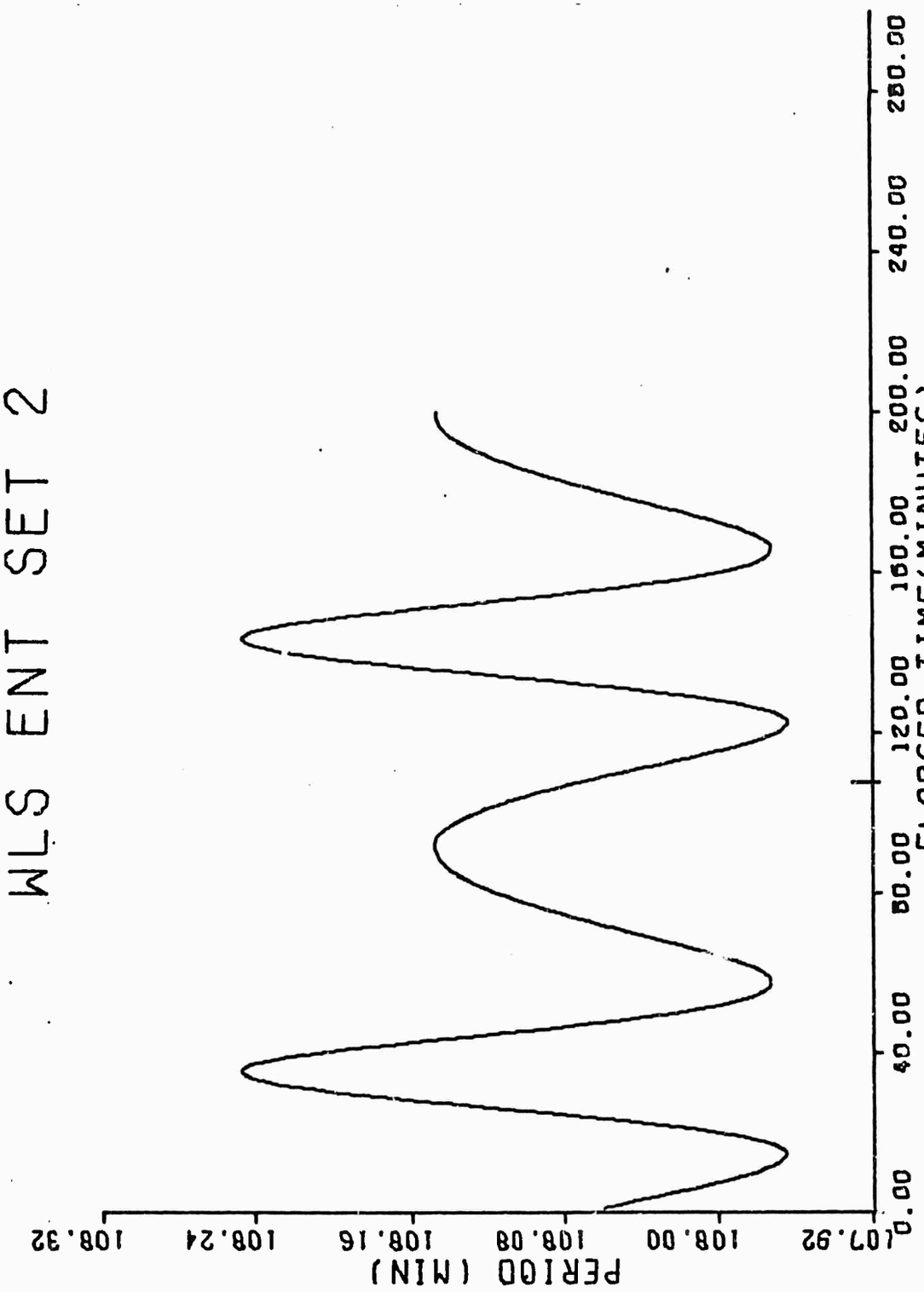

Figure 50. Period, WLS, Ent Set 2

Table XVI

Ent Data Set 2

Special Perturbations

Epoch Time: Day 215 Hour 10 Min 55 Sec 19.920

Elements	Kalman Reversed	Kalman Revised	WLS Predicted**
Semi-Major Axis (E.R.)	1.179962	1.179216	1.178903
Eccentricity	.123101	.122853	.123895
Angle of Inclination (Deg)	48.4691°	48.4544°	48.4364°
Line of Nodes (Deg)	255.3457°	255.3036°	255.2716°
Arg. of Perigee (Deg)	171.5305°	171.8982°	171.9950°
Period (Min)	108.294	108.191	108.148
Height at Perigee (Km)	221 km	219 km	209 km
Line of Nodes Rate (Deg/Day)	-3.8363		
Arg. of Perigee Rate (Deg/Day)	3.4751		
Radius (m)	8448541	8432774	8441018
Velocity (m/sec)	6436	6444	6438

**Converged in 5 iterations.

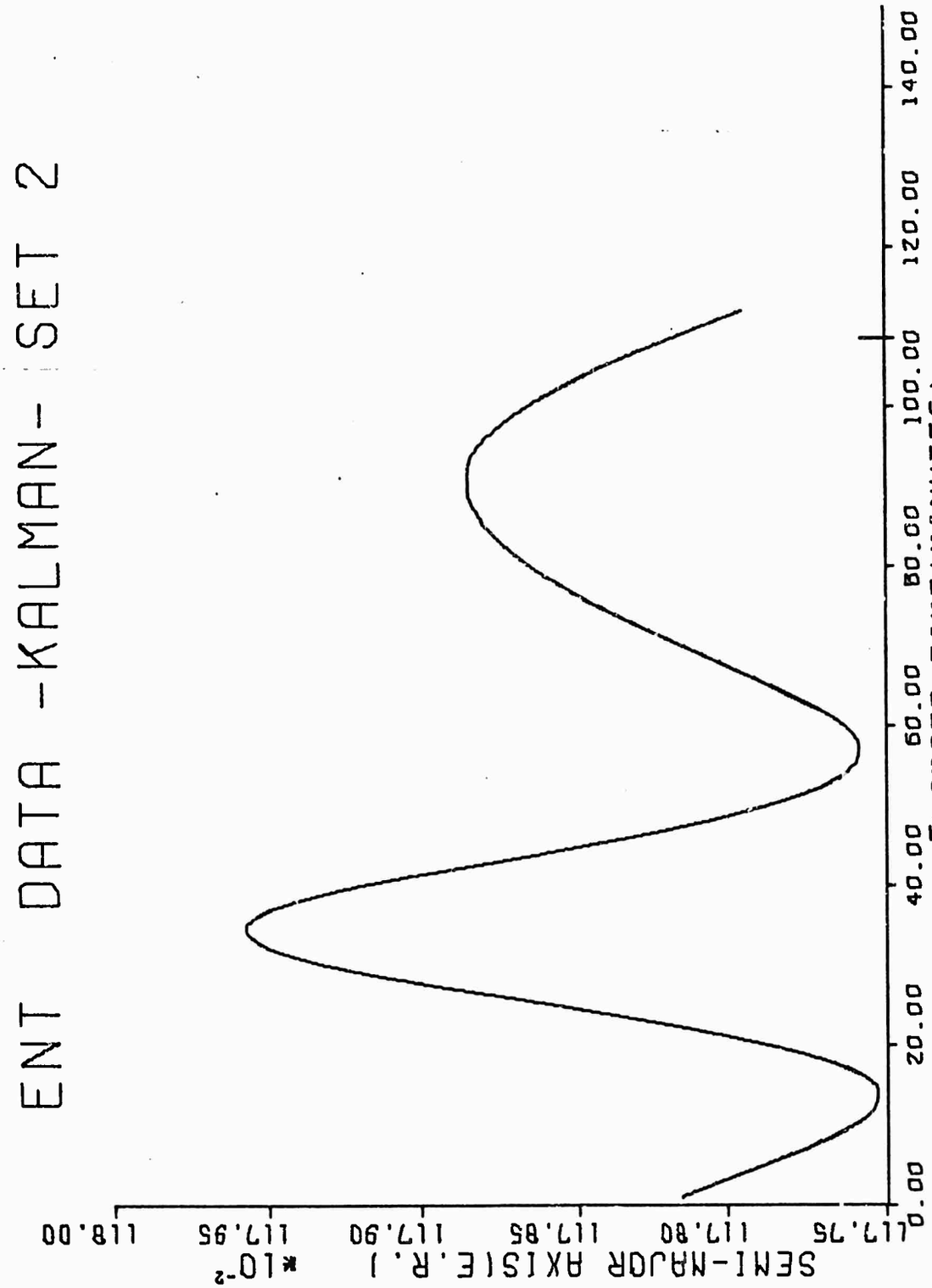

Figure 51. Semi-Major Axis, Kalman Revised, Ent Set 2

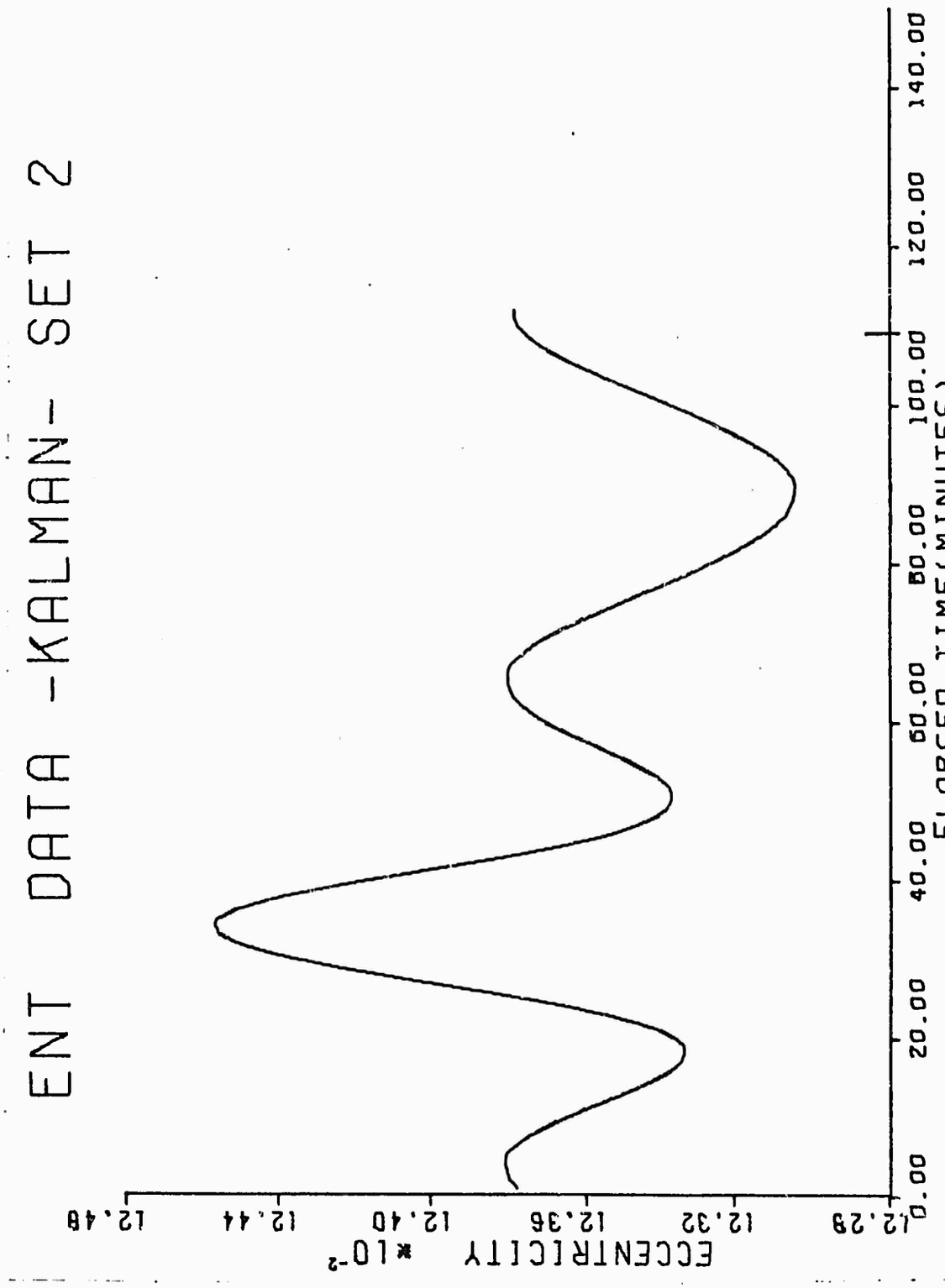

Figure 52. Eccentricity, Kalman Revised, Ent Set 2

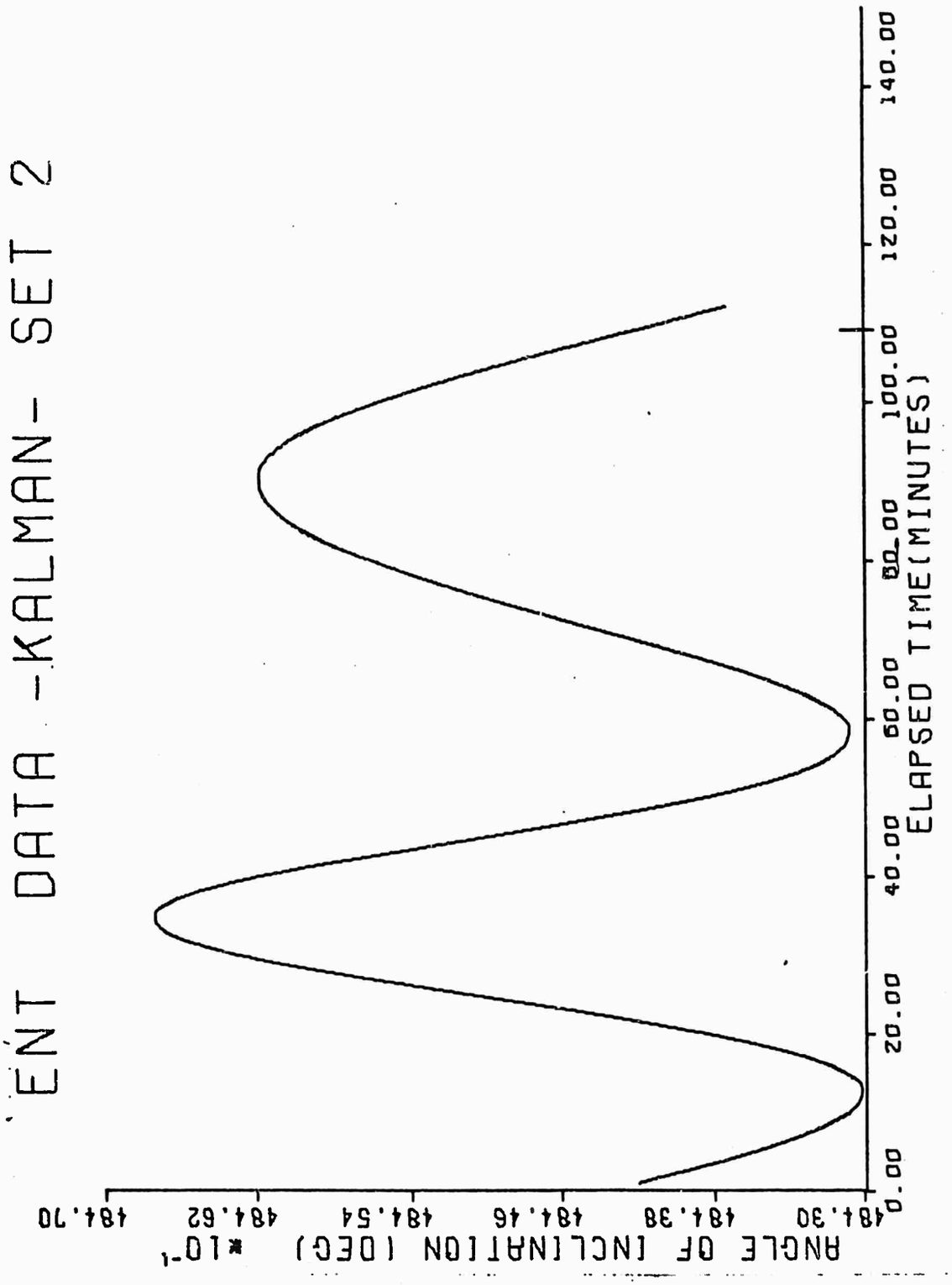

Figure 53. Angle of Inclination, Kalman Revised, Ent Set 2

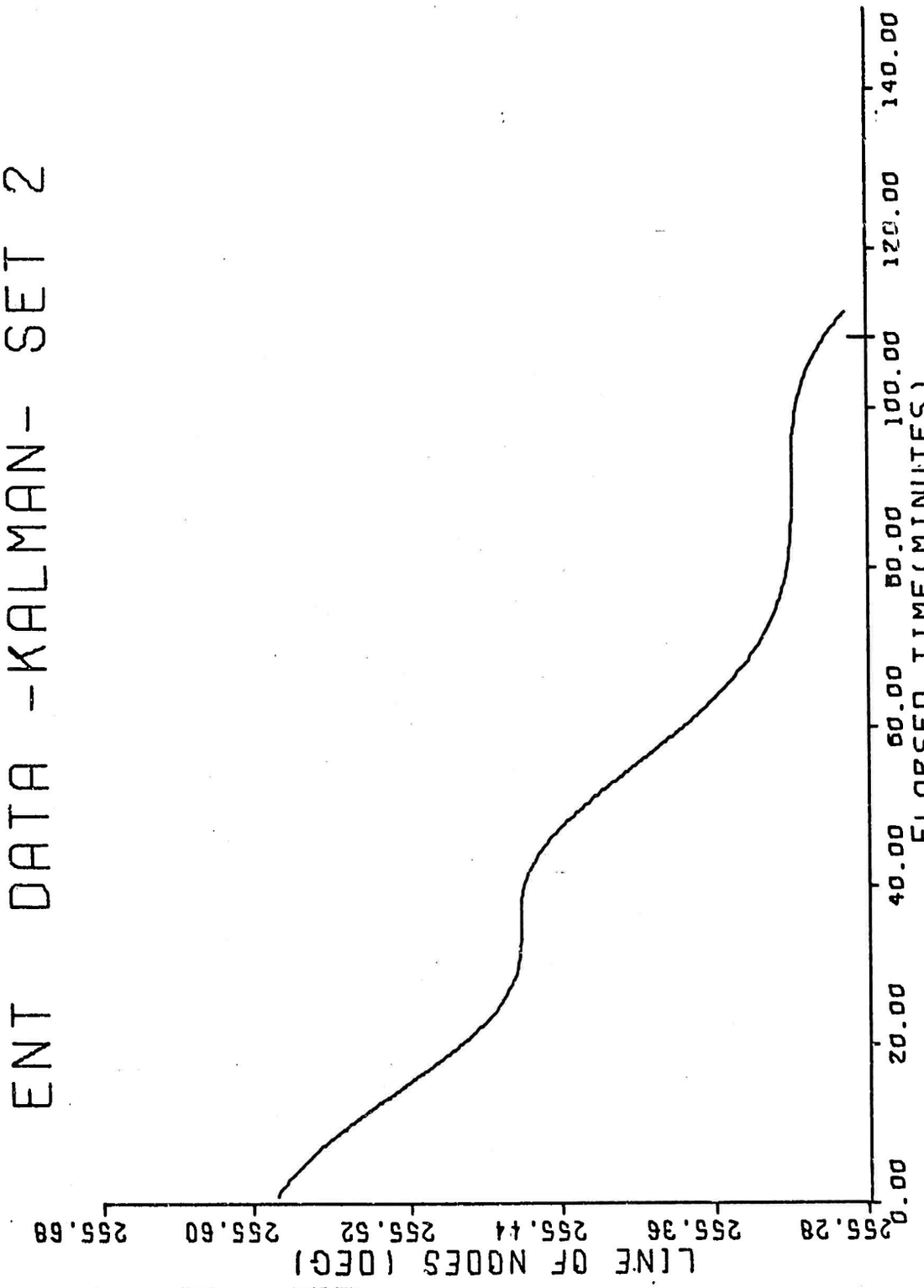

Figure 54. Line of Nodes, Kalman Revised, Ent Set 2

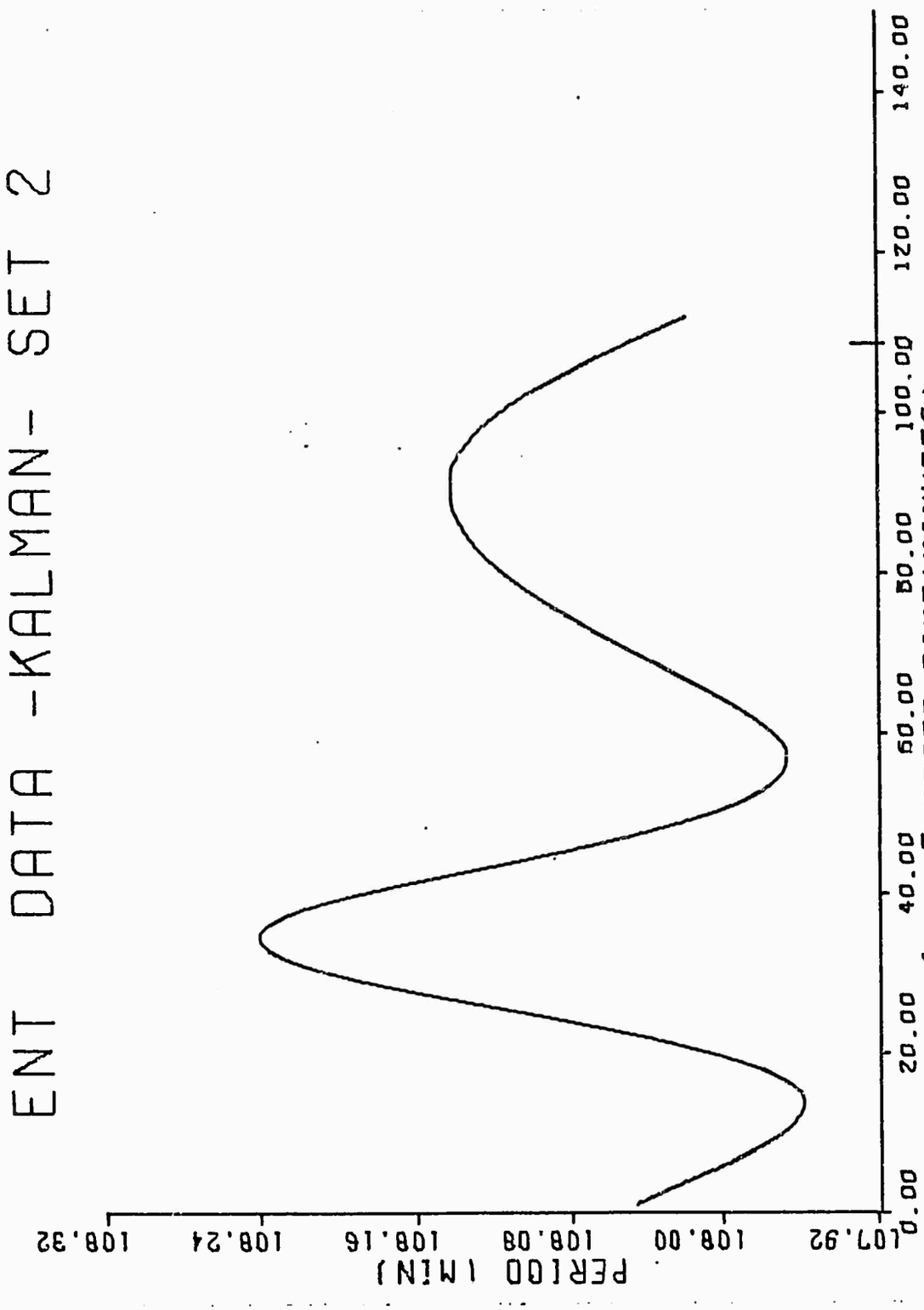

Figure 55. Period, Kalman Revised, Ent Set 2

However, the Kalman filter produced results which were less acceptable with respect to the orbit's period, and angle of inclination. A major cause of this problem was found to be attributable to the statistics supplied with the radar data. While the azimuth sigma was given as .426° actual analysis of the residuals produced by the convergent WLS filter showed that a value of about .025 would be much more acceptable. A similar discrepancy of approximately a factor of 10 was found in the elevation residuals. Repeated runs showed the WLS filter to be rather insensitive to the values chosen for the sigmas with a period of 108.06 minutes occurring repeatably at t_o. Having revised the values of sigma to correspond to those found with the residuals, the Kalman filter program was rerun with the results presented in Table XVI and figures 49 through 53. The new closer comparison with the values obtained by the WLS filter are more representative of the true values.

Kalman Smoothing. The results of the Kalman smoothing of the first observations of each pass are given in Table XVII. As was the case with real data, set 1, no significant results are obtained in pass 1 since insufficient measurements are present to allow a steady state value to be reached. However, pass 2 does achieve a steady state with the values being approximately those found by reverse integrating from the final state produced by the Kalman filter. Table XVII shows the smoothing results.

Covariance of the Filters. The final values of the covariance P are shown in Table XVIII for the orginal Kalman, the revised Kalman, and the WLS. No comparable values were supplied with the Ent data. The covariances of the revised Kalman filter are plotted in figures 54 through 57. The results are typical of those achieved with both the theoretical and Ent data set 1.

Table XVII

Smoothing Data at First Observations, Ent Set 2

Special Perturbations

	Kalman Reversed	WLS	Smoother
Pass 1 t=0., 30 observations used for smoothing.			
Semi-Major Axis (E.R.)	1.17904	1.17826	1.18091
Eccentricity	.12385	.12462	.12162
Angle of Inclination (Deg)	48.4443	48.4179	48.4743
Line of Nodes (Deg)	255.3169	255.5435	256.3354
Arg. of Perigee (Deg)	171.6493	171.7375	171.152
Period (Min)	108.167	108.060	108.425
Pass 2 t=6454., 44 observations used for smoothing			
Semi-Major Axis (E.R.)	1.17934	1.17828	1.17940
Eccentricity	.12383	.12458	.12379
Angle of Inclination (Deg)	48.4513	48.4184	18.4505
Line of Nodes (Deg)	255.3304	255.2564	256.4090
Arg. of Perigee (Deg)	171.8244	171.9750	171.5110
Period (Min)	108.208	108.063	108.216

Table XVIII

Final Covariances Ent Data Set 2

	Kalman Original	Kalman Revised Sigmas	WLS	WLS Revised Sigmas
P_{xx}	6.23×10^5	1.05×10^5	2.88×10^6	1.00×10^5
P_{yy}	2.17×10^6	5.61×10^4	1.20×10^6	9.90×10^4
P_{zz}	7.94×10^6	1.81×10^5	6.72×10^6	1.43×10^5
$P_{\dot{x}\dot{x}}$	32.45	1.13	37.20	1.15
$P_{\dot{y}\dot{y}}$	47.00	0.89	15.83	0.82
$P_{\dot{z}\dot{z}}$	456.42	7.01	386.90	6.74

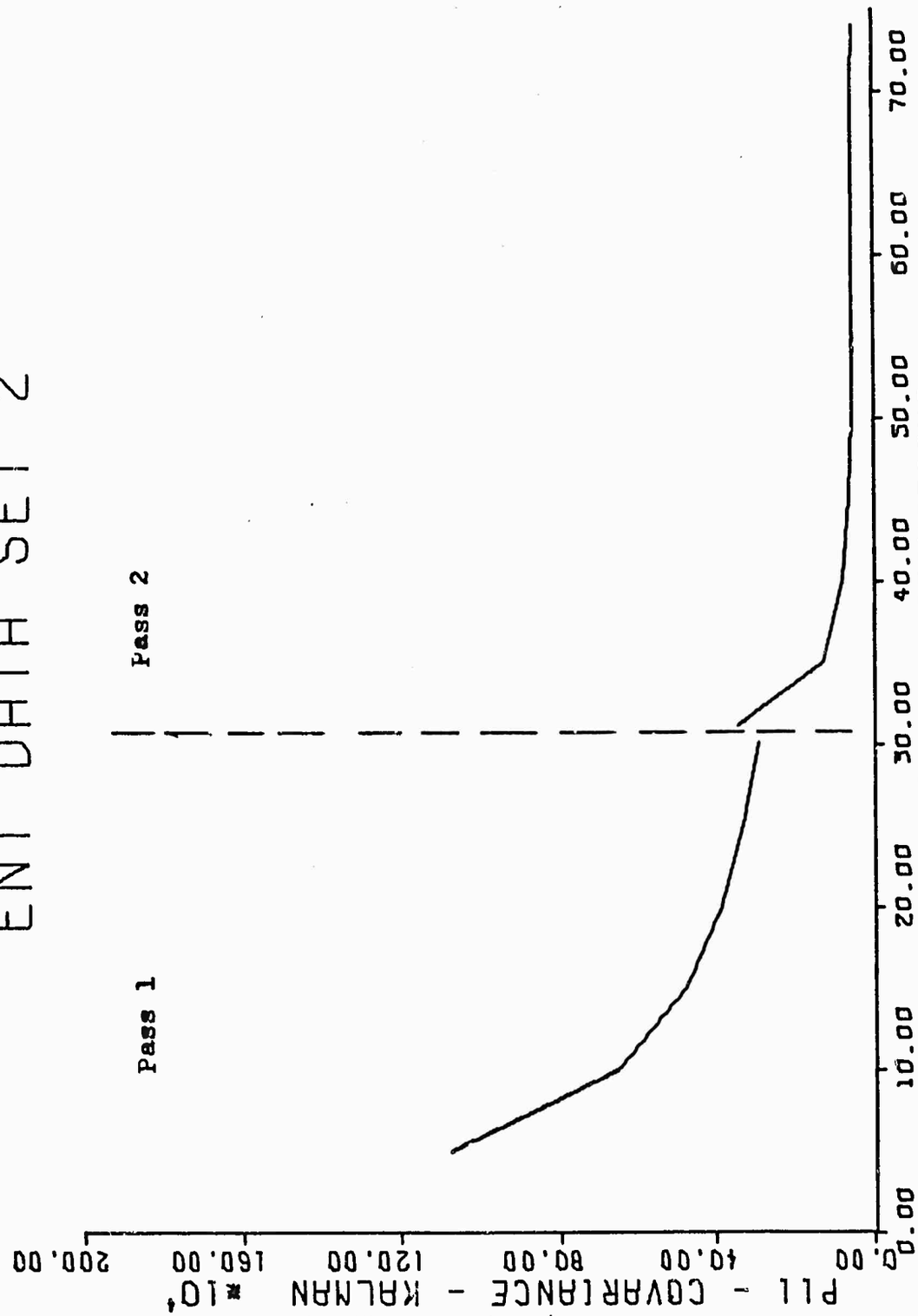

Figure 56. Covariance of P_{xx}, Kalman Revised, Ent Set 2

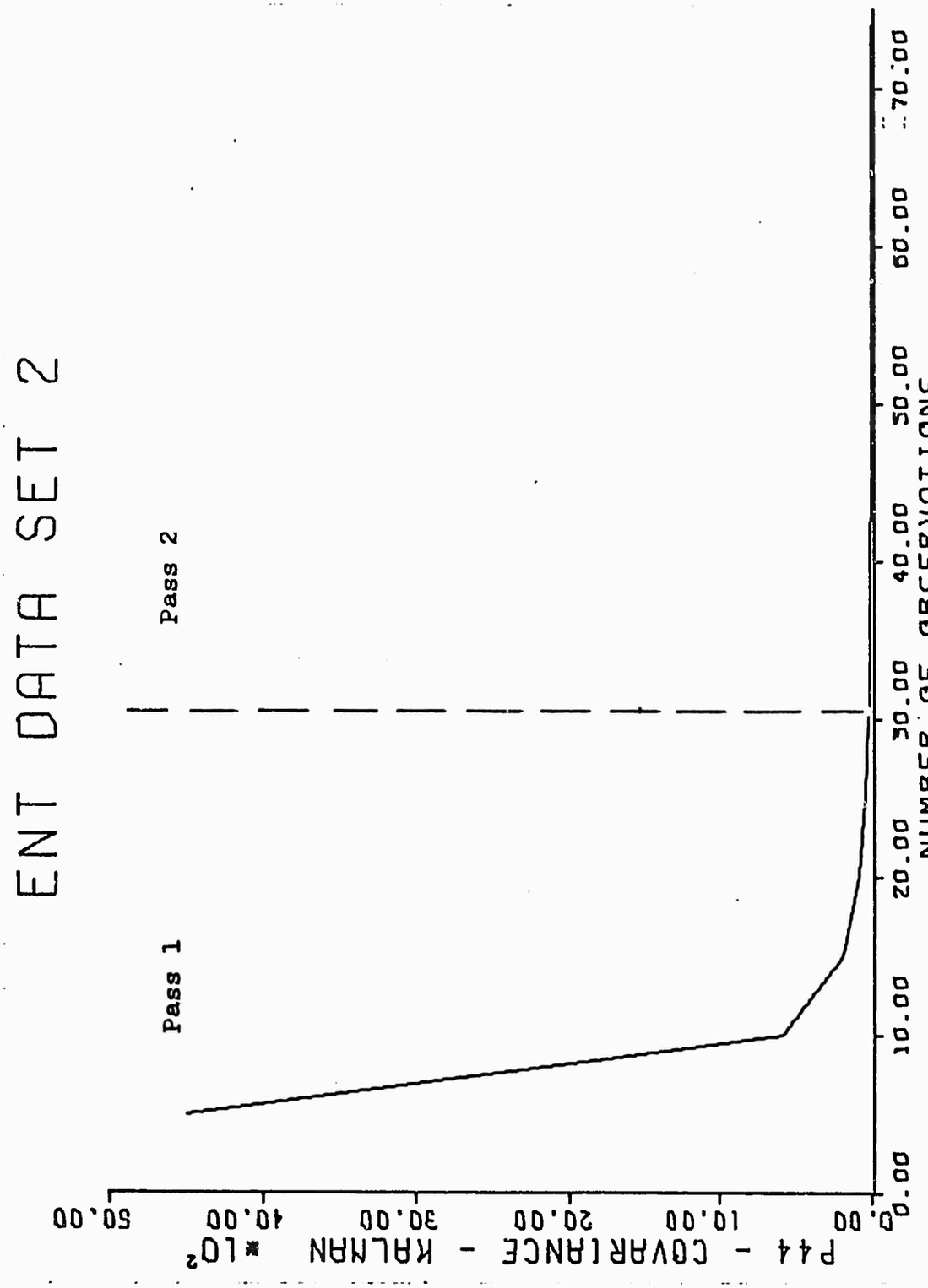

Figure 57. Covariance of P_{XX}^{+}, Kalman Revised, Ent Set 2

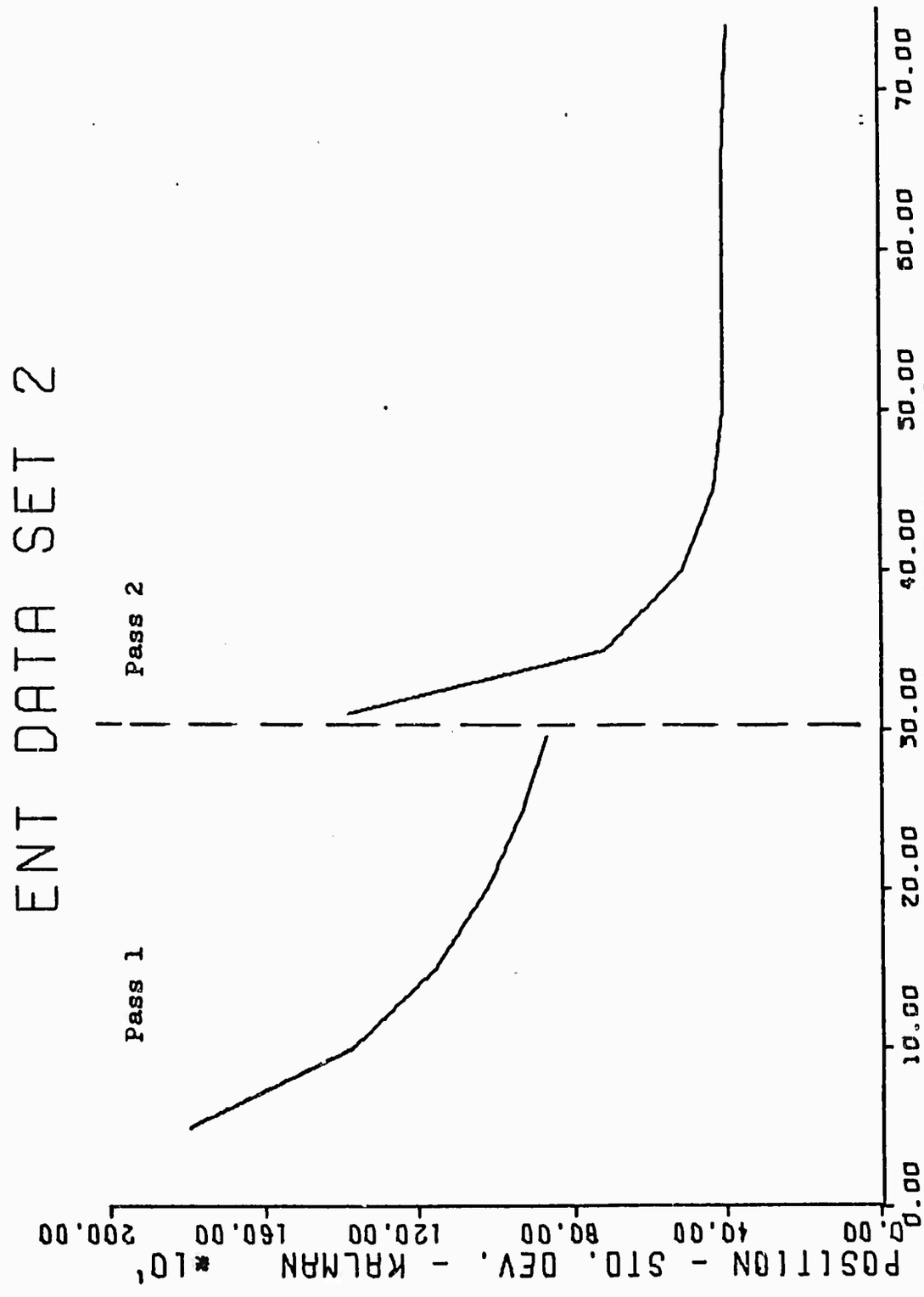

Figure 58. Standard Deviation of Position, Kalman Revised, Ent Set 2

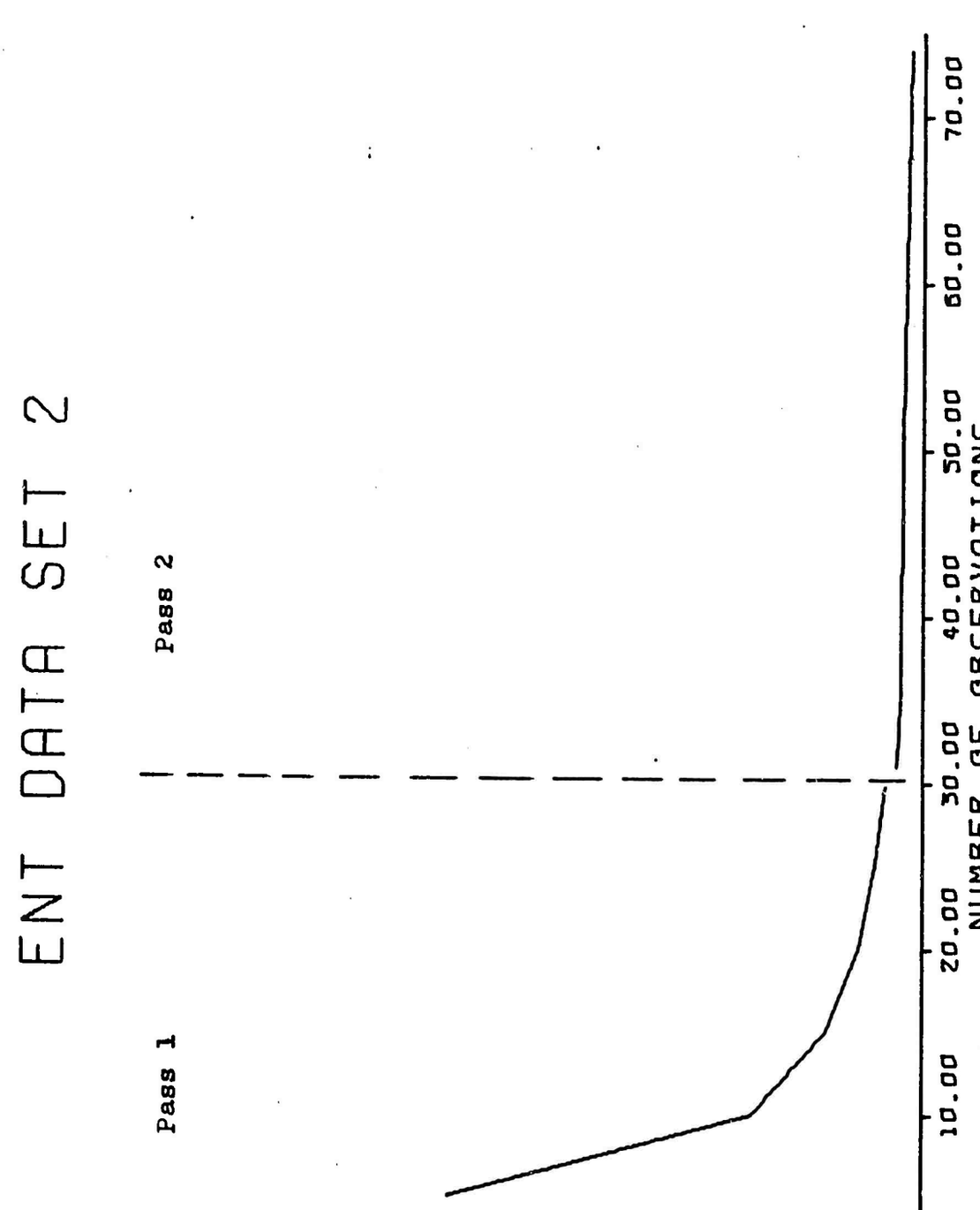

Figure 59. Standard Deviation of Velocity, Kalman Revised, Ent Set 2

Interpass Pointing Data. Due to the small number of measurements during pass 1, less accurate pointing data would be expected than was achieved in either the theoretical case or in data set 1. The pointing data is shown in Table XIX with an error of about 3° in azimuth and 1° in elevation. Although this would definitely limit the required field of scan, downrange detection with this pointing data will be more difficult.

Table XIX

Interpass Pointing Data Ent Set 2

Pass	Source	Range (meters)	Range Rate (meters/second)	Azimuth (Deg)	Elevation (Deg)
1-2	WLS	2789916	-3650	183.257°	24.56°
1-2	Kalman	2792497	-3655	183.341°	24.53°
1-2	Measurement	2712827	-3492	180.568°	25.64°

Chapter VIII

Conclusions and Recommendations

Conclusions. Based on the material presented in this thesis, as well as knowledge gained throughout the study of the near-earth orbital determination problem the following conclusions are drawn:

I. The simulated orbital analysis indicated that:

1. The Weighted Least Square error filter provides extremely accurate orbital parameters in the multi-pass problem with long data gap periods.

2. The Kalman Filter also provides equally accurate orbital parameters in the multi-pass problem with minimal data and long time gaps between observation passes.

3. The Kalman Fixed Point Smoother shows outstanding potential for the determination of orbital parameters if adequate measurements are available to cause the smoother to reach a steady state.

4. The existence of both short term and secular variations in the classical orbital parameters were demonstrated from the application of oblate earth modeling.

5. No conditions were encountered which caused either the WLS or Kalman filter to diverge. Interpass covariance remained well within the computational limits of the CDC 6600. The effects of the level I modification were not great due to the extreme computational capabilities of the CDC 6600.

6. The WLS filter took much longer to achieve the same results as the Kalman filter due to the necessity to batch compile the data and repeatedly integrate through that portion of the orbit in which there were no measurements, The approximate time ratio was 6 to 1.

7. Final covariances determined by the two methods were comparable.

8. Interpass pointing data was more accurate from the Kalman filter although no great difference was observed.

9. Modifications of filter parameters did not improve the speed or accuracy of the solution.

II. The actual data analysis indicated that:

1. Both the Kalman filter and the WLS filter showed the capability to accurately determine orbital parameters in a multi-pass multi-radar environment.

2. Kalman Smoothing failed to demonstrate the same degree of capability as in the theoretical case although when steady states were achieved the orbital parameters determined were accurate.

3. The same secular and short period perturbations seen in the theoretical data appeared in the orbital parameters for the actual data.

4. Both polar circular and low perigee elliptical orbits were able to be accurately determined.

5. The Kalman filter was found to be far more sensitive to errors or poor statistics on the noise covariance matrix, R.

6. Final covariances of both filters were comparable.

7. The WLS filter was seen to diverge on both sets of actual data until a modification to the process was made whereby the first pass data was converged and then used as the starting condition for the multi-pass data. Following the modification neither data set diverged.

8. The Kalman filter reached high interpass covariances on the order of 10^{11} during actual data processing. However, the filter always recovered on update and never diverged.

Recommendations: The following recommendations are made for continued study in this subject area and for improvement of the existing computer programs:

1. Modifications should be made to both programs to automate timing decisions during integration routines in order to maximize the use of information available from an observation.

2. Determination of θ_{g_o} should be written as a subroutine and added to both programs to increase program efficiency and minimize required input data. A constant update of θ_{g_o} should be made to achieve maximum accuracy.

3. Both programs should be modified to take the universal data format now employed at ENT.

4. The Kalman filter program should be expanded to include estimation of the ballistic coefficient, noise sigmas, noise biases, and net drag on the vehicle throughout the orbit. The estimation and application of the estimate of the noise covariance should improve Kalman filter operation.

5. A new orbital determination routine should be written employing the new Institute of Astronautics and Aeronautics orbital parameters.

6. A sensitivity analysis of both the WLS and Kalman filtering methods of orbital determination should be made.

7. Additional actual data should be applied to both programs to determine if the success found in the two cases tried in this thesis can be extended.

8. Additional applications of the smoothing algorithm should be made to determine if the smoother, when given adequate data, can

perform to the capability demonstrated in the simulated orbit case.

9. Both programs should be analyzed for possible reprogramming in order to reduce core requirements and decrease time requirements.

Bibliography

1. CIRA 1965, Amsterdam, North Holland Publishing Company, 1965.

2. Baker, Robert M. L. Astrodynamics. New York: Academic Press, Inc., 1967.

3. Baker, Robert M. L. and Maud W. Makemson. An Introduction to Astrodynamics (Second Edition). New York: Academic Press, Inc., 1967.

4. Britting, K. R. Inertial Navigation Systems Analysis, New York: Wiley Interscience, 1971.

5. Escobal, Pedro R. Methods of Orbit Determination. New York: John Wiley and Sons, Inc., 1965.

6. Ferguson, J. R., Jr. Comparison of the Extended Kalman Filter and Weighted Least Squares in Early-Orbit Determination. Air Force Institute of Technology, Master Thesis, Wright-Patterson AFB, Ohio, December 1971.

7. Filiatreau, Thomas R. and George E. Elliott. Application of the Kalman Filter to Orbit Determination. Air Force Institute of Technology, Master Thesis, Wright-Patterson AFB, Ohio, June 1970.

8. Gasposchkin, E. M. and Lambeck, K. 1969 Smithsonian Standard Earth (II) SAO Special Report No. 315. Smithsonian Institution Astrophysical Observatory, Cambridge, Massachusetts, May 18, 1970.

9. Hildebrand, F. B. Introduction to Numerical Analysis, McGraw-Hill, 1956.

10. Jazwinski, Andrew H. Stochastic Processes and Filtering Theory. New York: Academic Press, Inc., 1970

11. Jenson, J. et al. Design Guide to Orbital Flight. New York: McGraw-Hill, 1962.

12. King-Hele, Desmond. Theory of Satellite Orbits in an An Atmosphere. London: Butterworths, 1964.

13. Korn, . . and Korn . . Mathematical Handbook for Scientists & Engineers. New York: McGraw-Hill, 1968.

14. Meditch, J. S. Stochastic Optimal Linear Estimation and Control. New York: McGraw-Hill, 1969.

15. Nishimura, T. "Error Bounds of Continuous Kalman Filters and the Application to Orbit Determination Problems." IEEE Transactions on Automatic Control, 12:268-275 (June 1967).

16. Prislin, R. H. Trace66 Orbit Determination Program, Volume V: Differential Correction Procedure and Techniques. Aerospace Report No. TOR-0066 (9320)-2. Vol V. Los Angeles: The Aerospace Corp., 1970

17. Rogers, Charles E. and Christo Christodoulou. The Extended Kalman Filter Applied to the Determination of the Orbital Parameters of a Passive Earth Satellite. Air Force Institute of Technology, Master Thesis, Wright-Patterson AFB, Ohio, June 1971.

18. Sage, A. P. Optimum Systems Control. Prentice-Hall, Englewood Cliffs, New Jersey, 1968.

19. Schlee, F. H., et al, Divergence in the Kalman Filter. AIAA Journal, 5: 1114-1120 (1967).

20. Wackernagel, H. B. Spacetrack Earth Model 1966 (STEM66). Analysis Memorandum Number 66-3. Ent Air Force Base, Colorado: HQ 9th Aerospace Defense Division, June 1966.

21. Wolaver, L. E. Modern Techniques in Astrodynamics - An Introduction. Applied Mathematics Research Laboratory Technical Report # ARL 70-0278, Wright-Patterson Air Force Base, Ohio. (AD 718 963), 1970.

Appendix A

Derivation of the Gravitational Field of the Earth

The equations which describe the gravitational field of the earth are both long and complex. For this reason each of the three components of the gravitational field expressed in the geocentric rotating coordinate system will be determined term by term and combined finally as a summation of these individual terms.

Generally, the gravitational potential is given by

$$U = \frac{k_e{}^2 m}{r}\left(1 + \sum_{k=2}^{\infty}\left(\sum_{m=o}^{k}\left(\frac{P_k{}^{(m)}(\sin\phi)}{r^k}\right)\left(C_{k,m}\cos(m\lambda_E) + S_{k,m}\sin(m\lambda_E)\right)\right)\right) \tag{3}$$

However for this study adequate accuracy was considered achieved for

$$U = \frac{k_e{}^2 m}{r}\left(1 + \sum_{k=2}^{6}\left(\sum_{m=o}^{k}\left(\frac{P_k{}^{(m)}(\sin\phi)}{r^k}\right)\left(C_{k,m}\cos(m\lambda_E) + S_{k,m}\sin(m\lambda_E)\right)\right)\right) \tag{65}$$

In order to proceed further it is necessary to evaluate the associated Legendre Polynomials from P_2^0 to P_6^6. These functions are:

$$P_2{}^0 = .5(1-3x^2)$$

$$P_2{}^1 = 3x(1-x^2)^{1/2}$$

$$P_2{}^2 = 3(1-x^2)$$

$$P_3{}^0 = .5x(3-5x^2)$$

$$P_3{}^1 = 3/2(5x^2-1)(1-x^2)^{1/2}$$

$$P_3{}^2 = 15x(1-x^2)$$

$$
\begin{aligned}
P_3^3 &= 15(1-x^2)^{3/2} \\
P_4^0 &= .125x(3-30x^2 + 35x^4) \\
P_4^1 &= 2.5x(1-x^2)^{1/2}(7x^2 - 1) \\
P_4^2 &= 7.5(1-x^2)(7x^2 - 1) \\
P_4^3 &= 105x(1-x^2)^{3/2} \\
P_4^4 &= 105(1-x^2)^2 \\
P_5^0 &= .125(15-70x^2 + 63x^4)x \\
P_5^1 &= .125(1-x^2)^{1/2}(15-210x^2 + 315x^4) \\
P_5^2 &= .125(1-x^2)(-420x + 1260x^3) \\
P_5^3 &= .125(1-x^2)^{3/2}(-420 + 3780x^2) \\
P_5^4 &= .125(1-x^2)^2(7560x) \\
P_5^5 &= 945(1-x^2)^{5/2} \\
P_6^0 &= .0625(5-105x^2 + 315x^4 - 231x^6) \\
P_6^1 &= .0625(1-x^2)^{1/2}(210x - 1260x^3 + 1386x^5) \\
P_6^2 &= .0625(1-x^2)(210 - 3780x^2 + 6930x^4) \\
P_6^3 &= .0625(1-x^2)^{3/2}(-7560x + 27720x^3) \\
P_6^4 &= .0625(1-x^2)^2(-7560 + 83160x^2) \\
P_6^5 &= 10395(1-x^2)^{5/2}x \\
P_6^6 &= 10395(1-x^2)^3
\end{aligned}
\tag{66}
$$

We can then write

$$
\begin{aligned}
U = \frac{k_e^2 m}{r}\Bigg(1 &- \frac{J_2}{2r^2}\,(1-3\sin^2\phi) - \frac{J_3}{2r^3}\sin\phi(3-5\sin^2\phi) \\
&- \frac{J_4}{8r^4}(3-30\sin^2\phi + 35\sin^4\phi) - \frac{J_5}{8r^5}\sin\phi\,(15-70\sin^2\phi + 63\sin^4\phi) \\
&- \frac{J_6}{16r^6}(5-105\sin^2\phi + 315\sin^4\phi - 231\sin^6\phi) \\
&+ \sum_{k=2}^{6}\Bigg(\sum_{m=1}^{6}\left(\frac{P_k^m(\sin\phi)}{r^k}\right)(C_{k,m}\cos(m\lambda_E) + S_{k,m}\sin(m\lambda_E))\Bigg)\Bigg)
\end{aligned}
\tag{67}
$$

where the summation expresses the longitude dependent potential terms. The remainder of this equation can be expanded using the Legendre polynomials just given. From basic physics it can be shown that

$$G = \nabla U = \frac{\partial}{\partial x}\hat{i}_x + \frac{\partial}{\partial y}\hat{i}_y + \frac{\partial}{\partial z}\hat{i}_z\,(U) \tag{68}$$

By recalling that $\sin\phi = \frac{z}{r}$, $\cos\phi = \frac{\sqrt{x^2+y^2}}{r}$

$$\text{and} \qquad r = \sqrt{x^2+y^2+z^2} \tag{69}$$

$$\text{and} \qquad \sin\lambda_E = \frac{y}{\sqrt{x^2+y^2}} \;, \cos\lambda_E = \frac{x}{\sqrt{x^2+y^2}} \tag{70}$$

the various required derivatives can be obtained.

The following trigonometeris relations are also required:

$$\begin{aligned}
&\sin 2x = 2\sin x\cos x\\
&\cos 2x = \cos^2 x - \sin^2 x + 1 - 2\sin^2 x\\
&\sin 3x = 3\sin x - 4\sin^3 x\\
&\cos 3x = 4\cos^3 x - 3\cos x\\
&\cos 4x = 8\cos^4 x - 8\cos^2 x + 1\\
&\sin 4x = (8\cos^3 x - 4\cos x)\sin x\\
&\sin 5x = 5\sin x - 20\sin^3 x + 16\sin^5 x\\
&\cos 5x = 16\cos^5 x - 20\cos^3 x + 5\cos x\\
&\sin 6x = (32\cos^5 x - 32\cos^3 x + 6\cos x)\sin x\\
&\cos 6x = 32\cos^6 x - 48\cos^4 x + 18\cos^2 x - 1
\end{aligned} \tag{71}$$

After performing the required substitutions, the equations found in SUBROUTINE GRAVITY are obtained.

Complete copies of the programs used in this study including WLS, the Kalman filter, and the data generator are available from AFIT/ENE, Wright-Patterson AFB, Ohio.

Appendix B

Direction Cosine Matrices

Three coordinate systems are used in this study. These systems are all orthogonal systems such that the transpose of any direction cosine matrix is its inverse.

The following direction cosine matrix will transform a vector in the i system into the e system:

$$C_i^e = \begin{bmatrix} \cos(\omega_{ie}t + \theta_{g_o}) & \sin(\omega_{ie}t + \theta_{g_o}) & 0 \\ -\sin(\omega_{ie}t + \theta_{g_o}) & \cos(\omega_{ie}t + \theta_{g_o}) & 0 \\ 0 & 0 & 1 \end{bmatrix} \tag{72}$$

where θ_{g_o} is defined as in Appendix F.

This direction cosine matrix will transform a vector in the e system into the t system:

$$C_e^t = \begin{bmatrix} -\sin\phi\cos\theta & -\sin\phi\sin\theta & \cos\phi \\ \sin\theta & -\cos\theta & 0 \\ \cos\phi\cos\theta & \cos\phi\sin\theta & \sin\phi \end{bmatrix} \tag{73}$$

To go from the i system to the t system, premultiplication of the above direction cosine matrices is required such that

$$C_i^t = C_i^e C_e^t \tag{74}$$

Appendix C

Derivation of the System Matrix, F

The system matrix, F, is used in both the Weighted Least Squares Filter and the kalman filter. As defined by equation (22)

$$F = \frac{\partial f(x)}{\partial x}\Big|_{x=x(k+1;k)} \tag{75}$$

Now the derivative of a matrix with respect to a vector can be shown to be (Ref 18:553):

$$F = \begin{bmatrix} \frac{\partial \dot{x}_1}{\partial x_1} & \frac{\partial \dot{x}_1}{\partial x_2} & - & - & - & \frac{\partial \dot{x}_1}{\partial x_6} \\ \frac{\partial \dot{x}_2}{\partial x_1} & \frac{\partial \dot{x}_2}{\partial x_2} & - & - & - & \frac{\partial x_2}{\partial x_6} \\ \cdot & \cdot & & & & \cdot \\ \cdot & \cdot & & & & \cdot \\ \cdot & \cdot & & & & \cdot \\ \cdot & \cdot & & & & \cdot \\ \frac{\partial \dot{x}_6}{\partial x_1} & \frac{\partial \dot{x}_6}{\partial x_2} & - & - & - & \frac{\partial \dot{x}_6}{\partial x_6} \end{bmatrix} \tag{76}$$

Using the set of state equations given by equation (13) it can be seen that

$$F_{14} = F_{25} = F_{36} = 1$$

$$F_{41} = \frac{\partial^2 U}{\partial x^2} + \omega_{ie}^2 - v * x_4 * B \frac{*\partial \text{Density}}{\partial x} /2v$$

$$F_{42} = \frac{\partial^2 U}{\partial x \partial y} - v * x_4 * B * \frac{\partial \text{Density}}{\partial y} /2. \tag{77}$$

$$F_{43} = \frac{\partial^2 U}{\partial x \partial z} - v * x_4 * B * \frac{\partial \text{Density}}{\partial z} /2.$$

$$F_{44} = - v \cdot B \cdot \text{Density}/2 - x_4^2 \cdot B\text{-Density}/2v$$

$$F_{45} = 2\omega_{ie} - B \cdot \text{Density} \cdot x_4 x_5 / v$$

$$F_{46} = -B \cdot Density \cdot x_4 \cdot x_6 / v$$

$$F_{51} = \frac{\partial^2 U}{\partial y \partial x} - v\, x_5 \cdot B \cdot \frac{\partial Density}{\partial x} / 2.$$

$$F_{52} = \frac{+\partial^2 U}{\partial y^2} + \omega_{ie}^{\ 2} - v\, x_5\, B\, \frac{\partial Density}{\partial y} / 2.$$

$$F_{53} = \frac{\partial^2 U}{\partial y \partial z} - v \cdot x_5 \cdot B \cdot \frac{\partial Density}{\partial z} / 2.$$

$$F_{54} = -2\omega_{ie} - B \cdot Density \cdot x_4 \cdot x_5 / v$$

$$F_{55} = -v \cdot B \cdot Density/2 - x_5^2 \cdot B \cdot Density/2v$$

$$F_{56} = -B \cdot Density \cdot x_6 \cdot x_5 / v$$

$$F_{61} = \frac{\partial^2 U}{\partial z \partial x} - v \cdot x_6 \cdot B \cdot \frac{\partial Density}{\partial x} / 2.$$

$$F_{62} = \frac{\partial^2 U}{\partial z \partial y} - v x_6 \cdot B \cdot \frac{\partial Density}{\partial y} / 2.$$

$$F_{63} = \frac{\partial^2 U}{\partial z} - v x_6 \cdot B \cdot \frac{\partial Density}{\partial z} / 2.$$

$$F_{64} = -B \cdot Dense \cdot x_4 \cdot x_6 / v$$

$$F_{65} = -B \cdot Dense \cdot x_5 \cdot x_6 / v$$

$$F_{66} = -v \cdot B \cdot Dense/2 - x_6^2 \cdot B \cdot Dense/2v$$

where v = velocity

B = ballistic coefficient = .015

Appendix D

Measurement Sensitivity Matrix M

The measurement sensitivity matrix is made up of the partial derivatives of the measurements ρ, $\dot{\rho}$, A, and E with respect to the states evaluated at the current best estimate of the state of the satellite.

$$M = \left.\frac{\partial hi(x)}{\partial xj}\right|_{x=\hat{x}} = \begin{bmatrix} M(1) \\ M(2) \\ M(3) \\ M(4) \end{bmatrix} = \begin{bmatrix} \frac{\partial \rho}{\partial x} & \cdot & \cdot & \cdot & \frac{\partial \rho}{\partial \dot{z}} \\ \frac{\partial \dot{\rho}}{\partial x} & \cdot & \cdot & \cdot & \frac{\partial \dot{\rho}}{\partial \dot{z}} \\ \frac{\partial A}{\partial x} & \cdot & \cdot & \cdot & \frac{\partial A}{\partial \dot{z}} \\ \frac{\partial E}{\partial x} & \cdot & \cdot & \cdot & \frac{\partial E}{\partial \dot{z}} \end{bmatrix} \tag{78}$$

Where M(1), M(2), M(3), and M(4) are given by

$$M(1) = \left((x+X)/\rho,\ (y+Y)/\rho,\ (z+Z)/\rho,\ 0,\ 0,\ 0\right) \tag{79}$$

$$M(2) = \left(\frac{\dot{x}}{\rho} - \frac{\dot{\rho}(x+X)}{\rho},\ \frac{\dot{y}}{\rho} - \frac{\dot{\rho}(y+Y)}{\rho},\ \frac{\dot{z}}{\rho} - \frac{\dot{\rho}(z+Z)}{\rho},\ \frac{x+X}{\rho},\ \frac{y+Y}{\rho},\ \frac{z+Z}{\rho}\right) \tag{80}$$

$$M(3) = \left(1/(\rho^2 - z_T^2)\right)\left(-x_T \sin(\theta) - y_T \sin(\phi)\cos(\theta),\ x_T \cos(\theta) - y_T \sin(\phi)\sin(\phi),\ y_T \cos(\phi),\ 0,\ 0,\ 0\right) \tag{81}$$

$$M(4) = \left(1/\rho - z_T^2)^{1/2}\right)\left(\cos(\phi)\cos(\theta) - z_T(X-X)/\rho^2, \sin(\theta)\cos(\phi) - z_T\frac{(y-Y)}{\rho^2},\ \sin(\phi) - z_T(z-Z)/\rho^2,\ 0,\ 0,\ 0\right) \tag{82}$$

and where the state vector $\underline{x} = \begin{bmatrix} x_1 \\ x_2 \\ x_3 \\ x_4 \\ x_5 \\ x_6 \end{bmatrix} = \begin{bmatrix} x \\ y \\ z \\ \dot{x} \\ \dot{y} \\ \dot{z} \end{bmatrix}$ (83)

and x, y, and z are the negative of the station coordinates in the geocentric rotating frame and x_T, y_T, z_T are the position coordinates of the satellite in the tangent frame.

Appendix E

Gaussian Distribution Curves

The additional graphs contained in this appendix are included since they were the basis for the decision to make 25 runs of the Kalman and WLS programs and take statistical averages in order to satisfy theoretical requirements for a Guassian distribution.

The region of quantitization used on the graphs is .05. A finer grid would have led to graphs of more erratic behavior and a less fine grid would have camouflaged the true intent of the curve. It is seen that at 100 points the density appears to be hardly more than uniform. At more than 500 points, the density approaches the familiar bell-shaped Gaussian density curve. However, it should be emphasized that all of these samples passed a Kolomogorov Smirnov test with a significance level of .20 when compared with a true N(0,1) distribution.

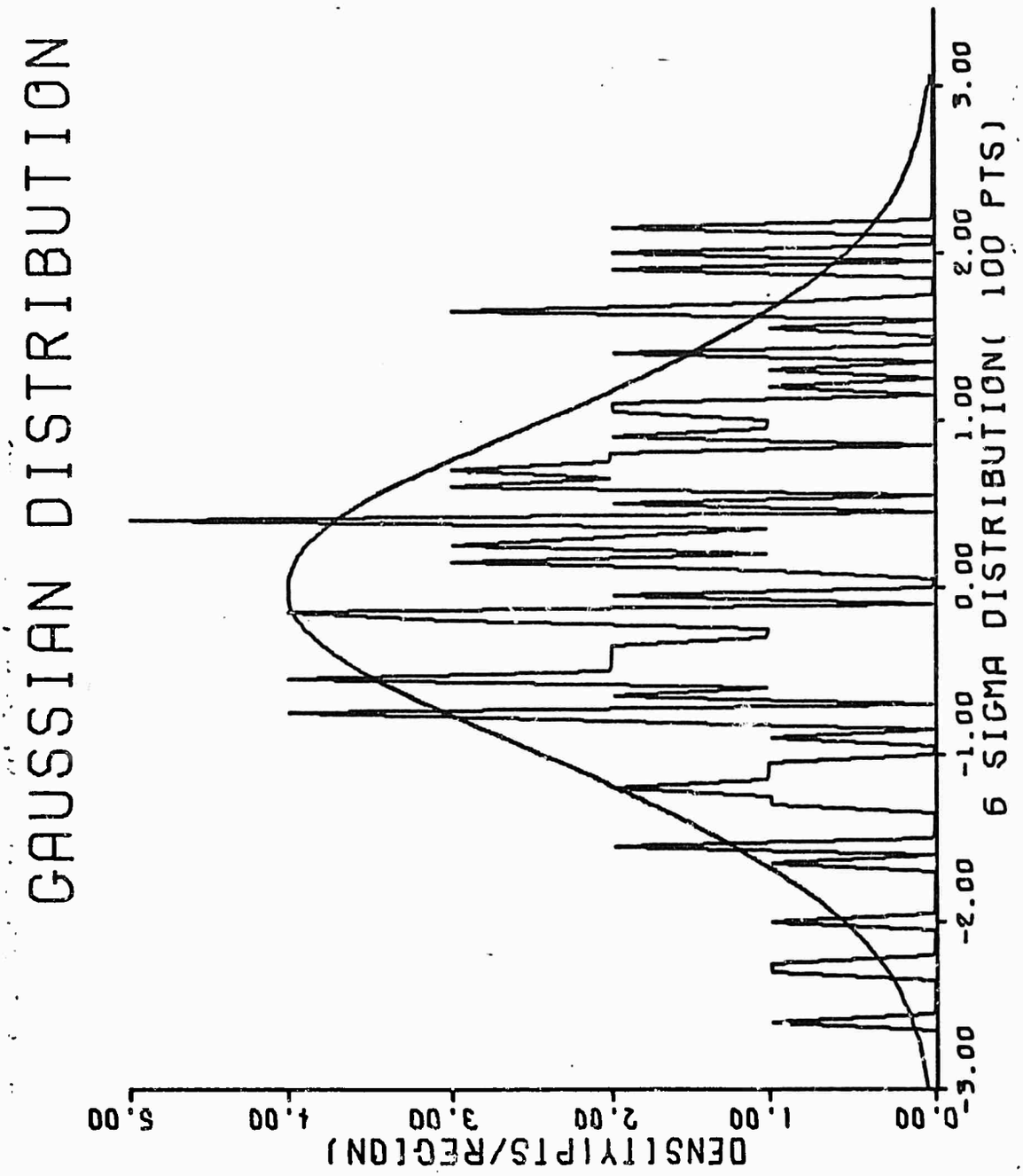

Figure 60. Gaussian Density Distribution 100 Points

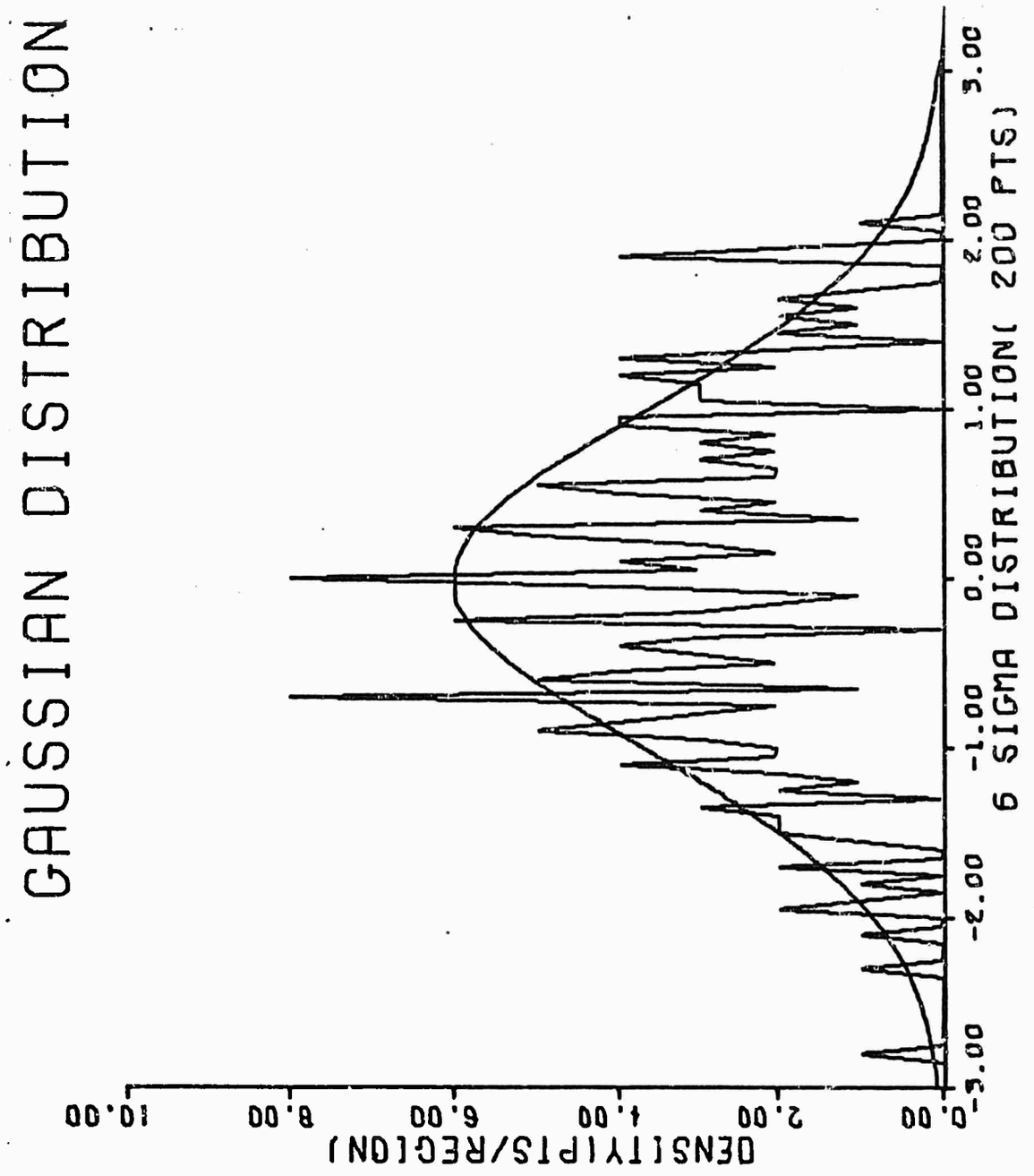

Figure 61. Gaussian Density Distribution 200 Points

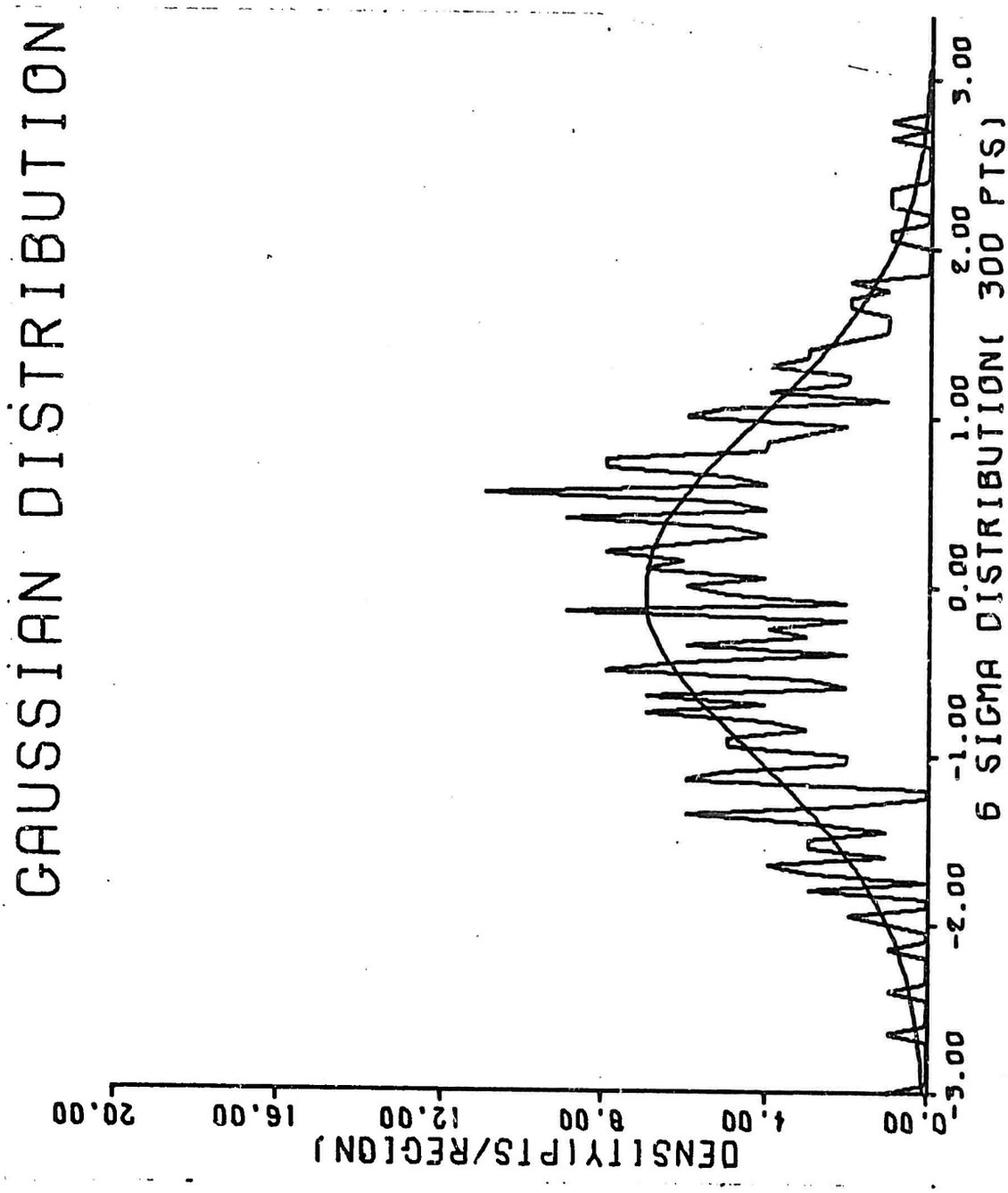

Figure 62. Gaussian Density Distribution 300 Points

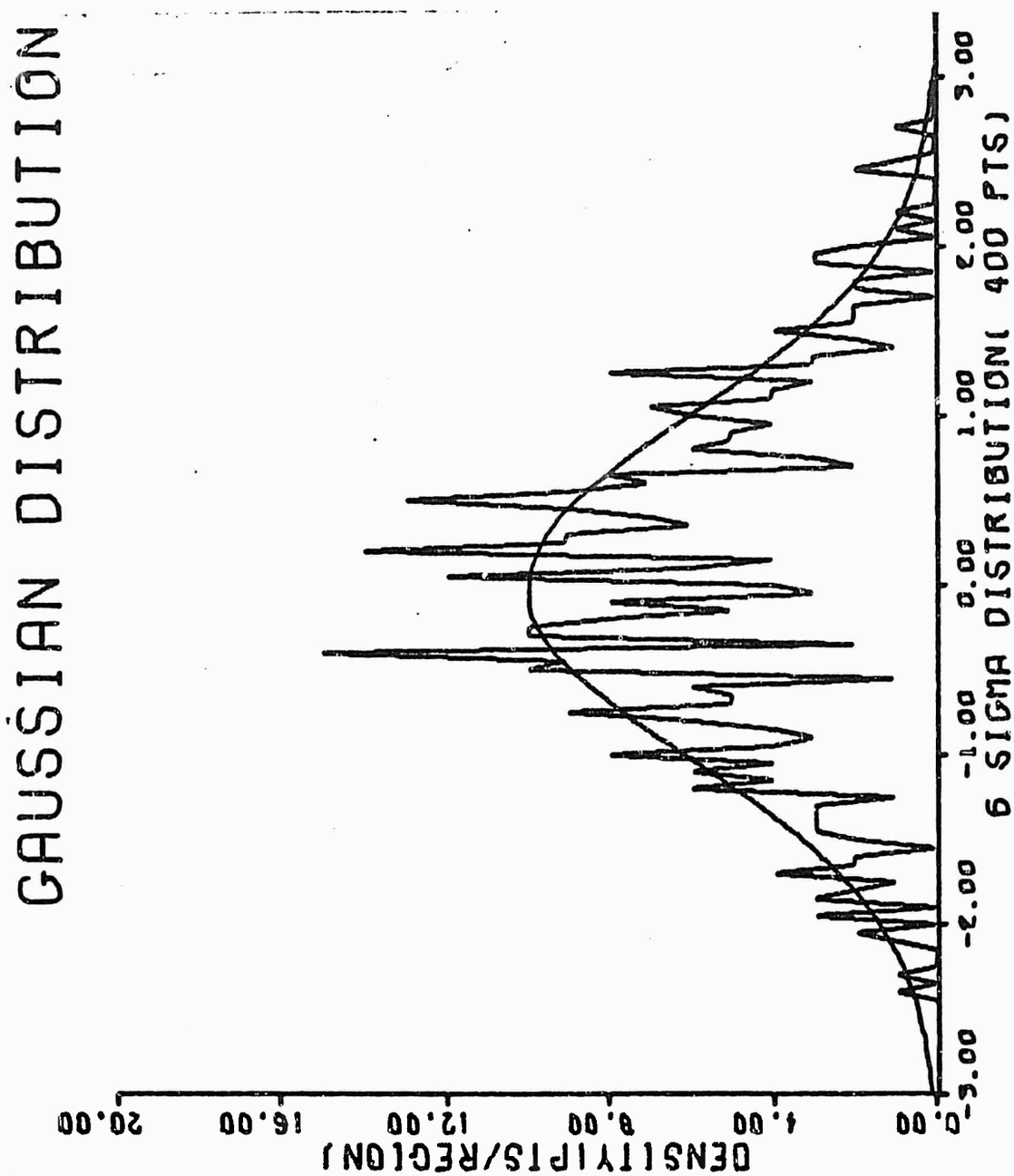

Figure 63. Gaussian Density Distribution 400 Points

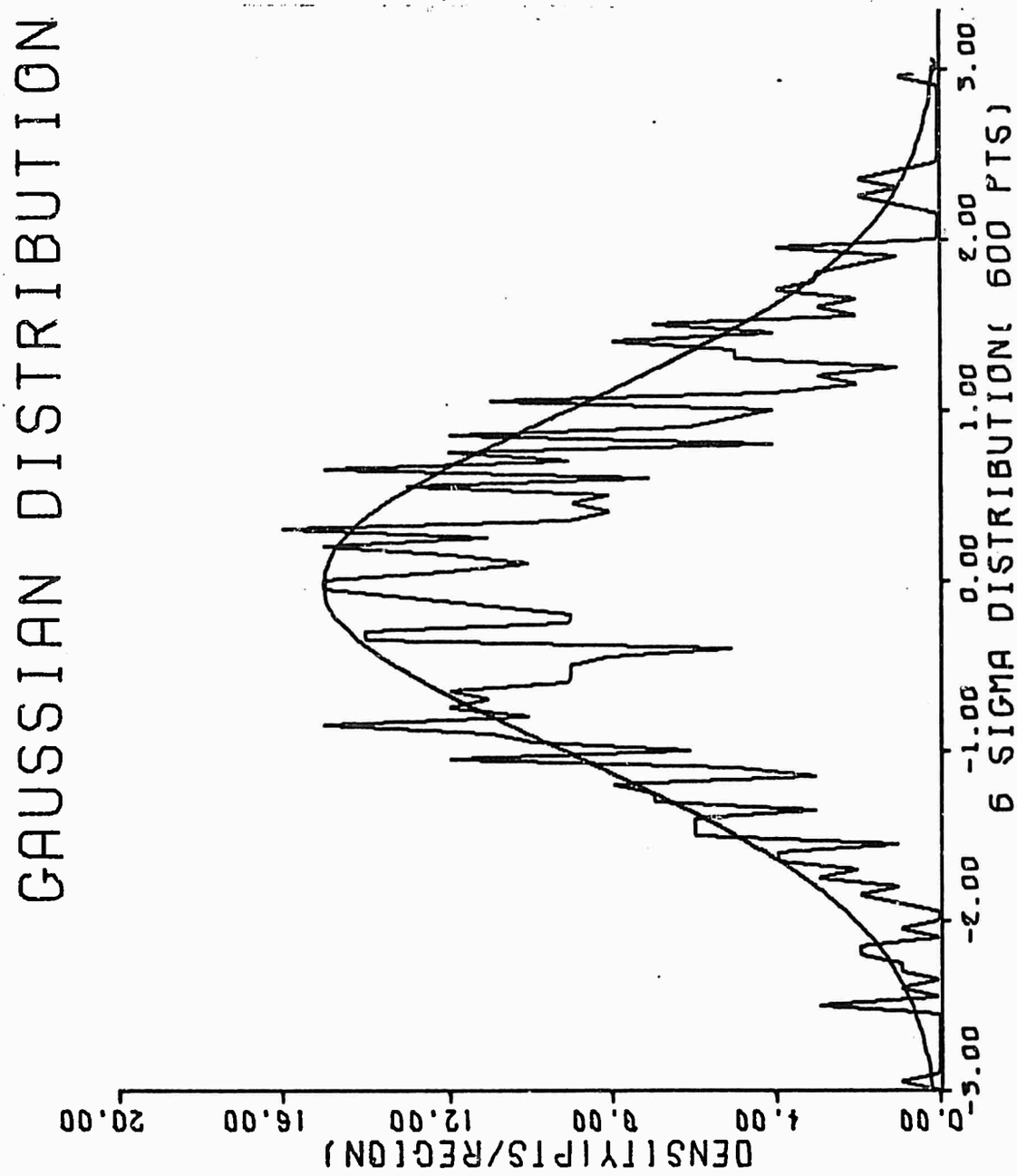

Figure 64. Gaussian Density Distribution 600 Points

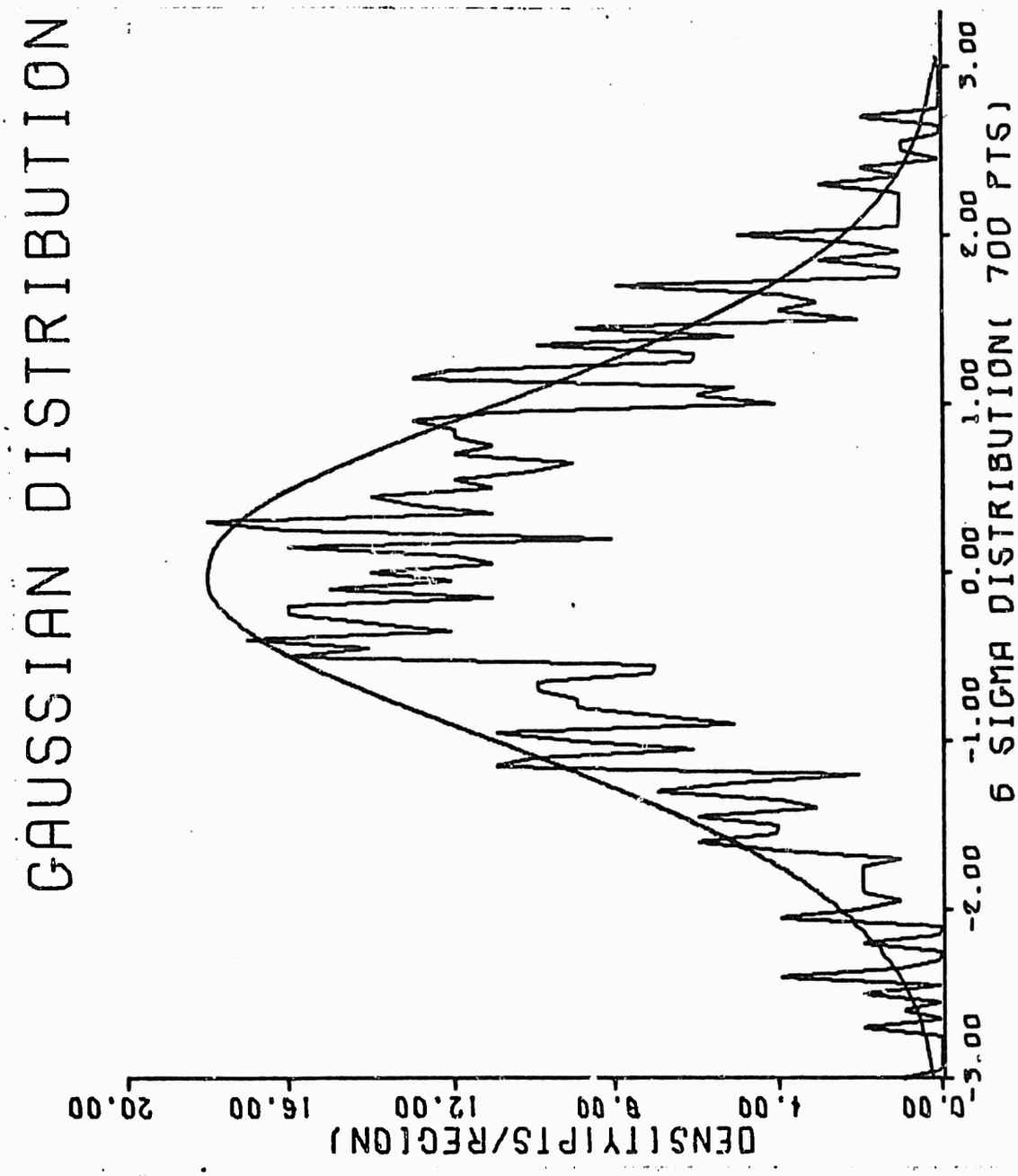

Figure 65. Gaussian Density Distribution 700 Points

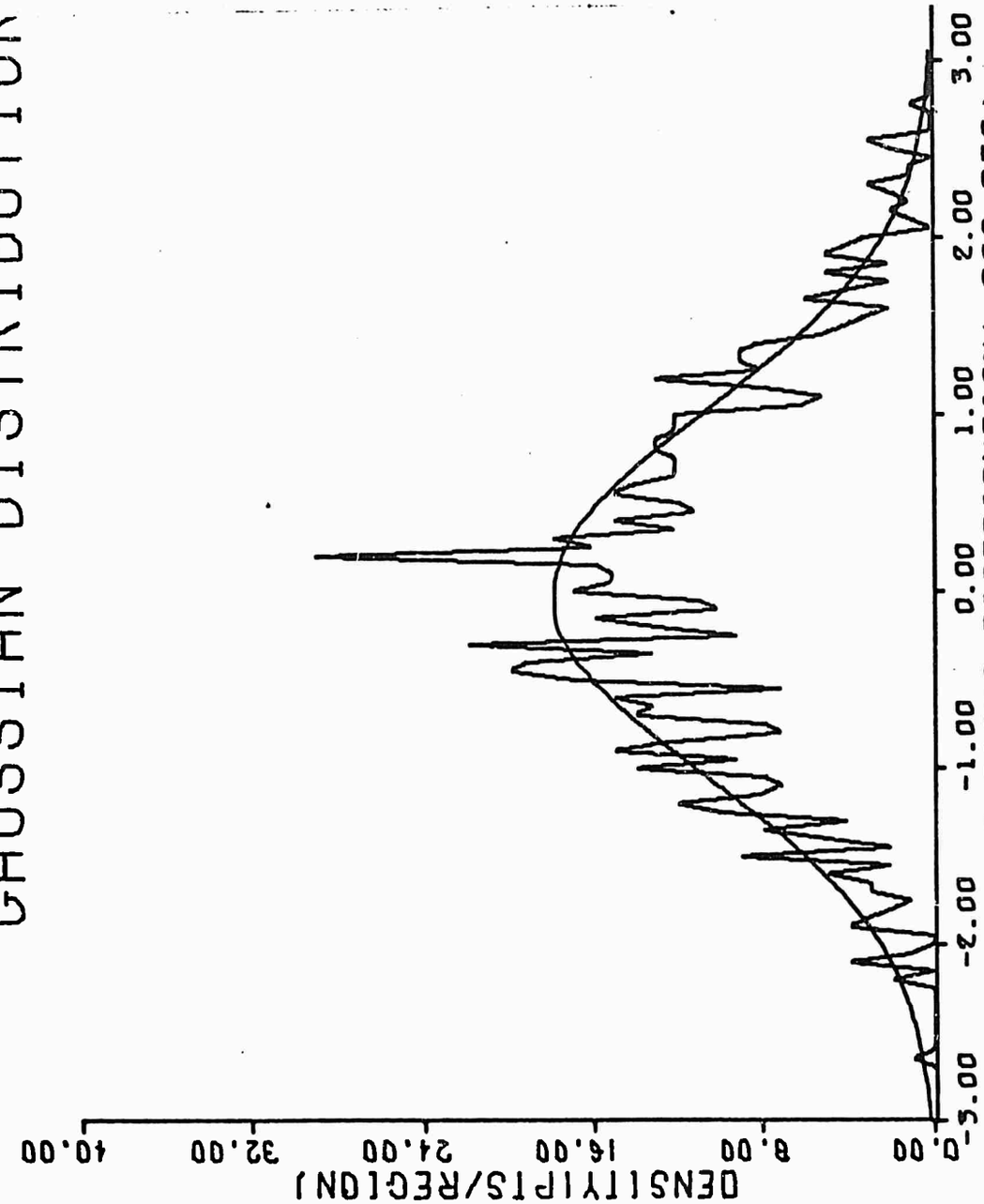

Figure 66. Gaussian Density Distribution 800 Points

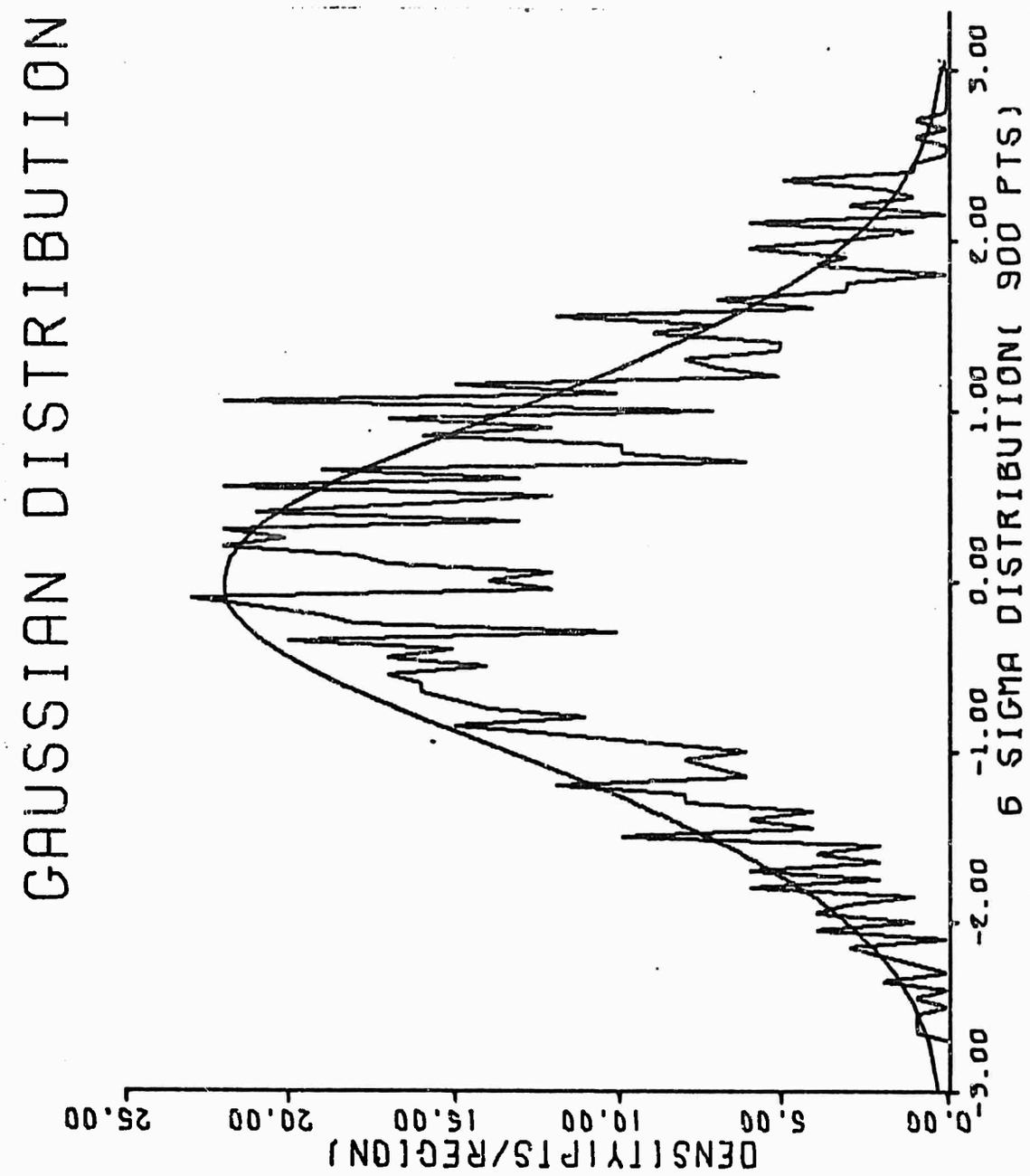

Figure 67. Gaussian Density Distribution 900 Points

Appendix F

Determination of θ_{g_o}

The determination of θ_{g_o} is necessary so that the inertial reference system may be properly located with respect to the rotating geocentric coordinate system. Specifically, θ_{g_o} is the hour angle between the Greenwich meridian and the vernal equinox (inertial x-axis) at 0 hrs GMT on the date under consideration.

This angle would normally be determined by use of an ephmeris. However, if the hour angle desired is for a date as recent as yesterday, such an ephemeris is likely to be unavailable. Therefore the following approximation was used:

$$\theta_{g_o} = 1.7294468 + [\text{Days Since 1950}] * .017202915 \quad (84)$$

where

$$[\text{Days Since 1950}] = [\text{yr-50}] * 365 + \text{INT}\left(\frac{\text{yr-1}}{4}\right) - 12 + \text{Day} \quad (85)$$

Reduce to less than 2π and INT means take the integer part of.

Example

Find θ_{g_o} for 190 day of 1972

then

$$\theta_{g_o} = 1.7294468 + [(72-50)*365 + \text{INT}\left(\frac{72-1}{4}\right) - 12 + 190]*.017202915$$

$$= 1.7294468 + [22*365 + 17 - 12 + 190]*.017202915$$

$$= 1.7294418 + (8225)*.017202915$$

$$= 1.7294468 + 141.4939759 = 143.2242268$$

$$= 4.99334607 \text{ rad} = 286.09765789^\circ = 19 \text{ hr } 4 \text{ min } 23.437884 \text{ sec}$$

Appendix G

Determination of Classical Orbital Parameters Using the State Vector

The determination of the classical orbital elements

a, the semi-major axis

e, the eccentricity

i, the angle on inclination

Ω, the line of nodes

and ω, the argument of perigee

from the state vector composed of the x,y,z components of position and the x,y,z components of velocity expressed in the geocentric rotating coordinate frame, e, is necessary to obtain many of the figures in this study. Additionally, the parameters

P, the period

and hp, the height at perigee

are of interest in many orbital problems. This appendix provides a method for obtaining these orbital parameters using the state vector.

The first step is to convert the state vector to the inertial computational frame, i, by use of the direction cosine matrix found in Appendix B.

In the inertial frame, the radius, r, and the velocity, $\dot{r}$, of the vehicle can be expressed as:

$$r = \sqrt{x^2 + y^2 + z^2} \tag{86}$$

$$\dot{r} = \sqrt{\dot{x}^2 + \dot{y}^2 + \dot{z}^2} \tag{87}$$

where the position states x, y, and z have been normalized using the astronomical distance unit r_e = 6,378,165 meters and the velocity states have been divided by the astronomical velocity unit, v_o = 7905.376 meters/second.

Since $\underline{r} \times \underline{v} = \underline{h}$ it is seen that

$$\begin{aligned} h_x &= y\dot{z}-z\dot{y} \\ h_y &= z\dot{x}-x\dot{z} \\ h_z &= x\dot{y}-y\dot{x} \end{aligned} \tag{88}$$

where h is the angular momentum and h_x, h_y, h_z are the x,y, and z components. Also

$$h = \sqrt{h_x^2 + h_y^2 + h_z^2} \tag{89}$$

since a vector magnitude is the square root of the sum of the squares of its components.

The eccentricity, e, is then found by

$$e = \sqrt{(r^2/h^2) + (h/r - 1.)^2} \tag{90}$$

The semi-major axis, a, is given by

$$a = h/(1.-e^2)(E.R.) \tag{91}$$

The period, P, can be found by

$$P = 2\pi((a\ r_e)^3/\omega)^{1/2}/60 \text{ min where } \omega = 3.986012\text{x}10^{14} \tag{92}$$

The height at perigee, h, can be found from

$$h_p = r_e(a-a\cdot e-1.) \text{ meters} \tag{93}$$

From geometric projections the following angles can be determined:

$$i = \cos^{-1}(hz/h) \text{ deg} \tag{94}$$

$$\Omega = \tan^{-1}(-hx/hy) \text{ deg} \tag{95}$$

One possible scheme for finding ω is

$$\omega = \tan^{-1}(z \cos i/(x \cos \Omega + y \sin \Omega)) - \cos^{-1}((h^2-\omega r)/eh^2) \text{ deg} \tag{96}$$

Care must be exercised on assigning the proper algebraic sign to the values of all of the inverse trigonometric functions with decisions based on the sign of h_z. (Ref 21:52-53).

Vita

Joseph John Pollard was born [redacted] He graduated [redacted] and entered [redacted] Institute of Technology where he majored in Electrical Engineering. In June 1965 he graduated with a Bachelor of Science degree in Electrical Engineering and an ROTC commission in the United States Air Force. His first active duty tour was at Holloman Air Force Base, New Mexico, where he served as a Center Plans Officer and later as Operations Officer in the SRAM (AGM-69) Test Division of the 6585 Test Group. Captain Pollard entered the Air Force Institute of Technology in August 1971 in pursuit of a Master's Degree in Electrical Engineering and will continue after graduation in Doctoral studies.

Permanent address: [redacted]

This thesis was typed [redacted]